USING GEOSPATIAL AND COMPUTER VISION TECHNIQUES FOR WEED DETECTION AND MAPPING IN AGRICULTURAL SYSTEMS

A Dissertation

by

BISHWA BANDHU SAPKOTA

Submitted to the Graduate and Professional School of
Texas A&M University
in partial fulfillment of the requirements for the degree of

DOCTOR OF PHILOSOPHY

Chair of Committee,	Muthukumar Bagavathiannan
Committee Members,	Nithya Rajan
	Scott Nolte
	Sorin Popescu
Head of Department	David D. Baltensperger

May 2022

Major Subject: Agronomy

ABSTRACT

Site-specific treatment of weeds in agricultural landscapes has been gaining importance in recent years due to economic savings and minimal impact on the environment. Weed detection and recognition is a major component of any site-specific treatment method. Different crop-weed complexities and weed control objectives may require the strategic implementation of various weed recognition approaches. This research aims at evaluating various weed detection and mapping approaches in different crops including cotton, corn, soybean, and wheat using remotely sensed digital RGB imageries. The first experiment was conducted in mid-season cotton infested with early-mid growth stage weeds to evaluate crop row detection methods for weed mapping and density estimation. The second experiment was conducted in wheat to evaluate the pixel-based detection approach for detecting Italian ryegrass and developing grid maps for competitive interactions. The third experiment was conducted to test the cross-crop species applicability of a convolutional neural networks (CNN)-based weed detection model trained for cotton over other row crops such as corn and soybean. The fourth experiment was conducted to explore various image synthesis techniques for training deep learning models to detect weeds in cotton. The first experiment revealed that the crop row detection approach can provide high accuracy levels for weed mapping and weed-density estimation. The second experiment showed that grass weeds such as Italian ryegrass can be effectively classified from wheat and competitive effects of ryegrass on wheat can be predicted early with reasonably high accuracy using the pixel-based machine learning approach. The third experiment indicated that a deep learning-based weed detection model trained for cotton can be used for soybean with more confidence compared to corn. The final experiment revealed that synthetic images can provide

comparable accuracy to real images for training weed detection models. In addition, the experiment showed that above-ground biomass of broadleaved weeds may be better predicted than grass using canopy mask results. Overall, these findings improve sensor-based weed detection, which is expected to advance precision weed management.

DEDICATION

To my dearly Mom and Dad

To my lovely wife Kisman Bhattarai

You are what made this worth it!

ACKNOWLEDGEMENTS

I first acknowledge the kindness and love of my mom and dad, who always dreamed me of attaining the highest level of education. They believed in my potential since when I was kid and always made sure I was not deprived of a good education.

I next acknowledge my mentor and major advisor Dr. Muthukumar Bagavathiannan. His sharp vision led to the foundation for my research and his encouragement pushed me on every front be rise professionally. His humble and meticulous personality is very admirable and inspiring.

I would like to thank my fantastic committee, Drs. Nithya Rajan, Scott Nolte, and Sorin Popescu for guiding me with their expertise throughout my Ph.D. journey. They have been great advisors, always willing to provide help when needed. I would like to thank my lab co-worker Mr. Chengsong Hu for being such a great friend and great co-worker. I thank you for responding to my queries always with great courtesy. My kudos to all the TAMU weed science lab members who supported one way or another.

I also like to thank my siblings, Sumitra, Barun, and Amrit for always being there as guardians. Truly indebted to you all. Last but not the least, I would like to thank my dear wife Mrs. Kisman Bhattarai for being there with me on every ups and downs during my Ph.D. journey. Thank you for taking on life's challenges with me. I adore you.

CONTRIBUTORS AND FUNDING SOURCES

Contributors

This work was supervised by a dissertation committee consisting of Dr. Muthukumar Bagavathiannan (Chair), Dr. Nithya Rajan (Soil and Crop Sciences), Dr. Scott Nolte (Soil and Crop Sciences), and Dr. Sorin Popescu (Ecosystem Science & Management).

Funding Sources

The experiment in Chapter 2 was funded by Texas A&M AgriLife Research—Cropping Systems Seed Grant Program (#111222), and Cotton Incorporated (#19-255).

The experiment in Chapter 3 was funded by a Texas A&M AgriLife Research Cropping Systems Seed Grant awarded to Dr. Bagavathiannan.

The experiment in Chapter 4 was funded in part by the USDA-Natural Resources Conservation Service-Conservation Innovation Grant (NRCS-CIG) program (award # NR213A750013G017) and Cotton Incorporated (award #20-739).

The experiment in Chapter 5 was funded in part by the USDA-Natural Resources Conservation Service-Conservation Innovation Grant (NRCS-CIG) program (award # NR213A750013G017) and Cotton Incorporated (award #20-739).

NOMENCLATURE

ANNs	Artificial Neural Networks
ANOVA	Analysis of Variance
AP	Average Precision
CNNs	Convolutional Neural Networks
DN	Digital Number
DNNs	Deep Neural Networks
ExG	Excess Greenness Index
FN	False Negative
FP	False Positive
GAN	Generative Adversarial Networks
GCPs	Ground Control Points
GLCM	Grey Level Co-occurrence Matrix
IoU	Intersection Over Union
IP	Instance Pool
LiDAR	Light Detection and Ranging
mAP	Mean Average Precision
MG	Morningglories
MLP	Multi Layer Perceptron
NDVI	Normalized Difference Vegetation Index
OA	Overall Accuracy
OBIA	Object Based Image analysis

PNG	Portable Network Graphic
PO	Paster Operations
RBGA	Red Blue Green Alpha
RGB	Red Green Blue
RM	Random Modifier
RMSE	Root Mean Square Error
RPN	Region Proposal Network
SIGP	Synthetic Image Generation Pipeline
SSWM	Site-Specific Weed Management
TGI	Triangular Greenness Index
TP	True Positive
UAS	Unmanned Aerial Systems
UAV	Unmanned Aerial Vehicle
USDA	United States Department of Agriculture
VARI	Visible Atmospheric Resistant Index
YOLO	You Only Look Once

TABLE OF CONTENTS

Page

LIST OF FIGURES

Page

LIST OF TABLES

Page

1. INTRODUCTION

1.1. Background

Weeds impact crop productivity and pose a serious threat to sustainable crop production (Hall et al., 1992; Oerke, 2005). Weed management is, therefore, a crucial but challenging agronomic intervention. Under current standard weed management interventions, broadcast herbicide applications are made periodically to control the weed emergence in the fields. Often, farms managed with standard herbicide plans may not bear heavy weed infestation following pre-emergence applications. Such managed farms may have a sporadic and more likely sparse distribution of weeds in the field. The broadcast application of herbicides under such situations may not be wise owing to two main reasons, a) unnecessary application can lead to increased herbicide costs b) excessive application can lead to environmental impacts (Christensen et al., 2009).

A site-specific weed management (SSWM) concept, which considers the spatio-temporal variabilities in weed species establishment and growth, can facilitate effective and economical weed management in such situations (Aracena, 2013; van Evert et al., 2017). The cost savings using the SSWM concept has been reported to be anywhere ranging from US$96.24 ha^{-1} to $104.76 ha^{-1} in soybean fields (Medlin and Shaw, 2000). However, this concept premises on precise detection and/or mapping of different weed species infesting crop fields. The progress made over the SSWM concept has remained optimistic so far. In general, SSWM is practiced under two approaches, a) real-time and b) post-mapping. In the real-time approach, robo-machines (e.g. Lottes et al., 2018; van Evert et al., 2011) are designed and programmed to scout for weeds in the field and apply control methods simultaneously. This approach is quicker because detection and control of weeds occur at the same time. However, this approach may not

be suitable when weeds are present at high density and/or at higher growth stages. The post-mapping approach (e.g. Castaldi et al., 2016; Lopez-Granados et al., 2015) on contrary is completed in two major steps, a) image acquisition and analysis to produce weed grid maps and b) weed control applications using weed grid maps. This approach is more suitable for weed control when high weed densities are found and management of such weed populations is possible with treatment zones.

Remote sensing is an integral part of post-mapping operations. Remote sensing is the process of characterizing a physical area by measuring the reflected and emitted radiation at a distance, generally from satellites or aircraft (Jensen, 2005). Remote sensing has been successfully used for weed infestation assessments across large areas (Lamb and Brown, 2001; Everitt et al., 2007; Lopez-Granados et al., 2015). Various satellites with unique sensor capabilities have been deployed to date to acquire a wide array of remote sensing images. However, at times, the spatial resolution of satellite images may be deemed inadequate for various agricultural applications including weed detection and mapping. As crops are typically small in size, very high spatial resolution images are required for canopy-level assessments. Recent advancements in Unmanned Aerial Systems (UAS) technologies have opened up new opportunities for acquiring high spatial resolution images at desired temporal resolutions (Shi et al., 2016). UAS technology has been successfully used for various agricultural applications, including soil and land mapping (Akar, 2017), drought stress monitoring (Ludovisi et al., 2017), crop disease detection (Mirik et al., 2011; Sugiura et al., 2016), and in-season yield estimation (Swain et al., 2010).

Weed detection and/or mapping using image processing and analysis techniques is a major component of these two approaches. Because their mode of operations in the field is

different, the image analysis techniques, however, must be tailored differently to obtain a domain-suitable end product. For example, in real-time operations, the digital images are analyzed to detect individual weeds, localize the positions, and acquire local coordinates for treating weeds with control systems while in post-mapping operations, images are analyzed to detect weeds at the individual level or map weeds across the regions to create prescription or treatment maps. In post-mapping, images can be analyzed to produce pixel-level or individual-plant-level information regarding the location and distribution of weeds throughout the field (Lopez-Granados et al., 2015). Such information can guide farmers in assessing weed-infested areas and developing management grids for site-specific treatments. For example, Castaldi et al. (2016) analyzed digital images to produce weed coverage maps in maize (*Zea mays* L.), which was further transformed into 2 m × 2 m grids. These grids were then classified into weed-free and weed-infested zones based on weed threshold and subsequently utilized for site-specific weed management. In addition, knowledge of weed distributions and densities across the field is beneficial for tailoring herbicide applications to weed spatial distribution in the field (Goudy et al., 2001).

The image analysis for weed detection in these approaches is performed using a series of computer vision and machine learning operations. Computer vision is the process of acquiring, processing, analyzing, and understanding digital images using computers (Klette, 2014). This technique enables a powerful extraction of useful information from digital images for further intelligence analysis. Machine learning is a computational method that involves recognizing the pattern in the data/information to make accurate predictions about the pattern in unseen data (Mohri et al., 2018). This method draws classification rules by iteratively minimizing the errors based on the user-fed training data. The rigorous iterative learning process thus leads to reliable

and repeatable decisions and results. In general, image analysis starts with the computer vision operations that generate a set of features for objects of interest followed by machine learning operations that utilize these features to learn the patterns.

Various computer vision and machine learning methods have been employed for SSWM purposes. Combining the object-based image analysis (OBIA) with random forest-based prediction, De Castro et al. (2018) analyzed UAV images and their derivatives to map weeds in cotton and sunflower fields. Chessboard segmentation was applied to the canopy height model to derive object height information, which was later fused with spectral features for classifying the segmented objects into weeds and non-weeds. Gao et al. (2018) fused row-detection algorithm results with OBIA-derived features to map weeds in maize fields using a random forest classifier. The Hough transformation algorithm was applied to detect cotton rows, which was then utilized for object segmentation and classification using machine learning algorithms. Gašparović et al. (2020) utilized a fusion of random forest-based supervised and K-means algorithm-based unsupervised classification methods to map oat (*Avena sativa* L.) using a low-cost UAV-borne RGB image.

In recent years, deep neural networks (DNNs) are increasingly used for several image localization and classification tasks. Among the different variants of DNNs, convolution neural networks (CNNs) have gained popularity for weed detection and classification due to their higher precision and accuracy. CNNs are the advanced form of neural networks that extract different hierarchies of information from the images and predict the location and extent of the target objects based on the extracted information (Chen et al., 2018). Although recently several studies have implemented CNNs for the detection and classification of weeds (Gao et al., 2020; Lottes et al., 2018; Sa et al., 2018), there is a great need for investigation into harnessing the

potential of CNNs for various crop-weed conditions. One of the areas that require great research is the applicability of the crop-specific weed detection model over other crops. This is particularly important as it's often expensive to train CNN models for weed detection due to large data requirements. Despite their promise, CNN models are data-hungry and prone to over-fitting if enough training data is not fed. In many cases, training data preparation and training process for these models is time-consuming and labor-intensive. Due to these reasons, it would be helpful to assess if synthetic images can be used in training these data-hungry models. This approach has already been embraced for various object detection and segmentation tasks, including weed detection (Gao et al., 2020; Hu et al., 202).

Studies have shown that the SSWM concept has great promise and prospects in agriculture (Medlin and Shaw, 2000; Pérez-Ruíz, 2005). Moreover, this technique is expected to ameliorate the herbicide resistance problem by cutting off the excessive usage of herbicide. However, the rate of adoption of this technique by farmers is not satisfactory (Lati et al., 2021). There are two major reasons why these technologies still lack widespread adoption. First, the technological and establishment cost exceeds the marginal benefits of the farmer. Initial purchasing and maintenance costs of robo-machines are extremely high. For example, Dino, a robot developed by a French AgTech startup costs a farmer about $220,000. The Post-mapping approach can also be very expensive because it involves multiple equipment and skillsets in the process. The second major reason is the inconsistency in the performance of these machines that causes insecurity in farmers for the investment. Part of the reason for performance inconsistency could be poor weed recognition techniques as weed recognition in complex agricultural background scenes can be difficult. Although considerable efforts have been placed since the early '90s, recognition systems still lack precision and accuracy. More research is needed to

improve the existing recognition systems and increase the diversity of techniques to combat unique weed detection problems. This dissertation customizes and evaluates various weed detection and mapping strategies pertaining to different crop-weed situations.

1.2. Objectives

1. Evaluate crop row detection approach for weed mapping across various density gradients in cotton using UAV-borne RGB images

2. Evaluate pixel-based machine learning approach and UAV-borne RGB images for detecting Italian ryegrass in wheat and predicting competitive interactions

3. Evaluate cross-crop species applicability of a crop-specific weed detection model over other row crops

4. Explore various synthetic image generation procedures for training a deep learning model for weed detection in row crops

2. MAPPING AND ESTIMATING WEEDS IN COTTON USING UNMANNED AERIAL SYSTEMS-BORNE IMAGERY*

2.1. Abstract

In recent years, Unmanned Aerial Systems (UAS) have emerged as an innovative technology to provide spatio-temporal information about weed species in crop fields. Such information is a critical input for any site-specific weed management program. A multi-rotor UAS (Phantom 4) equipped with an RGB sensor was used to collect imagery in three bands (Red, Green, and Blue; 0.8 cm/pixel resolution) with the objectives of (a) mapping weeds in cotton and (b) determining the relationship between image-based weed coverage and ground-based weed densities. For weed mapping, three different weed density levels (high, medium, and low) were established for a mix of different weed species, with three replications. To determine weed densities through ground truthing, five quadrats (1 m × 1 m) were laid out in each plot. The aerial imageries were preprocessed and subjected to Hough transformation to delineate cotton rows. Following the separation of inter-row vegetation from crop rows, a multi-level classification coupled with machine learning algorithms were used to distinguish intra-row weeds from cotton. Overall, accuracy levels of 89.16%, 85.83%, and 83.33% and kappa values of 0.84, 0.79, and 0.75 were achieved for detecting weed occurrence in high, medium, and low density plots, respectively. Further, ground-truthing based overall weed density values were fairly correlated (r^2 = 0.80) with image-based weed coverage assessments. Among the specific weed species evaluated, Palmer amaranth (*Amaranthus palmeri* S. Watson) showed the highest correlation (r^2 = 0.91) followed by red sprangletop (*Leptochloa mucronata* Michx) (r^2 = 0.88). The results highlight the utility of UAS-borne RGB imagery for weed mapping and density estimation in cotton for precision weed management.

*Sapkota B, Singh V, Cope D, Valasek J, Bagavathiannan M. Mapping and Estimating Weeds in Cotton Using Unmanned Aerial Systems-Borne Imagery. *AgriEngineering*. 2020; 2(2):350-366. https://doi.org/10.3390/agriengineering2020024

Keywords: digital agronomy; Hough transformation; machine learning; object-based image analysis; precision agriculture

2.2. Introduction

Weeds are the major pests of agricultural crops and a serious challenge to sustainable crop production (Hall et al., 1992; Oerke et al., 2005). A site-specific approach, which takes into account the spatio-temporal variabilities in weed species establishment and growth, can facilitate effective and economical weed management (Aracena et al., 2013; Van Evert et al., 2017). However, such an approach requires precise determination of different weed species infesting crop fields and their densities. Currently, weed infestation assessments are carried out by managers typically through manual weed scouting, which is often inefficient and inaccurate particularly in large production fields. Remote sensing has long been investigated as an alternative approach for weed infestation assessments across large areas (Everitt et al., 2006; Lamb et al., 2005; Lopez-Granados et al., 2015). Images acquired with remote sensing platforms can be analyzed to produce pixel-level or individual-plant-level information regarding the location and distribution of weeds throughout the field (Lopez-Granados et al., 2015). Such information can guide farmers in assessing weed infested areas and developing management grids for site-specific treatment. For example, Castaldi et al. (2016) analyzed digital imageries to produce coverage maps for weeds in maize (*Zea mays* L.), which were further transformed into 2 m × 2 m grids. These grids were classified into weed-free and weed-infested zones based on weed threshold and subsequently utilized for site-specific weed management. Moreover, knowledge of weed distributions and densities across the field is beneficial for tailoring herbicide applications to weed spatial dynamics in the field (Goudy et al., 2001).

Mapping weeds at early phenological growth stages requires higher spatial resolution imagery (Borra-Serrano et al., 2015; Lopez-Granados et al., 2015), although Borra-Serrano et al. (2015) found that as coarse as 5 cm of spatial resolution may provide satisfactory results. Traditional remote sensing platforms such as satellite imageries generally do not meet the spatial resolution standards required for weed detection, and also have limited capability to provide real-time data. Nonetheless, they have been used to map patches of weed species at field scale (Castro et al, 2013; De Castillejo-González et al., 2014). Recent advancements in Unmanned Aerial Systems (UAS) technologies have opened up new opportunities for acquiring high spatial resolution imagery at desired temporal resolutions (Shi et al., 2016; Singh et al., 2020) and have been successfully used in various agricultural research areas, including soil and land mapping (Akar, 2017), drought stress monitoring (Hoffman et al., 2016; Ludovisi et al., 2017) crop disease detection (Mirik et al., 2011; Suguira et al., 2016) and in-season yield estimation (Swain et al., 2010). The opportunities have expanded with the ability to extract 3D point-clouds from the UAS-based high resolution imagery, which have been extensively used in various agricultural and forestry studies (Comba et al., 2019; Mesas-carrascosa et al., 2020; Torres-Sanchez et al., 2018; Zermas et al., 2020). 3D point clouds can be analyzed to generate canopy height models and other 3D canopy metrics, which can be used as a supplement to spectral information. However, extraction of 3D information and processing of these metrics may be computationally complex and expensive. Over the years, with the increased ability to acquire imageries at sub-cm resolutions using UAS, several studies have experimented on the use of high-resolution imageries for weed mapping and classification (Castillejo-González et al., 2014; De Castro et al., 2018; Lopez-Granados et al., 2015; Louargant et al., 2018; Mink et al., 2018; Peña-Barragan et al., 2013; Rasmussen et al., 2013; Shi et al., 2016;). However, there is still a

lack of classification models to serve the unique needs of the farmer; thus, there is a strong need for developing case-specific classification models by further experimenting on different image analysis approaches.

With the rapid improvement in sensors, it has become possible to generate multi-band information, including thermal signatures, using UAS technology. These improvements have been adapted successfully in various agricultural applications, including weed detection and mapping. Due to the high ability of non-visible bands in discriminating plant species, several studies have used multispectral imagery (Lopez-Granados et al., 2015; Sa et al., 2018) and hyperspectral imagery (Atkinson et al., 2013; Gao et al., 2018; Mirik et al., 2013) for identifying and classifying weeds in crop fields and forest areas. The utility of thermal bands in plant stress detection (Calderon et al., 2015; Sankaran et al., 2013) has paved the way for using thermal imagery in weed detection and mapping. However, these improved sensors are costly, and computation and processing of the data acquired from such sensors can be resource intensive. In many circumstances, these sensors may not prove to be a better option than the relatively cheap and computationally simple visible bands such as red, green, and blue bands (i.e., RGB bands) (Lopez-Granados et al., 2015). Visible bands have long been utilized for various agricultural applications and have a great potential for use in weed species detection and differentiation (Borra-Serrano et al., 2015; Gao et al., 2018; Huang et al., 2018). For example, more recently, Lottes et al. (2017) classified weed species and sugarbeet using UAS-based RBG imagery, with an accuracy of 85% and 90%, respectively. Gao et al. (2018) detected weed species in maize using UAS-derived RGB imagery and developed highly accurate predictive models for weed density estimation. The accuracy of the weed detection process largely depends upon the model and training features used for the user-defined classes, in addition to spectral and spatial

resolution of the imageries. One of the most popular approaches utilized for image analysis is pixel-based approach. The traditional pixel-based approach involves the computational analysis at a pixel level and relies heavily upon spectral features, disregarding the potential for textural and spatial features to improve model accuracies (Blaschke et al., 2010). However, the recent evolution of convolutional neural networks (CNNs), that take into account the spectral, textural and spatial features of images, allow for improved classification accuracies.

CNN-based studies for distinguishing between weeds and crops have been increasing in recent times. Bah et al. (2018) used CNNs for detecting both intra- and inter-row weeds in spinach (*Spinacia oleracea* L.), beans (*Phaseolus vulgaris* L.), and beet (*Beta vulgaris* L.) in UAS-derived RGB images and achieved overall accuracies of 81%, 69%, and 93%, respectively. Using multispectral images, Sa et al. (2018) developed a CNN-based model to segment crops and weeds from the soil background and achieved an overall accuracy of 82%. Several other studies have validated the effectiveness of CNN-based models; however, these models are data intensive and highly suffer from data inadequacy. For some cases, especially when dealing with binary problems such as the presence or absence of a weed, CNNs may not be necessary. Instead, adequate image analysis can be carried out using much simpler methods such as the object-based image analysis (OBIA) (Blaschke et al., 2010).

The OBIA allows for the generation of large number of image objects, which can be further classified into user-defined classes (Sapkota and Liang, 2017; Sapkota & Liang, 2020). This approach was shown to be effective in mapping weeds in maize (Pena-Barragan et al., 2013) and sunflower (*Helianthus annuus* L.) (De Castro et al., 2018) when information such as crop row boundaries were fused with other set of features generated using OBIA. Such combined information would help segment inter-row weeds easily and minimize the misclassification

instances during the classification process. However, the effectiveness of the fusion approach could differ with variable weed densities, which may lead to fuzzy boundaries between crop rows and proximal weeds. Furthermore, the false crop boundary delineation could result in classification errors as any vegetation pixels outside of the crop row is considered a weed, which may not be the case when crop leaves extend outside of the row.

It is important to investigate the effectiveness of the above-mentioned approach by testing it on areas with varying weed densities. Moreover, it is equally important to develop a post-classification model to refine the classification and minimize errors due to false crop row detection. In this study, an improved methodology that addresses these issues has been tested and demonstrated in cotton (*Gossypium hirsutum* L.), which is an important crop in Texas and parts of the Southern United States (US). The specific objectives of this study are to (1) test the effectiveness of the improved fusion method (OBIA and crop row detection) to map various densities of weed infestation in a cotton field using high resolution UAS-based RGB imagery, and (2) determine the relationship between weed pixel coverage and ground-based weed densities.

2.3. Materials and Methods

2.3.1. Study Site and Establishment

The study was conducted at the Texas A&M AgriLife Research farm near College Station, TX, US (30°32′15.75″ N, 96°25′19.50″ W; elevation: 68 m) (Figure 2.1). The cotton crop was drill seeded in 1-m wide rows on 1 June 2017. Palmer amaranth (*Amaranthus palmeri* S. Watson) and red sprangletop (*Leptochloa mucronata* Michx) seed were broadcast planted with three different densities (low, medium, and high) (see Table 2.1) in 10 × 10 m plots within a 0.6

ha of field. Palmer amaranth is an annual plant native to the arid southwestern U.S. and northwestern Mexico and is one of the most problematic weeds in row crop production in the U.S. due to evolution of multiple herbicide resistance in this species [43]. Red sprangletop is an annual grass weed, widespread in the southern U.S. cultivated lands. Other weed species present in the experimental area, though in low frequencies, include morningglories (*Ipomoea* spp.), Texas millet (*Urochloa texana* Buckl.), and devil's claw (*Proboscidea louisianica* (Mill.) Thell.). Morningglory is a broadleaved, annual plant species with fast growth rates. Texas millet is an annual grass weed native to the southern U.S. and is a troublesome weed in row crops. Devil's claw is an annual broadleaved weed that is commonly found across the sandy, arid areas of west and south Texas. The study had three replications and were arranged in a randomized complete block design. The steps followed in image acquisition and weed mapping are summarized in the flowchart (Figure 2.2).

2.3.2. Data Collection

Multiple flights were conducted over the experimental area from May to July 2017; however, only the image acquired on 28 June 2017 was used for analysis in the current study due to high image quality in an early to mid-crop growth stage. The multi-rotor UAS Phantom 4 (DJI, China) equipped with a 12 MP on-board camera was used for capturing images in three bands (Red, Green, and Blue). Six ground control points (GCPs) were laid out throughout the study area for georeferencing the imagery, and global positioning system (GPS) coordinates were recorded for the GCPs using EMLID-GNSS receiver (EMLID Inc., Hong Kong, China). Three different radiometric calibration panels (white, gray, and black) were placed on the ground to enable radiometric calibration of the imagery during ortho-mosaicking process. Image data were collected at 15 m above ground level (AGL), with the auto-exposure mode, 70% side and

front overlapping rates, and forward UAV speed of 3 m/s. The flight was performed in a sunny day with wind speed of approximately 11 km h^{-1}. A total of 464 images (.JPG format) were captured during the flight mission. The .JPG format was chosen over raw image format during image acquisition as the flight planner used in this study only supported the earlier format. Moreover, Pix4D Mapper, the software used for stitching the images, could not support the raw image format.

Ground truthing data on weed species density were documented at the time of flight operations. For each plot, five quadrats (1 m × 1 m) were laid out throughout the experimental area. For each quadrat, the number of individual plants per each species were counted and density m^{-2} were determined for comparing with image-based coverage area. Reflectance values for cotton and the weed species were recorded from the imagery to observe the spectral overlap (Figure 2.3) and choose the appropriate techniques for further image processing.

2.3.3. Image Mosaicking and Radiometric Calibration

The images were mosaicked using the Pix4D Mapper software (Pix4D Inc., Lausanne, Switzerland) (Figure 2.4a). The GPS coordinates for the GCPs were post corrected and used in the mosaicking process. Among the several templates available in Pix4D, the 'Ag RGB' template was chosen to process the imagery since this template is recommended for mosaicking RGB imagery (Pix4D manual). The key point image scale was set to 'Full' mode and minimum number of key point matching was set to '3' for the point cloud densification in the template. The resulting ortho-mosaic imagery (Figure 2.4b) had a spatial and radiometric resolutions of 8 mm/pixel and 8 bits per pixel, respectively.

The digital number (DN) values were calibrated to reflectance values using the reflectance values of the spectral panel and their corresponding DN values in the imagery. Three

different datasets, each with 300 DN values of a band as the *X*-variable and the reflectance values as the *Y*-variable belonging to the pixels in the spectral panel were prepared. Further, simple linear regression analyses were conducted to derive three separate regression models (Equations (1)–(3)) for predicting reflectance values using prepared datasets. The model was then applied to predict the values for all the pixels in red, blue, and green bands.

$$(\sigma_j)_r = \mu 1 * (\lambda_j)_{r+c1} \quad (1)$$

$$(\sigma_j)_g = \mu 2 * (\lambda_j)_{g+c2} \quad (2)$$

$$(\sigma_j)_b = \mu 3 * (\lambda_j)b_{+c3} \quad (3)$$

where

$(\sigma_j)_r$ = predicted reflectance value of a *j*th pixel for the red band

$(\sigma_j)_g$ = predicted reflectance value of a *j*th pixel for the green band

$(\sigma_j)_b$ = predicted reflectance value of a *j*th pixel for the blue band

$(\lambda_j)_r$ = DN value of a *j*th pixel for the red band

$(\lambda_j)_g$ = DN value of a *j*th pixel for the green band

$(\lambda_j)_b$ = DN value of a *j*th pixel for the blue band

$\mu 1$, $\mu 2$ and $\mu 3$ are slope values for red, green, and blue band, respectively, whereas c1, c2, and c3 are constants for models for red, green, and blue band, respectively.

2.3.4. Image Preprocessing

Image preprocessing is an important step in image analysis and is required to prepare the image for further analysis. The experimental plots in the imagery were clipped into individual subsets and were subjected to further image processing. This process was completed in the following four steps:

2.3.4.1. Masking Non-Vegetative Area

In order to avoid potential misclassification of target objects with unnecessary objects, it is a good approach to mask the non-vegetative area upfront. For this purpose, excess green vegetation index (ExG) (Woebbecke et al., 1995) was calculated using Equation (4).

$$ExG=2G-R-BG+R+B \quad (4)$$

where G, R, and B indicate green, red, and blue channel pixel values, respectively.

The Otsu thresholding method (Otsu, 1979) was applied to identify an optimal threshold for developing a binary classification: vegetation vs. non-vegetation (Figure 2.4c).

2.3.4.2. Canny Edge Filtering

The canny edge algorithm (Canny, 1986) was applied over the Otsu's binary imagery to obtain the edges of the crop rows. The algorithm requires the user to input values for two different hyper parameters called "minVal" and "maxVal". MinVal and maxVal represent the lower and upper limits of the intensity gradient range such that for any potential edge candidates to be regarded as true edge, the curve to which it belongs should lie either completely or partially above the upper limit within the user-defined range. Several sets of lower and upper values were tested in a trial and error mode until the best visual results were obtained. A median filter was applied over the edge imagery to remove edge noises and highlight crop rows (Figure 2.4d).

2.3.4.3. Hough Line Transformation

To minimize potential misclassification, the classification algorithm was applied only after separating inter-row weeds from cotton by detecting crop rows using one of the popular crop row detection method called Hough transformation (Slaughter et al., 2008). This method determines positions of crop rows based on the parameters ρ and θ, where ρ is the perpendicular distance from the origin to the line and θ is the angle of perpendicular projection from the origin

to the line, clockwise from the positive *X*-axis of the image space (Slaughter et al., 2008). This method was implemented over the de-noised imagery using the "houghlineL" function in "OpenCV" package built in Python programming language to generate crop row lines (Figure 2.4e). The two hyper parameters for the function, ρ and θ, were chosen as 1000 and 0° to 180° respectively.

2.3.4.4. Generation of Crop-Row Strips

The row strip width (α) around each Hough line in each plot was determined using Equation (5), based on the width of cotton measured for 20 random plants within a plot.

$$\alpha = i = 120 wi20 \quad (5)$$

where α denotes mean width, *w* represents the width of the cotton plant measured from a tip of a leaf on one side to a tip of a leaf on another side in the direction perpendicular to row axis for the *i*th plant (1 to 20).

A particular width value was then used to generate crop-row strips for each of the rows in a plot.

2.3.5. Weed Detection and Regression

Following the establishment of row strips, the OBIA framework was implemented for both intra- and inter-row weed detection using eCognition Developer software (Trimble Inc., Munich, Germany). The chessboard segmentation analysis was then carried out over each plot imagery to produce grids of 5 × 5 pixels, which represented 4 cm × 4 cm area on the ground. Any grids pertaining to vegetation outside of the Hough transformation-derived strips (Figure 2.4f) were classified as inter-row weeds. After assigning the inter-row weeds, the next step was to classify the grids within a strip into cotton and intra-row weeds, as grids pertaining to soil/shadows had already been masked during image preprocessing steps. For this purpose, the

Random Forest (RF) method (Breiman, 1996), a non-parametric ensemble learning method, was used. This classifier creates a set of decision trees from a randomly selected subset of training dataset, which then aggregates the votes from different decision trees to decide the final class of the test object. The outcome in each decision tree is determined based on information gain, gain ratio, and Gini index (Breiman, 1996) for each attribute or feature. This classifier requires two hyper parameters 'ntree' (the number of decision trees to be formed during the decision process) and 'mtry' (the number of features to be used in the node for a decision tree) to be set by the user; in this study, 'ntree' and 'mtry' were set to '500' and 'the square root of total number of image features used in the classification', respectively.

A total of 18 grey level co-occurrence matrix (GLCM)-based textural features (Haralick et al., 1973) and five spectral features were constructed for clipped imageries (Table 2.2). A balanced sample size of 600 for each class (cotton and weed species) were selected randomly from the grid objects resulting from the chessboard segmentation to train the RF classifier. In addition, 200 samples for each class (cotton, weeds, and soil/shadows) were used for validation of mapping in each density treatments. Prior to the training process, it was necessary to discard the non-important features to optimize the computation cost and time. The "varImp.randomForest" function in "Caret" package in R programming language (R Foundation for Statistical Computing, Vienna, Austria) was used to compute the importance index for the features constructed in the study. The function uses the RF classifier-based wrapper selection method to calculate accuracy of each decision tree using out-of-bag samples for a given feature. The decrease in accuracy of decision tree when a feature is substituted with another feature is averaged across all the decision trees to calculate mean decrease in accuracy, which is further rescaled to 1–100 and termed as important index. In general, higher the mean decrease in

accuracy for a feature, higher the important index and better the feature. In this study, the features with index value greater than 50 in the scale of 1–100 were chosen, which includes two spectral features (red band and ExG) and four textural features (GLCM_Homogeneity for green band, GLCM_Contrast for green and red band, and GLCM_Entropy for red band).

In certain cases, leaves of inter-row weeds overlapped with that of cotton within the strip and could not be classified using the standard approach. In such cases, an iterative feature ratio rule was used to re-label the mis-labeled vegetation as weeds using Equation (6).

$$x=1, \quad 0.9<ExGij<1.1\ 0, \qquad \text{Otherwise} \quad (6)$$

where x is the rule to assign the specific grid *(j)* as weed (1) or non-weed (0), ExGij represents the ratio of ExG value of the grid for weeds immediately outside the row strip *(i)* to that of the grid immediately inside the row strip *(j)*.

Two model accuracy measures, namely overall accuracy (OA) and kappa values (K), were calculated. The OA is calculated using Equation (7) as the number of correctly classified grid objects over the total number of validation samples.

$$OA\ \%=A+E+IA+B+C+D+E+F+G+H+I \times 100 \quad (7)$$

where *A*, *E*, and *I* are the number of validation samples accurately classified as crop, weed, and soil/shadows, respectively; *D* and *G* are the number of crop samples that were inaccurately classified as weed and soil/shadow, respectively; *B* and *H* are the number of weed samples that were inaccurately classified as crop and soil/shadow; *C* and *E* are the number of soil/shadow samples that were inaccurately classified as crop and weed, respectively.

The Kappa value is a measure of deviation from the outcome by chance. The value ranges from 0 to 1, with 0 indicating no agreement and 1 indicating full agreement between the

observed and predicted values. The mathematical formula for computing kappa values was derived from Cohen (1960).

Following the generation of classification maps, the shapefiles for weed classes were extracted from the maps and loaded to the ArcMap software (ESRI Inc., Redlands, CA, USA). The area of all the shapefiles belonging to a particular quadrat (1 m × 1 m) was calculated, divided by the area of the quadrat, and recorded as image-derived weed coverage (%). A simple linear regression analysis was subsequently conducted in the R statistical software (R core team 2013) using the ground-based weed density (m^{-2}) dataset as the *Y*-variable and the image-derived weed coverage (%) dataset as the *X*-variable. In addition to the model for combined weed species in the quadrats, two separate individual models for two most dominant species in the experimental area, Palmer amaranth and red sprangletop were developed. For this purpose, quadrats (9 for Palmer amaranth and 11 for red sprangletop) that had >80% infestation of either species in the field were selected across the experimental area.

The whole data processing tasks were performed using a computer with a relatively high processing power comprising of Intel® core™ i7-5960X 3.00 gigahertz (GHz) central processing unit, 64 gigabytes of random-access memory (RAM), and 64-bit operating system. The data processing tasks, including image mosaicking, calibration, preprocessing, and weed detection and regression for all the density treatment plots takes approximately 2 h and 30 min. This includes only the time required for running the python scripts/software for corresponding data processing tasks and does not include the time associated with the preparation of necessary data for tasks such as image calibration, and training and validation of the classifier. The image mosaicking process consumed the majority of the time (approx. 70%), whereas the image

preprocessing step required the least time (5%).

2.4. Results and Discussion

2.4.1. Weed Mapping

The classification techniques used in the current study was effective in mapping the distribution of weeds in cotton with reasonably high accuracy levels. An overall accuracy (OA) of 89.16%, 85.83%, and 83.33% and kappa (K) value of 0.84, 0.79, or 0.75 were observed for low, medium, or high-density plots, respectively (Figure 2.5). The generally high accuracy levels obtained in the current study could be attributed to the implementation of the multi-step classification model wherein potential misclassification was minimized by first detecting and separating inter-row weeds, thereby subjecting only the intra-row weeds for machine learning-based classification. The classified maps and pixel density heat maps are shown in Figure 2.6.

Several studies have undertaken a similar multi-step classification approach and achieved high classification accuracies. For example, De Castro et al. (2018) mapped both broadleaved and grass weed species in sunflower and cotton fields and achieved an average weed detection accuracy index of 73% and 75% for cotton and sunflower field, respectively. López-Granados et al. (2015) mapped johnsongrass (*Sorghum halepense* (L.) Pers.) in maize (*Zea mays* L.) using a multistep approach, wherein the maize rows were first delineated using an iterative strip formation process, the inter-row johnsongrass was detected, and then normalized difference vegetation index (NDVI) and Excess Greenness Index (ExG) were used to classify intra-row johnsongrass from maize with an accuracy of 89% and 82% for multispectral and visual imagery, respectively. In another study, Gao et al. (2018) combined the pixel-based method with OBIA to map weeds in a maize crop; Hough transformation was followed by Random Forest

(RF) classifier using spectral, GLCM-based textural, and geometrical features to classify intra-row weeds with OA and K values of 94.5% and 0.91, respectively.

A unique aspect of the current study is that it implemented the multi-step approach under three different weed density levels and provided an outlook on how the accuracies are affected. Moreover, the majority of existing studies have focused on classifying weeds at an early crop stage when the weeds are sparsely distributed or there is a clear delineation of crop rows due to an absence of overlapping intra-row weeds. Such scenarios would minimize the complexity of generating crop row lines and further image processing tasks, leading to high classification accuracies. However, the current study successfully classified intra- and inter-row weeds even under high density levels.

The robustness of classification of inter-row weeds was dependent on how accurately the crop rows were delineated (Lopez-Granados et al., 2015; Gao et al., 2018) using the crop row detection method. In the current study, this method was very effective, given the straight cotton rows in the field. However, additional processing may be required to remove redundant crop row lines in cases of non-linearity or under very high weed density levels wherein the green pixels of inter-row weeds may overlap with crop pixels, making it difficult for the algorithm to identify edges of rows. Apart from the field structure, crop row detection can also be influenced by the noises during binarization, edge detection, and other related preprocessing steps (Gee et al., 2008). One of the several reasons for the inaccurate binarization could be the higher spectral similarity between shadow and underexposed vegetation pixels. The lower leaves are affected by shadow from upper leaves, which could lead to spectral confusion between underexposed leaves and gaps in crop canopy. The inaccurate masking of crop pixels, especially at the edge of the

crop rows, might significantly affect crop row detection results and thus may lead to inaccurate crop row lines.

Low weed density plots had low instances of inter-row weeds and extremely low intra-row weeds. However, intra-row weeds were relatively frequent in the medium and high-density plots. Lower OA in high-density plots, as compared to low-density plots, could be attributed to frequent occurrence of intra-row weeds in high density plots and difficulty associated with classifying intra-row weeds from cotton using the OBIA method. High instances of intra-row weeds increased the risk of spectral similarity and obscure the textural uniqueness of plants due to canopy interlockings. This situation was found in every replication of the high-density plots. The standard deviations of OA and kappa for different density plots were low and quite similar, probably due to high similarity in spatial configuration and amount of inter-row and intra-row weeds in cotton. In addition, segmented objects (group of pixels) were used as the validation samples, in contrast to pixels, which may have lowered the chances of variability in accuracy measures.

Morningglories showed high spectral (all three bands) and textural confusion with cotton, compared to Palmer amaranth and red sprangletop. The morningglories were often seen creeping into the cotton rows in the ground, adding more complexity in spectral distinction. Red sprangletop in particular had very low spectral overlap with cotton, compared to other weed species. These weeds were only the major grass species found in the area and were visually distinct in the ground. Though Palmer amaranth had high spectral similarity with cotton, the GLCM-based textural attributes based on 5 × 5 pixel kernels were different for these species, as implied by differences in leaf sizes and canopy structure. Thus, a combination of spectral and textural features yields high classification accuracies (Lin et al., 2017; Wu et al., 2009).

However, it should also be noted that spectral similarity observed here between cotton and weeds may not be the case in other situations. The spectral confusion is primarily dependent on the spectral, spatial, and radiometric resolution of the imagery; growth stage of the crop and weed; and the crop production system. For example, inclusion of non-visible bands in the analysis may help increase the spectral separability between crops and weeds. Further, increase in radiometric resolution adds more gradients of pixel values and thus provides more details/information at the pixel level.

2.4.2. Relationship between Weed Density and Pixel Coverage

The relationship between the image-based weed coverage data (i.e., area covered by weed pixels) and ground-based weed density assessments (plants m^{-2}) for total weed species, and individually for Palmer amaranth and red sprangletop was determined using a simple linear regression analysis. A fairly high coefficient of determination ($r^2 = 0.80$) was achieved for total weed species present in a quadrat, indicating that the density of weeds in the crop field could be estimated based on weed pixel coverage (Figure 2.7). The ability for assessing weed densities using aerial images has been demonstrated previously. For example, Gao et al. [36] obtained, using a very high-resolution imagery (1.78 mm/pixel), high coefficient of determination ($r^2 = 0.89$) between image-based weed density and manually assessed weed density in a maize field. Although the coefficient of determination in the current study ($r^2 = 0.80$) was slightly lower compared to that of Gao et al. [36], current study provided considerably high accuracy even with a coarser spatial resolution (8 mm/pixel).

The degree of relationship between ground-based manual assessments and aerial image-based assessments can be affected by several factors including weed and crop species being studied, growth stages of weeds, and environmental factors. First, the accuracy of weed pixel

coverage determination in aerial imagery depends on how well the weeds are classified and distinguished from the crop. Second, inter-locked growth of weed species can lead to inaccurate estimation of pixel coverage since the coverage area of two interlocking weed plants may be lesser than the actual value. It is also possible that the dominant weeds can partially or completely mask other species growing underneath them, affecting the total pixel values (Lin et al., 2017; Connolly et al., 2017). Among the individual weed species assessed in the present study, high coefficient of determination was achieved for red sprangletop ($r^2 = 0.88$) (Figure 2.8a) and Palmer amaranth ($r^2 = 0.91$) (Figure 2.8b). Higher accuracies with Palmer amaranth compared to that of red sprangletop could be largely attributed to the differences in growth pattern between the two species; red sprangletop plants had higher overlapping with each other, with more variable growth sizes compared to Palmer amaranth.

In this study, we aimed at demonstrating if and how UAS can be used to map different densities of early- to mid-season weeds in cotton and estimate their densities. We do not anticipate our regression models to be as accurate under alternative experimental settings (e.g., different flight heights, growth stage of weeds, forward speed, lighting conditions, etc.). Rather, we anticipate that the study informs that true color UAV images can indeed be used to map early- to mid-season weeds. Nonetheless, we are confident that our methodology can be adopted and expanded by other studies with a similar focus. The prime reason for this adaptability is that the supervised classification method implemented in this study is based on the local training data. The regression model for weed estimation depends upon the classification-based weed canopy coverage area, which in turn depends upon the training samples collected by the researcher. This whole process is similar for any weed size in cotton. Following points highlight the significance of the experimental plan and the outputs of this study:

a. The study has demonstrated if and how early- to mid-season weeds can be mapped in cotton using true color UAS-borne imagery.

b. The study has shown that vegetation indices such as excess greenness index and textural features can be used in mapping early- to mid-season weeds, at least for high spatial resolution true color imagery. This information can guide future researchers with shared ideas.

c. The study has illustrated that high spatial resolution true color imagery-based weed coverage area could be an effective determinant of weed density in cotton at early- to mid-growth stage of weeds.

d. The study has also demonstrated how high spatial resolution imagery can be utilized to detect early- to mid-season cotton rows and use the information to easily segment out inter-row weeds.

2.5. Conclusions

This study demonstrated a methodology for mapping weed infestations in cotton utilizing RGB imagery and non-conventional image analysis techniques. Advanced computer vision techniques were tested to map weeds under different density levels and determine the relationship between image-based weed coverage estimates and ground-based weed density assessments. The current study has successfully demonstrated that they can be applied across different levels of weed densities. The spatial maps and density prediction models can be great resources for farmers/consultants for robust assessment of weed infestations and making informed management decisions. Furthermore, with a successful application of RGB imagery for this purpose, the study also emphasizes the usefulness of RGB imagery for weed assessment.

This study, however, has few limitations: (a) the results presented here were based on the experiment carried out on a specific weed growth stage (Table 2.1) and thus the predictive model for weed densities may not be applicable to other weed growth stages. However, our study proved the effectiveness of the computer vision techniques in weed density assessments, and this approach can be expanded to other scenarios as well. (b) the quadrats used for regression analysis for individual weed species were selected such that the specific weed densities were >80% within each quadrat. This was necessary due to difficulties with distinguishing different weed species using RGB imagery at this level of image resolution (8 mm/pixel). Such high densities of a single weed species may not be typical in all field scenarios and occurrence of a mix of multiple weed species can complicate prediction accuracies. However, ongoing technological improvements may improve weed classification and provide a solution to this challenge. Future research should focus on utilizing multispectral and hyperspectral imageries and develop improved classification algorithms for weed infestation assessments.

2.6. References

Ali, A., Streibig, J.C., Andreasen, C., 2013. Yield loss prediction models based on early estimation of weed pressure. Crop Protection 53, 125–131. https://doi.org/10.1016/j.cropro.2013.06.010

Aracena, P.A., n.d. A spatially-explicit decision support system for invasive weed species managment (Ph.D.). University of Montana, United States -- Montana.

Atkinson, J.T., Ismail R., Robertson, M., 2014. Mapping bugweed (*Solanum mauritianum*) infestations in *Pinus patula* plantations using hyperspectral imagery and support vector

machines. IEEE Journal of Selected Topics in Applied Earth Observations and Remote Sensing 7, 17–28. https://doi.org/10.1109/JSTARS.2013.2257988

Bah, M.D., Dericquebourg, E., Hafiane, A., Canals, R., 2019. Deep Learning Based Classification System for Identifying Weeds Using High-Resolution UAV Imagery, in: Arai, K., Kapoor, S., Bhatia, R. (Eds.), Intelligent Computing, Advances in Intelligent Systems and Computing. Springer International Publishing, Cham, pp. 176–187. https://doi.org/10.1007/978-3-030-01177-2_13

Blaschke, T., 2010. Object based image analysis for remote sensing. ISPRS Journal of Photogrammetry and Remote Sensing 65, 2–16. https://doi.org/10.1016/j.isprsjprs.2009.06.004

Borra-Serrano, I., Peña, J.M., Torres-Sánchez, J., Mesas-Carrascosa, F.J., López-Granados, F., 2015. Spatial quality evaluation of resampled unmanned aerial vehicle-imagery for weed mapping. Sensors 15, 19688–19708. https://doi.org/10.3390/s150819688

Breiman, L., 1996. Bagging predictors. Machane Learning 24, 123–140. https://doi.org/10.1007/BF00058655

Calderón, R., Navas-Cortés, J., Zarco-Tejada, P., 2015. Early detection and quantification of verticillium wilt in olive using hyperspectral and thermal imagery over large areas. Remote Sensing 7, 5584–5610. https://doi.org/10.3390/rs70505584

Canny, J., 1986. A computational approach to edge detection. IEEE Transactions on Pattern Analysis and Machine Intelligence PAMI-8, 679–698. https://doi.org/10.1109/TPAMI.1986.4767851

Castaldi, F., Pelosi, F., Pascucci, S., Casa, R., 2017. Assessing the potential of images from unmanned aerial vehicles (UAV) to support herbicide patch spraying in maize. Precision Agriculture 18, 76–94. https://doi.org/10.1007/s11119-016-9468-3

Castillejo-González, I.L., Peña-Barragán, J.M., Jurado-Expósito, M., Mesas-Carrascosa, F.J., López-Granados, F., 2014. Evaluation of pixel- and object-based approaches for mapping wild oat (Avena sterilis) weed patches in wheat fields using QuickBird imagery for site-specific management. European Journal of Agronomy 59, 57–66. https://doi.org/10.1016/j.eja.2014.05.009

Cohen, J., 1960. A coefficient of agreement for nominal scales. Educ. Psychol. Meas. 20, 37–46.

Comba, L., Biglia, A., Ricauda Aimonino, D., Tortia, C., Mania, E., Guidoni, S., Gay, P., 2019. Leaf Area Index evaluation in vineyards using 3D point clouds from UAV imagery. Precision Agriculture. https://doi.org/10.1007/s11119-019-09699-x

Connolly, J., Sebastià, M.-T., Kirwan, L., Finn, J.A., Llurba, R., Suter, M., Collins, R.P., Porqueddu, C., Helgadóttir, Á., Baadshaug, O.H., Bélanger, G., Black, A., Brophy, C., Čop, J., Dalmannsdóttir, S., Delgado, I., Elgersma, A., Fothergill, M., Frankow-Lindberg, B.E., Ghesquiere, A., Golinski, P., Grieu, P., Gustavsson, A.-M., Höglind, M., Huguenin-Elie, O., Jørgensen, M., Kadziuliene, Z., Lunnan, T., Nykanen-Kurki, P., Ribas, A., Taube, F., Thumm, U., De Vliegher, A., Lüscher, A., 2018. Weed suppression greatly increased by plant diversity in intensively managed grasslands: A continental-scale experiment. Journal of Applied Ecology 55, 852–862. https://doi.org/10.1111/1365-2664.12991

De Castro, A.I., López-Granados, F., Jurado-Expósito, M., 2013. Broad-scale cruciferous weed patch classification in winter wheat using QuickBird imagery for in-season site-specific control. Precision Agriculture 14, 392–413. https://doi.org/10.1007/s11119-013-9304-y

De Castro, A.I., Torres-Sánchez, J., Peña, J.M., Jiménez-Brenes, F.M., Csillik, O., López-Granados, F., 2018. An automatic random forest-OBIA algorithm for early weed mapping between and within crop rows using UAV imagery. Remote Sensing 10, 285.

Everitt, J.H., Fletcher, R.S., Elder, H.S., Yang, C., 2008. Mapping giant salvinia with satellite imagery and image analysis. Environmnetal Monitoring Assessment 139, 35–40. https://doi.org/10.1007/s10661-007-9807-y

Gao, J., Liao, W., Nuyttens, D., Lootens, P., Vangeyte, J., Pižurica, A., He, Y., Pieters, J.G., 2018a. Fusion of pixel and object-based features for weed mapping using unmanned aerial vehicle imagery. IJAEO 67, 43–53. https://doi.org/10.1016/j.jag.2017.12.012

Gao, J., Nuyttens, D., Lootens, P., He, Y., Pieters, J.G., 2018b. Recognising weeds in a maize crop using a random forest machine-learning algorithm and near-infrared snapshot mosaic hyperspectral imagery. Biosystems Engineering 170, 39–50. https://doi.org/10.1016/j.biosystemseng.2018.03.006

Gée, C., Bossu, J., Jones, G., Truchetet, F., 2008. Crop/weed discrimination in perspective agronomic images. Computer and Electronics in Agriculture 60, 49–59. https://doi.org/10.1016/j.compag.2007.06.003

Gée, Ch., Bossu, J., Jones, G., Truchetet, F., 2008. Crop/weed discrimination in perspective agronomic images. Computers and Electronics in Agriculture 60, 49–59. https://doi.org/10.1016/j.compag.2007.06.003

Goudy, H.J., Bennett, K.A., Brown, R.B., Tardif, F.J., 2001. Evaluation of site-specific weed management using a direct-injection sprayer. wees 49, 359–366. https://doi.org/10.1614/0043-1745(2001)049[0359:EOSSWM]2.0.CO;2

Hall, M.R., Swanton, C.J., Anderson, G.W., 1992. The critical period of weed control in grain corn (Zea mays). Weed Sci. 40, 441–447. https://doi.org/10.1017/S0043174500051882

Haralick, R.M., Shanmugam, K., Dinstein, I., 1973. Textural Features for Image Classification. IEEE Transactions on Systems, Man, and Cybernetics SMC-3, 610–621. https://doi.org/10.1109/TSMC.1973.4309314

Hoffmann, H., Jensen, R., Thomsen, A., Nieto, H., Rasmussen, J., Friborg, T., 2016. Crop water stress maps for an entire growing season from visible and thermal UAV imagery. Biogeosciences 13, 6545–6563. https://doi.org/10.5194/bg-13-6545-2016

Huang, H., Deng, J., Lan, Y., Yang, A., Deng, X., Zhang, L., 2018. A fully convolutional network for weed mapping of unmanned aerial vehicle (UAV) imagery. PloS one 13, e0196302. https://doi.org/10.1371/journal.pone.0196302

Lamb, D.W., Brown, R.B., 2001. PA—Precision Agriculture: Remote-sensing and mapping of weeds in crops. JAER 78, 117–125. https://doi.org/10.1006/jaer.2000.0630

Lin, F., Zhang, D., Huang, Y., Wang, X., Chen, X., 2017. Detection of corn and weed species by the combination of spectral, shape and textural features. Sustainability 9. https://doi.org/10.3390/su9081335

López-Granados, F., Torres-Sánchez, J., Serrano-Pérez, A., de Castro, A.I., Mesas-Carrascosa, F.J., Peña, J.-M., 2016. Early season weed mapping in sunflower using UAV technology: variability of herbicide treatment maps against weed thresholds. Precision Agriculture 17, 183–199. https://doi.org/10.1007/s11119-015-9415-8

Lottes, P., Khanna, R., Pfeifer, J., Siegwart, R., Stachniss, C., 2017. UAV-based crop and weed classification for smart farming. Presented at the 2017 IEEE International Conference on Robotics and Automation (ICRA), pp. 3024–3031. https://doi.org/10.1109/ICRA.2017.7989347

Louargant, M., Jones, G., Faroux, R., Paoli, J.-N., Maillot, T., Gée, C., Villette, S., 2018. Unsupervised classification algorithm for early weed detection in row-crops by combining spatial and spectral information. Remote Sensing 10, 761.

Ludovisi, R., Tauro, F., Salvati, R., Khoury, S., Mugnozza Scarascia, G., Harfouche, A., 2017. UAV-Based thermal imaging for high-throughput field phenotyping of black poplar response to drought. Frontiers in Plant Science 8. https://doi.org/10.3389/fpls.2017.01681

Mesas-Carrascosa, F.-J., de Castro, A.I., Torres-Sánchez, J., Triviño-Tarradas, P., Jiménez-Brenes, F.M., García-Ferrer, A., López-Granados, F., 2020. Classification of 3D point clouds using color vegetation indices for precision viticulture and digitizing Applications. Remote Sensing 12, 317.

Mink, R., Dutta, A., Peteinatos, G.G., Sökefeld, M., Engels, J.J., Hahn, M., Gerhards, R., 2018. Multi-temporal site-specific weed control of cirsium arvense (L.) Scop. and rumex crispus L. in maize and sugar beet using unmanned aerial vehicle based mapping. Agriculture 8, 65.

Mirik, M., Ansley, R.J., Steddom, K., Jones, D.C., Rush, C.M., Michels, G.J., Elliott, N.C., 2013. Remote distinction of a noxious weed (Musk Thistle: CarduusNutans) using airborne hyperspectral imagery and the support vector machine classifier. Remote Sensing 5, 612–630.

Mirik, M., Jones, D.C., Price, J.A., Workneh, F., Ansley, R.J., Rush, C.M., 2011. Satellite remote sensing of wheat infected by wheat streak mosaic virus. Plant Disease. 95, 4–12.

Oerke, E.C., 2006. Crop losses to pests. JAS 144, 31–43. https://doi.org/10.1017/S0021859605005708

Otsu, N., 1979. A threshold selection method from gray-level histograms. IEEE transactions on systems, man, and cybernetics 9, 62–66.

Peña, J.M., Torres-Sánchez, J., de Castro, A.I., Kelly, M., López-Granados, F., 2013. Weed mapping in early-season maize fields using object-based analysis of unmanned aerial vehicle (UAV) images. PloS one 8.

Quiquerez, A., Chevigny, E., Allemand, P., Curmi, P., Petit, C., Grandjean, P., 2014. Assessing the impact of soil surface characteristics on vineyard erosion from very high spatial resolution aerial images (Côte de Beaune, Burgundy, France). CATENA 116, 163–172. https://doi.org/10.1016/j.catena.2013.12.002

Rasmussen, J., Nielsen, J., Garcia-Ruiz, F., Christensen, S., Streibig, J.C., 2013. Potential uses of small unmanned aircraft systems (UAS) in weed research. Weed Research 53, 242–248. https://doi.org/10.1111/wre.12026

Sa, I., Popović, M., Khanna, R., Chen, Z., Lottes, P., Liebisch, F., Nieto, J., Stachniss, C., Walter, A., Siegwart, R., 2018. WeedMap: A large-scale semantic weed mapping framework using aerial multispectral imaging and deep neural network for precision farming. Remote Sensing 10, 1423.

Sankaran, S., Maja, J.M., Buchanon, S., Ehsani, R., 2013. Huanglongbing (citrus greening) detection using visible, near infrared and thermal imaging techniques. Sensors (Basel) 13, 2117–30. https://doi.org/10.3390/s130202117

Sapkota, B.B., Liang, L., 2018. A multistep approach to classify full canopy and leafless trees in bottomland hardwoods using very high-resolution imagery. Journal of Sustainability in Forest 37, 339–356. https://doi.org/10.1080/10549811.2017.1409637

Sapkota, B.B., Liang, L., 2020. High-resolution mapping of ash (Fraxinus spp.) in bottomland hardwoods to slow Emerald Ash Borer infestation. Science of Remote Sensing 1, 100004. https://doi.org/10.1016/j.srs.2020.100004

Shi, Y., Thomasson, J.A., Murray, S.C., Pugh, N.A., Rooney, W.L., Shafian, S., Rajan, N., Rouze, G., Morgan, C.L.S., Neely, H.L., Rana, A., Bagavathiannan, M.V., Henrickson, J., Bowden, E., Valasek, J., Olsenholler, J., Bishop, M.P., Sheridan, R., Putman, E.B., Popescu, S., Burks, T., Cope, D., Ibrahim, A., McCutchen, B.F., Baltensperger, D.D., Avant, R.V., Vidrine, M., Yang, C., 2016. Unmanned Aerial Vehicles for High-Throughput Phenotyping and Agronomic Research. PloS one 11, e0159781–e0159781. https://doi.org/10.1371/journal.pone.0159781

Singh, V., Rana, A., Bishop, M., Filippi, A.M., Cope, D., Rajan, N., Bagavathiannan, M., 2020. Chapter Three - Unmanned aircraft systems for precision weed detection and management: Prospects and challenges, in: Sparks, D.L. (Ed.), Advances in Agronomy. Academic Press, pp. 93–134.

Slaughter, D.C., Giles, D.K., Downey, D., 2008. Autonomous robotic weed control systems: A review. Comput. Electron. Agric. 61, 63–78. https://doi.org/10.1016/j.compag.2007.05.008

Sugiura, R., Tsuda, S., Tamiya, S., Itoh, A., Nishiwaki, K., Murakami, N., Shibuya, Y., Hirafuji, M., Nuske, S., 2016. Field phenotyping system for the assessment of potato late blight

resistance using RGB imagery from an unmanned aerial vehicle. Biosystems Engineering 148, 1–10.

Swain, K.C., Thomson, S.J., Jayasuriya, H.P.W., 2010. Adoption of an unmanned helicopter for low-altitude remote sensing to estimate yield and total biomass of a rice crop. Transactions of the ASABE 53, 21–27. https://doi.org/10.13031/2013.29493

Torres-Sánchez, J., de Castro, A.I., Peña, J.M., Jiménez-Brenes, F.M., Arquero, O., Lovera, M., López-Granados, F., 2018. Mapping the 3D structure of almond trees using UAV acquired photogrammetric point clouds and object-based image analysis. Biosystems Engineering 176, 172–184. https://doi.org/10.1016/j.biosystemseng.2018.10.018

van Evert, F.K., Fountas, S., Jakovetic, D., Crnojevic, V., Travlos, I., Kempenaar, C., 2017. Big Data for weed control and crop protection. Weed Research 57, 218–233. https://doi.org/10.1111/wre.12255

Ward, S.M., Webster, T.M., Steckel, L.E., 2013. Palmer Amaranth (Amaranthus palmeri): A review. Weed Technology. 27, 12–27. https://doi.org/10.1614/WT-D-12-00113.1

Woebbecke, D.M., Meyer, G.E., Von Bargen, K., Mortensen, D.A., 1995. Color indices for weed identification under various soil, residue, and lighting conditions. Trans. ASAE 38, 259–269. https://doi.org/10.13031/2013.27838

Wu, L., Wen, Y., 2009. Weed/corn seedling recognition by support vector machine using texture features. African Journal of Agricultural Research 4, 840–846.

Zermas, D., Morellas, V., Mulla, D., Papanikolopoulos, N., 2020. 3D model processing for high throughput phenotype extraction – the case of corn. Computer and Electronics in Agriculture 172, 105047. https://doi.org/10.1016/j.compag.2019.105047

2.7. Table and Figures

Table 2.1. Weed infestation levels in the low, medium, and high density plots in the experimental area.

Species	Average Weed Density (m^{-2})			
	Low	Medium	High	Size *
Palmer amaranth (*Amaranthus palmeri* S. Watson)	2	5	10	4 to 6 leaf stage (10–15 cm tall)
Red sprangletop (*Leptochloa mucronata* Michx.)	2	8	15	4 to 10 tiller stage (8–15 cm tall)
Morningglories (*Ipomoea* spp.)	1	2	3	1 to 4 leaf stage
Texas millet (*Urochloa texana* Buckl.)	0	1	3	2 to 7 tiller stage (7–10 cm tall)
Devil's claw (*Proboscidea louisianica* (Mill.) Thell.)	1	2	2	1 to 4 leaf stage
Total	6	18	33	

* Size at the time of capturing the aerial image used in this research.

Table 2.2. Full set of image features tested in the study.

Feature Type	Feature Name [a]	Description
Spectral (N = 4)	B, G, R, ExG	Mean values of all three channels and derived features for each grid object
Textural (N = 18)	GLCM Homogeneity at 45° for R, G, and B GLCM Homogeneity at 270° for R, G, and B GLCM Contrast at 45° for R, G, and B GLCM Contrast at 270° for R, G, and B GLCM Entropy at 45° for R, G, and B GLCM Entropy at 270° for R, G, and B	Second-order textural statistics based on Haralick et al. [49]

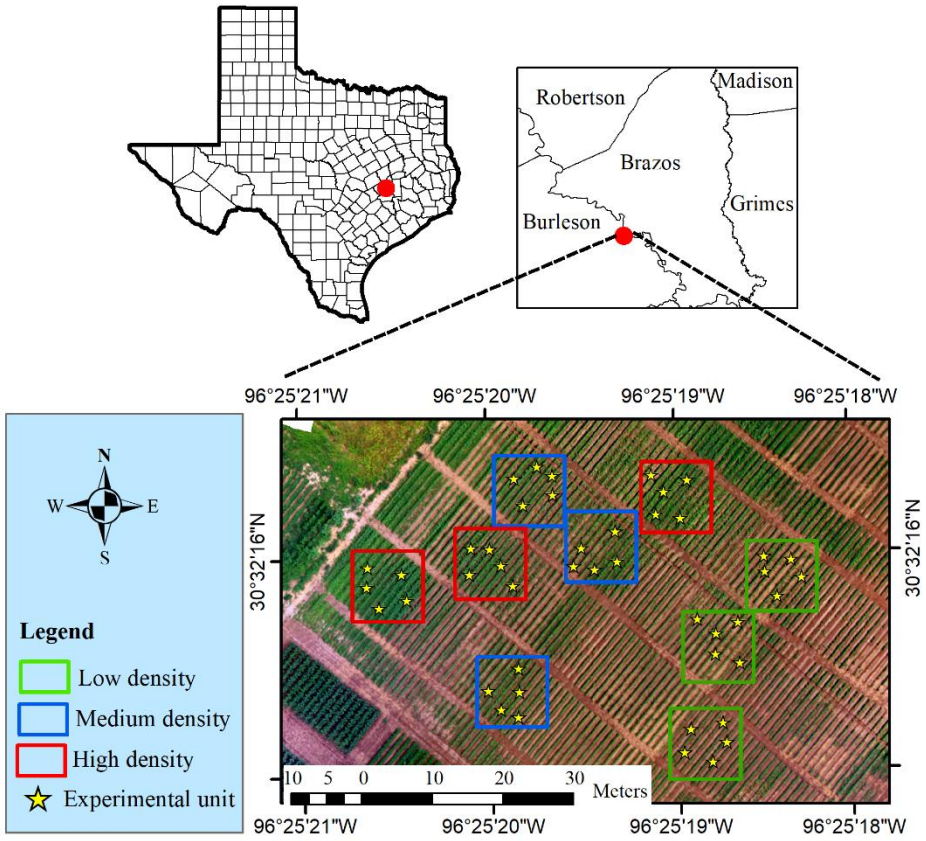

Figure 2.1. The experimental field (0.6 ha) with spatial distribution of treatment plots representing low (green polygons), medium (blue), and high (red) weed densities. Yellow star within the density plots represent the location for experimental unit, which is a quadrat (1 m × 1 m) in our case. Each treatment plot has five experimental units.

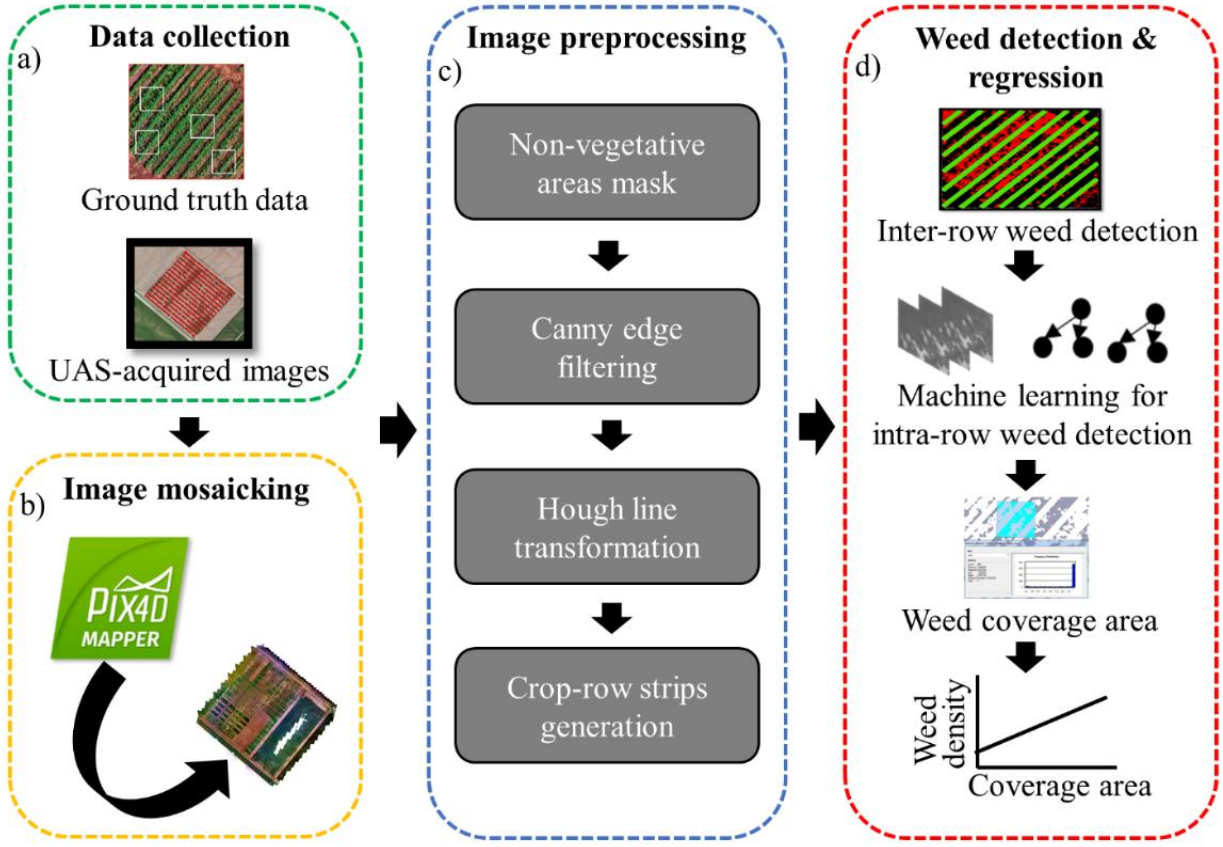

Figure 2.2. Flowchart for the overall methodology followed in this research for mapping weeds in a cotton field. The specific steps included (shown in dashed boxes) are: (a) data collection, (b) image mosaicking, (c) image preprocessing, and (d) weed detection and regression.

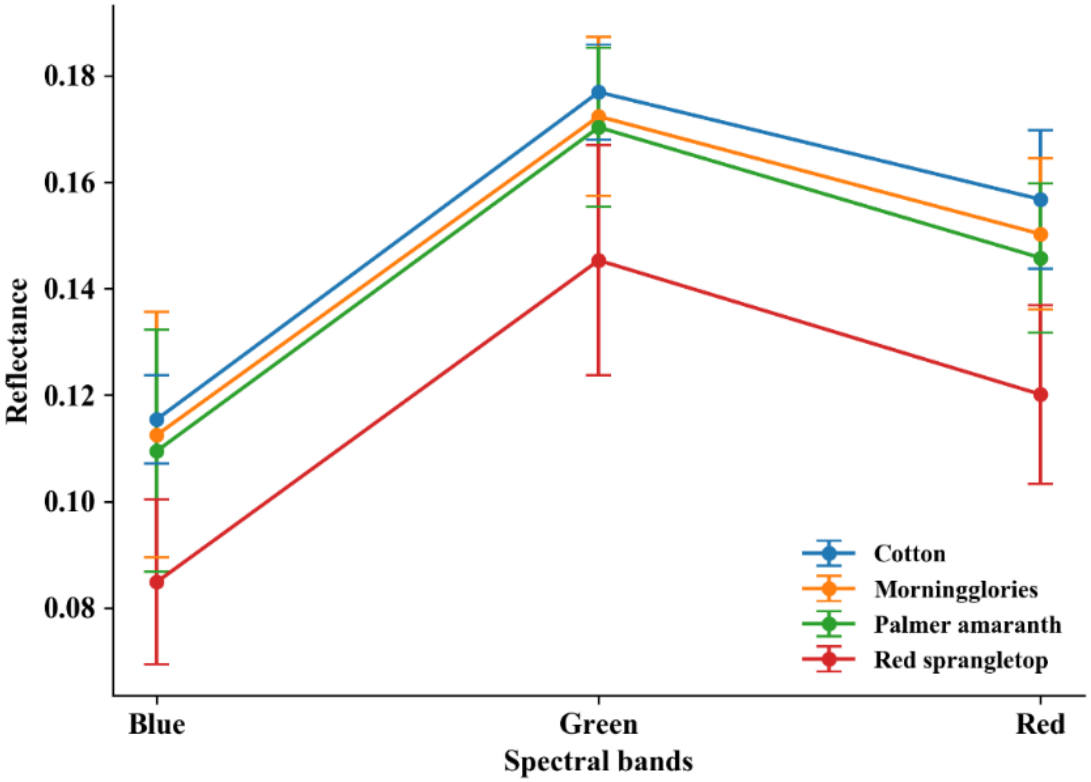

Figure 2.3. Reflectance values for the three most dominant weed species in the experimental area, compared with cotton for red, green, and blue bands in the visual imagery.

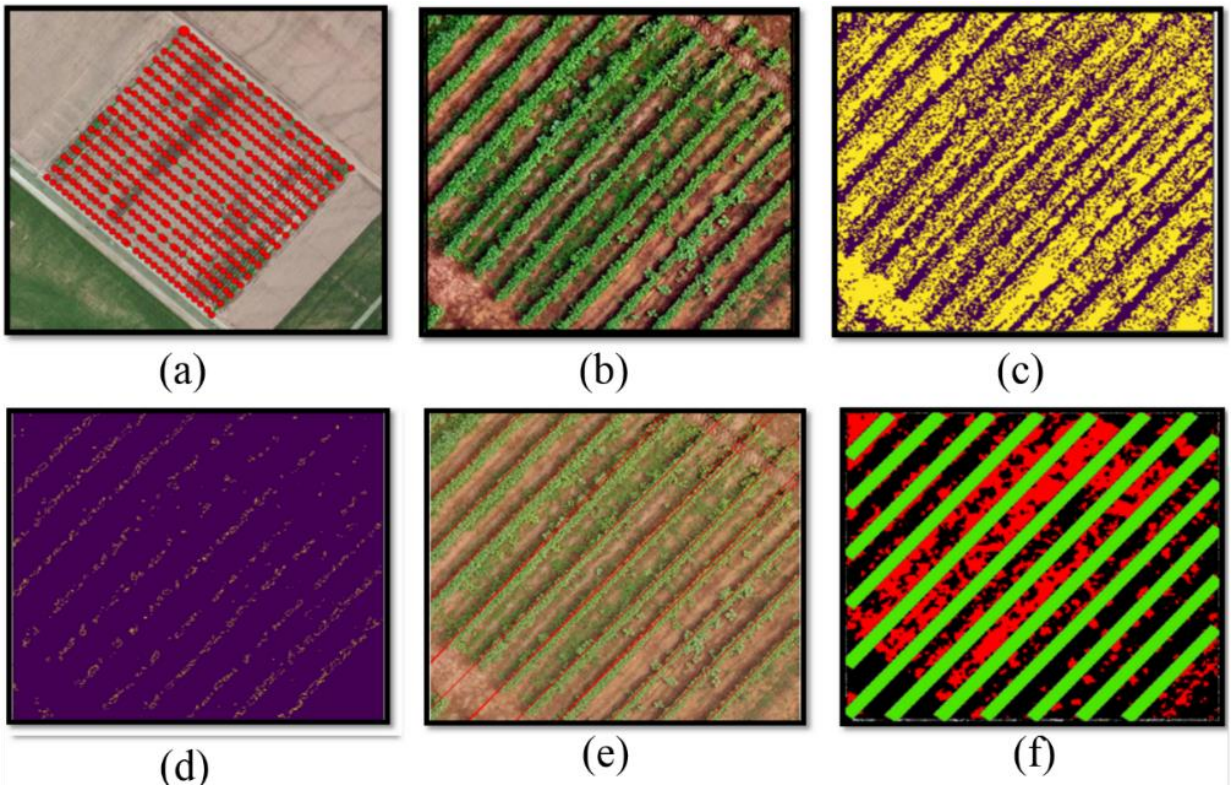

Figure 2.4. Various stages of image pre-processing: (a) Loading raw images in Pix4D software for mosaicking, (b) Clipping RGB imagery pertaining to each 10 m × 10 m treatment plot, (c) Otsu-thresholding, (d) Applying canny-edge algorithm and median filtering, (e) Generating Hough lines over the RGB imagery, and (**f**) Creating strips around Hough lines (green lines); here red pixels represent inter-row weeds and black pixels represent soil/shadows.

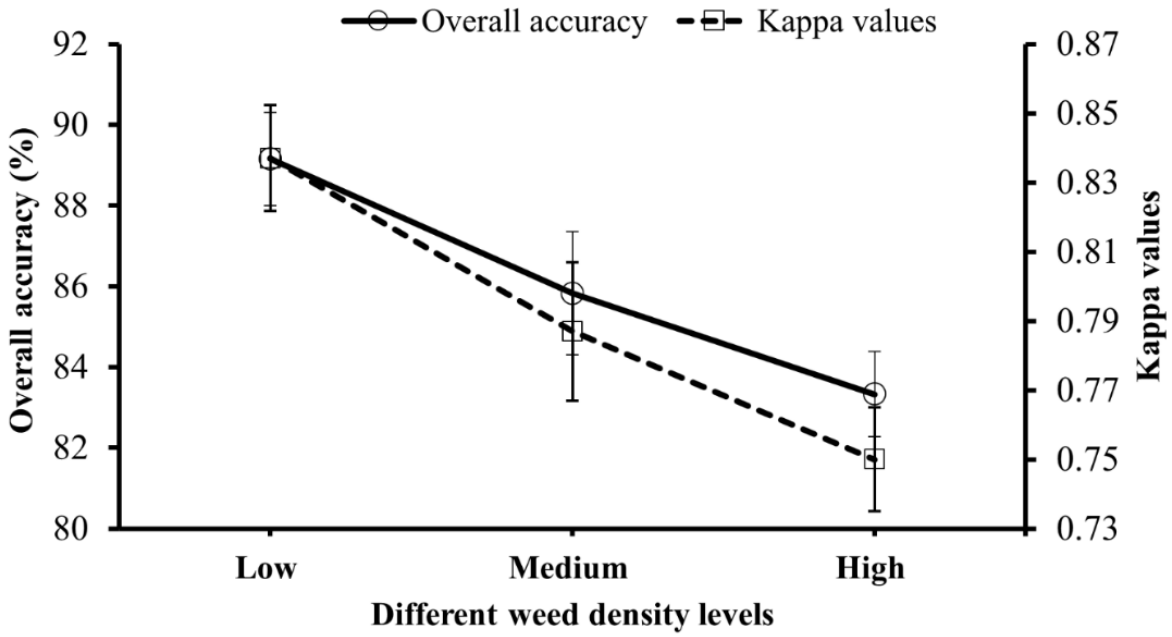

Figure 2.5. Accuracy measures for various levels (low, medium, and high) of weed densities established in the experiment.

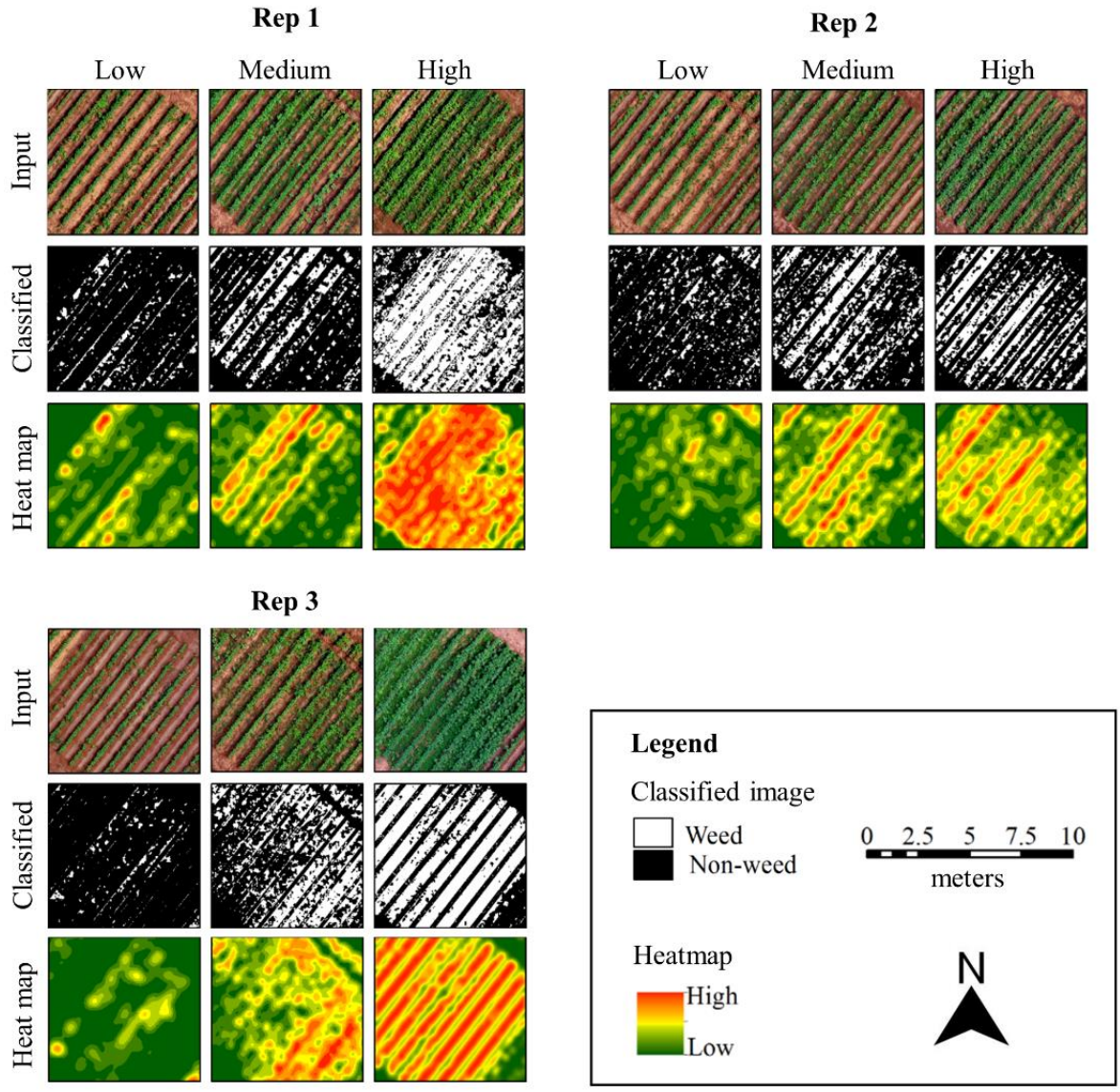

Figure 2.6. Results showing weed coverage in each replication (Rep 1, Rep 2, and Rep 3 on the upper-left, upper-right, and bottom-left panels, respectively) for three different density treatment plots (low, medium, and high). The pixels pertaining to weeds and crop in the classified maps were analysed using a multi-step approach involving separation of inter-row weeds first using Hough transformation and then detection of intra-row weeds using random forest classifier. The weed pixel density heat maps were derived by first converting the classified pixels to point shape files and performing point kernel density analysis on the shapefiles.

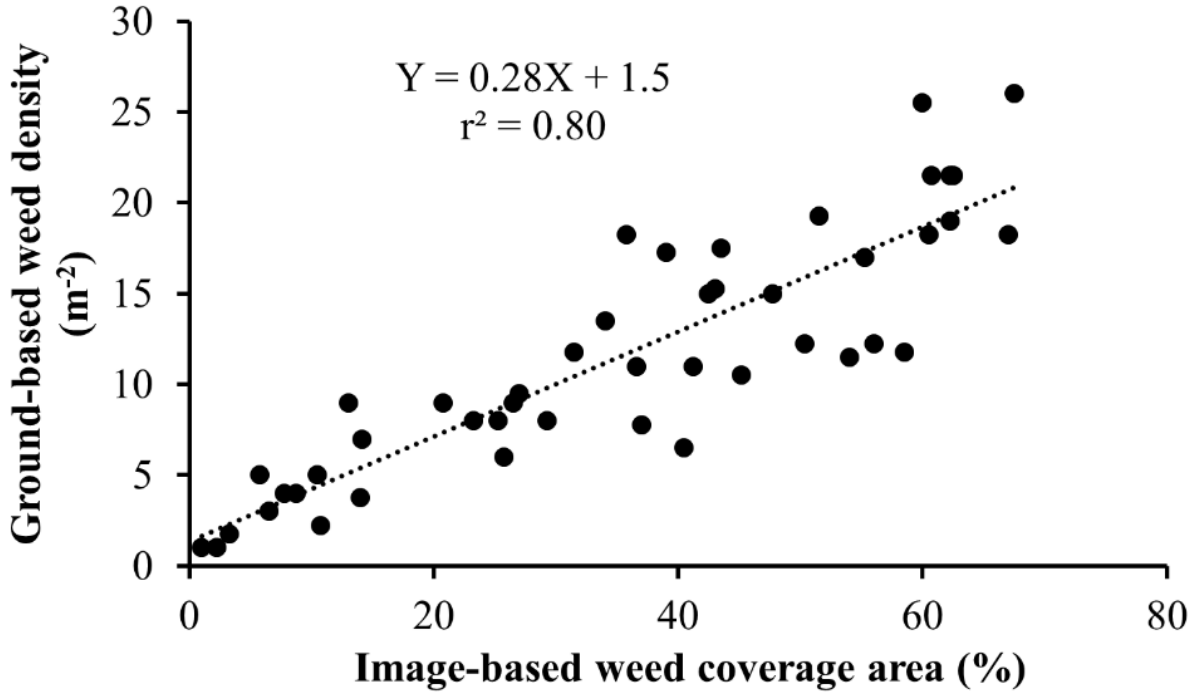

Figure 2.7. Linear regression showing the strength of association between weed pixel coverage (%) quantified using aerial imagery and overall weed density (no. of weeds m−2) in the quadrats determined by ground truthing.

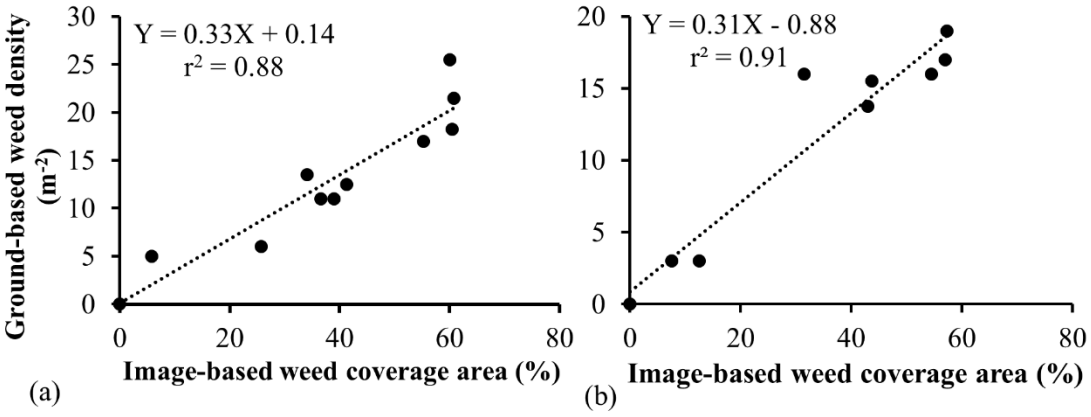

Figure 2.8. Regression analysis of weed pixel coverage (%) obtained using aerial imagery and ground-based weed density (m−2) for (a) red sprangletop and (b) Palmer amaranth.

3. DETECTION OF ITALIAN RYEGRASS IN WHEAT AND PREDICTION OF COMPETITIVE INTERACTIONS USING REMOTE SENSING AND MACHINE LEARNING TECHNIQUES*

3.1. Abstract

Italian ryegrass (*Lolium perenne* ssp. *multiflorum* (Lam) Husnot) is a troublesome weed species in wheat (*Triticum aestivum*) production in the United States, severely affecting grain yields. Spatial mapping of ryegrass infestation in wheat fields and early prediction of its impact on yield can assist management decision making. In this study, unmanned aerial systems (UAS)-based red, green and blue (RGB) imageries acquired at an early wheat growth stage in two different experimental sites were used for developing predictive models. Deep neural networks (DNNs) coupled with an extensive feature selection method were used to detect ryegrass in wheat and estimate ryegrass canopy coverage. Predictive models were developed by regressing early-season ryegrass canopy coverage (%) with end-of-season (at wheat maturity) biomass and seed yield of ryegrass, as well as biomass and grain yield reduction (%) of wheat. Italian ryegrass was detected with high accuracy (precision = 95.44 ± 4.27%, recall = 95.48 ± 5.05%, F-score = 95.56 ± 4.11%) using the best model which included four features: hue, saturation, excess green index, and visible atmospheric resistant index. End-of-season ryegrass biomass was predicted with high accuracy (R^2 = 0.87), whereas the other variables had moderate to high accuracy levels (R^2 values of 0.74 for ryegrass seed yield, 0.73 for wheat biomass reduction, and 0.69 for wheat grain yield reduction). The methodology demonstrated in the current study shows great potential

*Sapkota, B.; Singh, V.; Neely, C.; Rajan, N.; Bagavathiannan, M. Detection of Italian Ryegrass in Wheat and Prediction of Competitive Interactions Using Remote-Sensing and Machine-Learning Techniques. *Remote Sens.* **2020**, *12*, 2977. https://doi.org/10.3390/rs12182977

for mapping and quantifying ryegrass infestation and predicting its competitive response in wheat, allowing for timely management decisions.

Keywords: computer vision; deep neural networks; precision agriculture; site-specific management; unmanned aerial systems; UAVs; weed-crop interactions

3.2. Introduction

Italian ryegrass (*Lolium perenne* ssp. *multiflorum* (Lam) Husnot) is one of the most problematic weeds in wheat (*Triticum aestivum* L.) production in the United States (U.S.) (Tucker et al., 2006). Italian ryegrass is a cool-season winter annual weed that thrives best under a temperature range of 20 to 25 °C. It has faster leaf expansion rate than wheat and its competition can negatively impact tiller production, uptake of soil nutrients, photosynthesis and overall growth of wheat, resulting in significant crop yield loss (Carson et al., 1999; Stone et al., 1998). Italian ryegrass densities as low as 1 plant m^{-2} can reduce wheat grain yield by 0.4% (Leibl, 1987). Early management of this species is vital to prevent yield loss, given its high competitive ability with wheat (Leibl, 1987).

Advancements in precision agriculture can facilitate site-specific weed management (SSWM) (Singh et al., 2020), which involves variable application rates for effective weed management based on weed distribution, location, and density in crops (Thompson et al., 1991). This approach can assist with effective management of herbicide resistance in weeds such as Italian ryegrass (Caio and Bradley, 2018; Mingyang et al., 2016). Given the vital need for early-season weed control to prevent crop yield loss, information on weed distribution through effective detection and mapping in crop fields is of paramount importance (Shaner and Beckie, 2014). Furthermore, an ability to predict the outcomes of weed-crop competitive interactions,

particularly crop yield reduction and weed seed production, using early-season weed infestation levels can facilitate informed management decisions for timely action (Ali et al., 2013).

Precise detection and mapping of Italian ryegrass in wheat fields, especially during early growth stages, is a challenge, generally due to high morphological similarities and indistinct canopy boundaries. Although Italian ryegrass has a characteristic pale green color and could stand out visually from wheat plants, such differences may not be obvious or too intricate to recognize in spectral data. These challenges in the classification of grass weed species, such as wild oat (*Avena sterilis* L.) and rigid ryegrass (*Lolium rigidum* L.), in a grass crop such as wheat based on spectral signatures have already been reported (Gómez-Casero et al., 2010; López-Granados et al., 2008). Few other attempts have been made to classify ryegrass from wheat using digital imagery (Golzarian and Frick, 2011; Kodagoda et al., 2008) but primarily using traditional classification approaches that may be less robust.

Addressing the challenge of grass weed detection in a cereal crop would require solutions on two major fronts: acquiring high spatial resolution imageries of production fields and developing effective image analysis models for precise species detection. Although varying spatial resolution of imageries and maps could have a differential impact on model uncertainties (Cottter et al., 2003; Singh, 2017), high-resolution imageries have proven effective for detection of weeds at the individual plant level even at early growth stages (Gao et al., 2018). Mapping ryegrass at individual plant canopy level allows for better estimation of weed infestations across the crop field and thus effective implementation of SSWM. Unmanned aerial systems (UAS), one of the popular remote-sensing platforms, have been successfully utilized in obtaining high-resolution aerial imageries for weed detection and mapping (De Castro et al., 2018; López-Granados et al., 2016; Pena et al., 2013; Sapkota et al., 2020; Tamouridou et al., 2017).

However, the benefits of high-resolution imagery can be fully exploited only if the image analysis/classification approach used for the problem is robust.

Several machine-learning classification approaches have been employed for various classification problems in the agricultural sector, including mapping of crops and weeds using aerial imageries. Yang et al. (2017) applied the single feature probability technique to generate features, which were later trained with decision trees and maximum likelihood classifier to map rice fields and assess lodging. Gašparović et al. (2020) utilized a fusion of random forest-based supervised and K-means algorithm-based unsupervised classification methods to map oat (*Avena sativa* L.) in fields using a low-cost unmanned aerial vehicle (UAV)-borne red, green and blue (RGB) imagery. Combining the object-based image analysis (OBIA) with random forest-based prediction, De Castro et al. (2018) analyzed UAV imagery and its derivatives to map weeds in cotton and sunflower fields. Gao et al. (2018) fused row-detection algorithm results with OBIA-derived features to map weeds in maize fields using a random forest classifier.

Every classification problem poses a unique level of intricacy and therefore demands a suitable classification mechanism. For discriminating among different grass species, a powerful classification approach accompanied by a machine-learning classifier may be desirable. One of the effective ways in this regard is to generate multiple features, select the best and most informative features, and make inferences using a powerful machine-learning algorithm. The feature selection process ensures the elimination of irrelevant features, which would otherwise compromise the ability of the machine-learning models (Kanellopoulos et al., 1997). Artificial neural networks (ANNs), one of the most powerful and advanced machine-learning classifiers, have been frequently used for weed detection and mapping (Gutiérrez et al., 2008; Li et al., 2008; Yang et al., 2003). ANNs, in general, are the computing systems that mimic the biological

neural networks, comprising of three main systems namely the input layer to receive the data, hidden layer(s) to learn the pattern in the data, and output layer to provide the best parameters for classification (Rumelhart et al., 1986).

The current study utilizes deep neural networks (DNNs) for detection and mapping of Italian ryegrass in wheat fields. DNNs are ANNs with more than one hidden layer, designed to improve the ability to learn complex patterns. With the increase in the number of hidden layers, the neural networks become denser with an enhanced ability for pattern recognition (Goodfellow et al., 2016). Here, we apply a rigorous hyperparameter tuning process and exhaustive feature selection to improve the DNN-based classification accuracy. The specific objectives of this study were to: 1) detect and map Italian ryegrass in wheat fields using UAS-derived imageries and DNNs; and 2) develop and test models to predict the impact of early-season Italian ryegrass infestations determined using UAS-derived imagery on end-of-season productivity of wheat and ryegrass.

3.3. Materials and Methods

3.3.1. Location and Experimental Setup

The study was conducted in 2018 at two distinct sites (0.2 ha each) at the Texas A&M AgriLife Research (Site A, 30° 32' 15" N, 96° 25' 35" W, elevation: 70 m) and Extension farms (Site B, 30° 30' 37" N, 96° 25' 13" W, elevation: 68 m) located in Burleson County, TX (Figure 3.1). The locations are characterized by a sub-tropical climate, with average monthly maximum and minimum temperatures during the study period/winter wheat growing season (November–May) of 20° C and 8.5° C, respectively. The total rainfall during the growing season in 2018 for

this area was 889 mm. The sites mainly varied in soil composition; the soil type of Site A was Weswood silty clay loam, whereas that of Site B was Belk clay (Soil Survey Staff, 2020).

The winter wheat crop (TAM 304) was drill-seeded at a seeding rate of 120 kg ha^{-1} and 19 cm row spacing on 15 November 2018 at Site A and 20 November 2018 at Site B. An Italian ryegrass biotype sourced locally was broadcast planted in the plots immediately after planting wheat. The experimental area was divided into model training (red polygons in Figure 3.1) and validation sections (blue polygons in Figure 3.1). The training area consisted of three Italian ryegrass density (low, moderate, and high) treatments and a weed-free check, replicated four times (16 total plots; plot size: 2 m x 3 m, with 2 m buffer in all sides) in a randomized complete block design. Within each training plot, a 1 m^2 quadrat was established at the center which served as the sampling unit for image analysis and ground-truth data collection. In the quadrats, the ryegrass seedlings were thinned to simulate a gradient of different densities across sites, with achieved final densities of 20, 50, and 80 plants m^{-2} for Site A, and 50, 100, and 150 plants per m^{-2} for Site B. The validation area (25 m x 9 m) had a random gradient of densities of Italian ryegrass inter-mixed in wheat, and a total of 5 quadrats were established within the validation area for each site as the sampling units for model validation. Wheat was raised as a rain-fed crop, and nitrogen fertilizer (150 kg ha^{-1}) was split-applied at 45 days after planting (DAP) (50 kg ha^{-1}) and at 90 DAP (100 kg ha^{-1}). No pest control treatments were required.

3.3.2. General Workflow

The experiment began with image collection during the early growth stage of weed, followed by an end-of-season collection of ground-truth data for both weed and crop. The next step was to process the imagery, which was conducted in three sub-steps, including image mosaicking and calibration, feature extraction and selection, and image classification and

validation. Regression modelling was performed to develop predictive models using image- and ground-based information. Finally, the models were implemented on the validation plots to build a heatmap for different measured variables (Italian ryegrass biomass and seed production, and wheat biomass and grain yield reduction) and validate the accuracy of the models. Figure 3.2 shows the schematics of the general workflow followed in this research.

3.3.3. Data Collection

3.3.3.1. Image Collection

In order to collect early-season information required for the study, aerial flights were carried out on 6 March 2019 and 13 March 2019 at Site A and Site B, respectively. The timing coincided with the peak tillering stage of wheat and ryegrass, at about 90 DAP on both sites. A quadcopter UAV "DJI Phantom 4 Pro" (DJI, China) attached with an RGB sensor (12 megapixels) was flown at an altitude of 10 m to acquire aerial images at three different bands (Red, Green, and Blue) during ±2 hours of solar noon (10 AM to 2 PM) in both sites. The average wind speed was 9.6 kmph for Site A and 8 kmph for Site B throughout the flight duration. Images were acquired at an overlapping mode (75% for both side and end overlap), the exposure was set to automatic mode, and the flight plan was executed in a grid structure at an operating speed of 5 m/s. The flight mission was executed using the mobile application "Pix4Dcapture" (Pix4D, Lausanne, Switzerland) and was completed in 20 minutes at each site. Reflectance panels/tarps were placed in the field at the time of flights to perform spectral calibration in the imagery at a later stage.

3.3.3.2. Ground-Truth Data Collection

Upon wheat maturity, ground-truth data pertaining to ryegrass biomass, ryegrass seed yield, wheat biomass, and wheat grain yield were obtained from each quadrat on 23 May 2019,

to develop regression models between early-season ryegrass densities and end-of-season biophysical parameters of ryegrass and wheat. In order to account for potential ryegrass seed loss due to shattering prior to harvest, a visual estimate of seed shattering was documented at the time of harvest. The ryegrass and wheat plants were manually harvested from each quadrat at the ground level, separated by species, placed in individual paper bags, and dried in an oven at 63 °C for 36 hours prior to the estimation of dry biomass. Wheat plants from each experimental unit were threshed to obtain grain yield. Ryegrass spikes were hand threshed and seed yield was determined after adjusting for shattering loss.

3.3.4. Image Processing

3.3.4.1. Image Mosaicking and Calibration

Images acquired for each site were stitched together using the Pix4D mapper software (Pix4D, Lausanne, Switzerland) to generate qualitative, high-resolution (3 mm/pixel) orthomosaic imageries. Generating qualitative orthomosaic imageries can sometimes be challenging as the process depends heavily upon several factors, including camera internal and external orientation parameters, flight parameters, and the robustness of the image-matching algorithm (Conte et al., 2018; Pérez et al., 2013). Failure to optimize the camera parameters can result in distortion of the imageries. The Pix4D mapper mitigates this issue by optimizing the camera parameters during the initial run and allowing users to re-run the process with the optimized parameters. In this study, camera model parameters were initially loaded from the exchangeable image file format metadata, generated automatically by the UAV during the image acquisition process, into the Pix4D mapper. To further improve the quality, the initial calibration phase was re-run using the optimized parameters. A detailed description of how Pix4D mapper generates an orthomosaic imagery from sets of UAV-borne imageries can be found in this link

(https://support.pix4d.com/hc/en-us/articles/204272989-Offline-Getting-Started-and-Manual-pdf). Following the orthomosaic generation, the digital number (DN) values of the imageries were calibrated to reflectance values using the three different custom spectral panels (black, grey, and white). Three different datasets, each with 300 DN or pixel values of a band as the X-variable and the reflectance values of corresponding pixels in the spectral panels derived using Analytical Spectral Devices FieldSpec Pro HandHeld spectroradiometer (Analytical Spectral Devices, Boulder, CO, USA) as the Y-variable were prepared. Furthermore, simple linear regression analyses were conducted for the X- and Y-variables to derive three separate regression models (Equations 1–3) for predicting reflectance values using prepared datasets. The model was then applied to predict the values for all the pixels in red, blue, and green bands.

$$(\sigma_j)_r = \mu 1*(\lambda_j)_r + c1 \quad 1)$$

$$(\sigma_j)_g = \mu 2*(\lambda_j)_g + c2 \quad 2)$$

$$(\sigma_j)_b = \mu 3*(\lambda_j)b + c3 \quad 3)$$

where, σj= predicted reflectance value of a j^{th} pixel for the red (r), green (g), and blue (b) band; λj = DN value of a j^{th} pixel for the red (r), green (g), and blue (b) band; $\mu 1, \mu 2,$ and $\mu 3$ are slope values derived from the linear equations for red, green, and blue band, respectively; and c1, c2, and c3 are intercepts for models for red, green, and blue band, respectively.

3.3.4.2. Feature Extraction and Selection

Following the spectral calibration, 12 feature layers were extracted and/or computed for further image-processing purposes (Table 3.1). Optimizing the feature subset is required before

feeding into machine-learning algorithms for improving the classification process and making it cost- and time-efficient [34]. For this purpose, first, 1000 training samples for each of the user-defined classes (in this case, 5-classes: Ryegrass-A, Ryegrass-B, Non-ryegrass vegetation, Bareground, and Shadow) were collected from the imageries of both sites. Ryegrass-A and B represent different categories of ryegrass pixels in the imagery, indicating normal green pixels (A) and illuminated pixels (B). A considerable number of illuminated ryegrass pixels were observed in the experiment area, and the two categories were treated separately since combining them might compromise the prediction ability of the classifier. Second, the distribution of features within/across the user-defined classes were explored to select the best feature combination qualitatively. However, such a selection approach was too complex since there was much variation in the distribution of these features (Figure 3.3). Therefore, a wrapper-based feature selection approach called "exhaustive selection" was employed to select the 10 best feature combinations (hereafter referred to as feature models) using one-fourth of the training samples for each class (i.e. 250).

3.3.4.3. Image Classification and Validation

After the selection of best feature models, each feature model was tested for classifying images sampled in each quadrat (1 m x 1 m) (hereafter referred to as quadrat images) into user-defined classes using the supervised machine-learning system. The back-propagation multilayer perceptron (MLP), a commonly used and widely available ANN structure (Atkinson and Tatnall, 1997), was used as the machine-learning system in this study. Keras, a high-level neural networks application programming interface (API) written in python computer language was used to build the MLP-based custom DNN system. Various hyperparameters were tested for several values prior to final training process to derive the best set of values (Table 3.2), using the

same subset of training samples used for exhaustive feature selection. Categorical crossentropy was fixed for the loss function and “adam”, a very popular stochastic gradient descent-based weight optimization technique, was fixed for the optimizer in the tuning and training process.

This best set of parameters was then used in the custom DNN system to train each feature model. One-half of the training samples for each class (i.e. 500) were used for training purposes. Each trained DNN model was finally implemented over each quadrat image and in total 10 different classification outputs were generated for 10 different feature models for each image. Once the quadrat image was classified into user-defined classes, post-classification operations such as filtering, smoothing, and generalization were carried out to remove any speckled appearance and improve the quality of the classified output. For accuracy purposes, different indicators such as precision, recall, and F-score were calculated for each feature model using an independent set of validation samples [i.e., remaining one-fourth of training samples (250) for each class] and the best feature model was determined. Precision was measured as the number of correctly classified samples of a class divided by the number of samples labeled as that class by the system (Equation 4). Recall was calculated as the number of correctly classified positive samples of a class divided by the number of validation samples allocated for that class (Equation 5). F-score is a combination of both precision and recall (Equation 6).

$$\text{Precision} = \frac{TP}{TP + FP} \qquad 4)$$

$$\text{Recall} = \frac{TP}{TP + FN} \qquad 5)$$

$$\text{F-score} = 2 \times \frac{\text{Precision} \times \text{Recall}}{\text{Precision} + \text{Recall}} \quad 6)$$

where, TP, FP, and FN represent true positive, false positive, and false negative instances, respectively.

3.3.5. Regression Modeling

With the classification of imageries and evaluation of the models, the best classified output, i.e. classified imagery for each quadrat (altogether 32, including both sites) were used in the regression modelling procedure. Each classified imagery comprised of pixels classified into either of the user-defined classes. First, both ryegrass classes (i.e., Ryegrass-A and B) were merged into a single class. Then, the ryegrass pixels pertaining to this class within each classified imagery were enumerated and the number of enumerated pixels was divided by total number of pixels in the imagery to calculate ryegrass canopy coverage area (%). In the next step, four separate models were developed by regressing the canopy coverage area of ryegrass (%) as the predictor variable, while considering ryegrass biomass (g), ryegrass seed yield (g), wheat biomass reduction (%), and wheat grain yield reduction (%) as predicted variables. Wheat biomass and grain yield reduction (%) were calculated as a relative measure with weed-free check plots. Altogether, 32 pairs of predicted and predictor variables (16 pairs corresponding to the quadrats for each site) were used in the regression analysis for ryegrass biomass and seed yield, whereas only 24 pairs were used for wheat biomass reduction (%) and grain yield reduction (%). Finally, the coefficient of determination (R^2) and root mean square error (RMSE) were calculated as statistical measures of how well the regression predictions approximated the datapoints.

3.3.6. Predictive Model Implementation and Validation

The validation areas (Figure 3.1) were demarcated within the experimental field and the orthomosaic imageries were clipped to their extent for spatial implementation of the predictive models and independent model validation. The best feature model was also applied to the clipped imageries to obtain the classified outputs (i.e., early-season ryegrass canopy coverage maps), followed by all the post-classification operations described earlier to improve the results. The classified map was partitioned into several (1 m × 1 m) grids and the ryegrass canopy coverage area (%) was calculated for each of the grid. The predictive models developed earlier were then applied to the grids to obtain the values for all the predicted variables. Ground truth values for the 5 quadrats in each validation area pertaining to ryegrass biomass (g), ryegrass seed yield (g), wheat biomass reduction (%), and wheat grain yield reduction (%) were assessed against predicted heatmap values for those corresponding grids to determine the reliability of the whole classification and predictive model framework. RMSE and coefficient of determination (R^2) were calculated as the measure of agreement between predicted and observed variables.

3.4. Results

3.4.1. Ryegrass Detection Using Feature Combinations

Among the approximately 4000 model runs of various features and their combinations tested in the study, the top 10 best performing models had a combination of four or more features, illustrating the robustness of multivariate analysis for species detection. Based on independent validation samples, the average F-score values ranged between 89% and 96% for different feature models (i.e., feature combinations) tested (Table 3.3). The highest average F-score (95.5%) was achieved with the model that combined color transformed features (hue and

saturation) with vegetation indices (Excess Green Index (ExG) and Visible Atmospheric Resistant Index (VARI)) for machine learning (Model #10 in Table 3.3), which was closely followed by the model that used Red, Blue, Sat, VARI, ExG and Wavelet_Mean (Model #9; F-score: 95.3%). However, the model #10 was chosen for mapping Italian ryegrass (Figure 3.4) since it was more parsimonious compared to #9.

For model #10, the user-defined classes Bareground and Shadow were classified with the highest precision, recall and F-score (>98%), compared to the other classes namely Ryegrass-A, Ryegrass-B and Non-Ryegrass (Figure 3.5). As explained by boxplots for different features (Figure 3.3), Bareground and Shadow had very distinct boundaries from other classes for several features. The lightly shaded portion of Italian ryegrass and wheat leaves were expected to be classified as Shadow (i.e., formed underneath the canopy) due to spectral similarities; however, a meticulous training of these regions greatly reduced potential misclassification, which is indicated by the high precision (>98%) and recall (>98%) values for Shadow. The classification for Non-Ryegrass vegetation had the lowest accuracy (Figure 3.5; F-score: 91%), which is likely since this class encompassed a mixture of primarily wheat and few other weed species, resulting in fuzzy, instead of distinct, boundaries for different features. As a result, there could have been several instances of misclassification with either Shadow and/or Ryegrass-A. Ryegrass-B had a higher F-score (94%) compared to Ryegrass-A (92.5%) and Non-Ryegrass vegetation (91%), which could be attributed to brighter pixels of Ryegrass-B compared to the rest of the vegetation pixels, leading to distinct separation for several features. However, Ryegrass-B and Bareground overlapped for several features, as a result of reflectance from debris present on the soil surface which often produced bright reflectance.

3.4.2. Prediction of Competitive Outcomes between Italian Ryegrass and Wheat

The canopy coverage area (%) for Italian ryegrass (predictor variable) was computed from each classified map of quadrat image (Figure 3.6) and regressed against the ground truth data (predicted variables). In general, Italian ryegrass biomass and seed production increased with an increase in their canopy coverage area (as determined through image analysis) for the densities simulated here, with a concurrent decline in wheat biomass production and grain yield. The highest coefficient of determination (R^2 = 0.87; RMSE = 66.03) was achieved for prediction of ryegrass biomass, followed by ryegrass seed yield (R^2 = 0.74; RMSE = 32.44), wheat biomass reduction (%) (R^2 = 0.73; RMSE = 9.27), and wheat grain yield reduction (%) (R^2 = 0.69; RMSE = 10.94) (Figure 3.7). Results showed that Italian ryegrass coverage had a linear relationship with its biomass, and a curvilinear relationship with its seed production as well as biomass and grain yield reduction of wheat.

3.4.3. Model Validation

The early-season ryegrass canopy coverage maps developed with the DNN model for validation area in each site (Figure 3.8, top panel) and the competition models described above were utilized together to produce heat maps (1 m x 1 m grid size). These heat maps provide a visual representation of weed/crop competitive outcomes at the end of the season in terms of biomass and seed yield (Figure 3.8, bottom panel). Validation results showed that the coefficient of determination based on predicted (heat map-based) and observed values (ground-based) was the highest (R^2 = 0.83; RMSE: 69.8) for Italian ryegrass biomass, followed by ryegrass seed yield (R^2 = 0.72; RMSE = 17.9), wheat biomass reduction (%) (R^2 = 0.63; RMSE: 10.57), and grain yield reduction (%) (R^2 = 0.60; RMSE = 16.23) (Figure 3.9). Thus, the validation analysis

showed that the models developed in this study were generally robust in predicting end-of-season productivity for Italian ryegrass as well as wheat.

3.5. Discussion

The results provide strong evidence that a combination of multiple classification features is more effective in species detection compared to employing individual features, but the choice of features is important. In this study, color-transformed features (hue and saturation) and vegetation indices (VARI and ExG) were found to be the most effective combination in detecting Italian ryegrass in wheat. Hue and saturation are invariant to brightness variation (Chaves-González et al., 2010) and, therefore, are least affected by illumination differences by ryegrass leaves. Given the pale green color of ryegrass leaves compared to that of wheat, the difference in the greenness level was obvious with hue and saturation values. Several studies have credited hue and saturation for their ability to differentiate plants based on the greenness level (Burks et al., 2002; Hemming et al., 2001). Additionally, ExG was shown to be useful in separating plant tissues from other backgrounds (soil and weathered plant residue) (Yang et al., 2015). VARI was designed to be minimally sensitive to atmospheric effects, allowing precise estimation of the vegetative fraction of different plant species. Recently, VARI was found to be very useful in classifying real shadows from non-sunlit plant leaves in the canopy (Milas et al., 2017). This property of the index may have helped in reducing misclassification between shadow and non-sunlit wheat/ryegrass plant canopies in our study, as there were several non-sunlit plant pixels with shadow-like appearance in both experimental sites.

A very limited number of studies have detected/classified grass weeds in wheat using digital images (either handheld camera or UAS-derived) to date. Golzarian and Frick (2011) used very high-resolution true-color images (0.26 mm/pixel) for differentiating annual ryegrass and

wheat, with an accuracy of 88%. It should be noted that the current study utilized relatively lower spatial resolution (3 mm/pixel; Figure 3.4) and still achieved a higher accuracy (F-score: 95%). This is particularly advantageous for optimizing computational costs and complexity when scaling up this approach for vast production fields. The reasons for the improvement in classification accuracy compared to that of Golzarian and Frick (2011) could be the use of DNNs, which have been proven to solve increasingly complicated applications with increasing accuracy over time (Goodfellow et al., 2016). However, the current study classified ryegrass at a relatively larger seedling stage compared to what was studied by Golzarian and Frick (2011), which may also have affected the learning capability of the classification model.

Kodagoda et al. (2008) used an overhead imaging system fitted with color and near-infrared cameras to capture high-resolution digital images in order to differentiate between wheat and two weed species, cobbler's peg (*Bidens pilosa* L.) and rigid ryegrass (*Lolium rigidium* L.). Hue, saturation, and texture information of plant leaves were extracted from the digital images and fed into traditional machine learning algorithms such as k-means clustering and Mahalanobis distance. Although their model worked fairly well for differentiating cobbler's peg from wheat (accuracy: 85%), it failed to detect and classify ryegrass from wheat (accuracy: 26%). Similarities of these two species in the distributions of hue, saturation, and texture cues were concluded to be the prime reason for the very low performance of the model. The current study also observed an overlap in the distribution of hue and saturation between ryegrass and non-ryegrass vegetation (Figure 3.3); however, supplementing with vegetation indices such as ExG and VARI was beneficial for classification.

Recently, convolutional neural networks (CNNs) have been widely appreciated for their high potential for detecting and mapping weeds (Gao et al., 2020; Huang et al., 2018; Sa et al.,

2018). However, training a CNN model for segmentation generally requires a relatively large number of annotated labels for weeds and crop canopy boundaries, making the procedure labor-intensive and time-consuming (Gao et al., 2020). The complexity in training data preparation manifolds due to the intricate labeling procedure for grasses caused by the extreme interlocking of leaves. Moreover, this annotation process is almost impossible if the resolution of the imagery is not high enough to clearly delineate leaf boundaries. Instead of a time-consuming and intricate weed annotation procedure, this study adopted the relatively easier training sample selection approach. The most representative pixels for each user-defined class were selected as the training samples and deep neural network system was trained over the samples to achieve higher accuracy. With the intensive feature optimization technique, this study generated various feature models and tested independently to obtain the most accurate model. Feature optimization processes, such as that described in the current research, are often reported to boost machine learning performance (Xue et al., 2013).

To the best of our knowledge, very few studies have utilized DNN-based predictive models for understanding weed–crop interaction and explored the feasibility of predicting biomass and seed yield using plant canopy coverage information. Most of the existing yield prediction studies have heavily relied upon vegetation indices, especially Normalized Difference Vegetation Index (NDVI) (Fassnacht et al., 1997; Shanahan et al., 2001; Xue et al., 2007). However, several studies have reported that NDVI becomes saturated at high leaf-area index levels, which in turn may lead to inaccurate prediction of biomass and yield (Fassnacht et al., 1997; Turner et al., 1999). This study, in contrast, utilizes vegetation indices and other promising features to classify the pixels pertaining to the class of interest and then uses the number of

pixels as the predictor variable for biomass and seed yield. Thus, this method avoids the risk of saturation and seasonal variability of vegetation indices, and leads to a better prediction.

Relatively lower correlation for wheat biomass and grain yield reduction (%) compared to ryegrass biomass and seed yield in this study could be attributed to the use of ryegrass canopy coverage area (%) as the predictor variable. In particular, wheat grain yield reduction (%) had lower coefficient of determination compared to wheat biomass because grain yield is a complex trait and is affected by several factors including environmental and genetic factors (Slafer et al., 1996; Yagbasanlar et al., 1995). Although biomass has been reported to be one of the primary determinants of grain yield, other factors such as grains per spike and spikelets per plant may also have an influence (Slafer et al., 1996). Thus, the competitive effect of ryegrass on wheat grain yield may not be proportional to the effect on wheat biomass, as explained by different coefficient of determination for wheat biomass and grain yield in this study.

The ryegrass infestation map developed during the early season may help facilitate management interventions, including site-specific weed management (Thompson et al., 1991). The infestation maps can also be useful for monitoring ryegrass distribution and dynamics spatially and temporally. The predictive models and the spatial heatmap representation of weed-crop competitive interactions as presented in this study can be highly useful for management decision making (Heather et al., 2001). Predicting weed-crop interference early-on can inform weed control thresholds required to minimize yield loss (Swanton et al., 1999). These spatial heatmaps together with weed control thresholds can be utilized to create management grids. It should also be noted that heat map representation of competitive interactions at the 1 m × 1 m grid level in this study can be scaled-up to various grid sizes to fit different management needs.

Furthermore, recommendations for the features and hyperparameters made in the study could be utilized in similar studies to improve the efficiency.

This study, however, has some limitations: 1) only ANNs were tested for weed detection where several machine-learning classifiers such as random forest and support vector machine were available and already used for weed detection and mapping in the past. Future research should test these classifiers independently or maybe fused with more advanced deep-learning methods such as the CNNs; 2) broader applicability of the classification model presented here in wheat fields with varying geographies and environmental conditions is unknown. Wheat varieties may widely differ in leaf color and composition and thus may exhibit different spectral signatures. The model can be generalized and empowered with diverse training samples; 3) the competition models developed here were based solely on ryegrass canopy coverage area estimated from the aerial imageries. As such, this study did not attempt to utilize/evaluate already established weed-crop competitive models that were based on variables such as weed density (Cousens, 1985), biomass (Christensen, 1994; Colbach et al., 2014), and leaf-area index (Kropff et al., 1991). The effectiveness of the canopy/ground cover-based prediction compared to the previously established approaches is unknown. Future research should test and ensemble these approaches to improve the accuracy and feasibility of weed–crop interaction assessments; and 4) scaling this approach to large production fields may be challenging due to high computational demands.

3.6. Conclusions

This study successfully identified and demonstrated a UAS-based remote-sensing approach that combined both color transformed features and vegetation indices for improved

detection and mapping of Italian ryegrass in wheat (Highest F-score: 95.56 ± 4.11%). In addition, this study provided evidence that deep learning-based estimation of early-season plant canopy coverage can be a better predictor for competitive interactions, with relatively higher R^2 values for developed models [0.87 for ryegrass biomass (g), 0.74 for ryegrass seed yield (g), 0.73 for wheat biomass reduction (%), and 0.69 for wheat seed yield reduction (%)]. This study also highlighted the value of affordable, computationally less complex, and less storage demanding RGB imageries in assisting farmers with weed assessment and precision weed management. The machine learning-based classification model and the weed–crop competition models developed and employed in the study will be helpful in devising suitable agronomic interventions.

3.7. References

Ali, A., Streibig, J.C., Andreasen, C., 2013. Yield loss prediction models based on early estimation of weed pressure. Crop Protection 53, 125–131. https://doi.org/10.1016/j.cropro.2013.06.010

Atkinson, P.M., Tatnall, A.R.L., 1997. Introduction Neural networks in remote sensing. International Journal of Remote Sensing 18, 699–709. https://doi.org/10.1080/014311697218700

B. Xue, M. Zhang, W. N. Browne, 2013. Particle swarm optimization for feature selection in classification: A multi-objective approach. IEEE Transactions on Cybernetics 43, 1656–1671. https://doi.org/10.1109/TSMCB.2012.2227469

Burks, T.F., Shearer, S.A., Green, J.D., Heath, J.R., 2002. Influence of weed maturity levels on species classification using machine vision. Weed Science 50, 802–811. https://doi.org/10.1614/0043-1745(2002)050[0802:IOWMLO]2.0.CO;2

Caio, A.C.G.B., Bradley, D.H., 2018. Multiple herbicide–resistant italian ryegrass [*Lolium perenne* L. spp. *multiflorum* (Lam.) Husnot] in california perennial crops: characterization, mechanism of resistance, and chemical management. Weed Science. 66, 696–701. https://doi.org/10.1017/wsc.2018.50

Carson, K.H., Cralle, H.T., Chandler, J.M., Miller, T.D., Bovey, R.W., Senseman, S.A., Stone, M.J., 1999. *Triticum aestivum* and *Lolium multiflorum* interaction during drought. Weed Sci. 47, 440–445. https://doi.org/10.1017/S0043174500092055

Chaves-González, J.M., Vega-Rodríguez, M.A., Gómez-Pulido, J.A., Sánchez-Pérez, J.M., 2010. Detecting skin in face recognition systems: A colour spaces study. DSP 20, 806–823. https://doi.org/10.1016/j.dsp.2009.10.008

Conte, P., Girelli, V.A., Mandanici, E., 2018. Structure from Motion for aerial thermal imagery at city scale: Pre-processing, camera calibration, accuracy assessment. ISPRS Journal of Photogrammetry and Remote Sensing 146, 320–333. https://doi.org/10.1016/j.isprsjprs.2018.10.002

Cotter, A.S., Chaubey, I., Costello, T.A., Soerens, T.S., Nelson, M.A., 2003. Water quality model output uncertainty as affected by spatial resolution of input data. Journal of the American Water Resources Association 39, 977–986. https://doi.org/10.1111/j.1752-1688.2003.tb04420.x

De Castro, A.I., Torres-Sánchez, J., Peña, J.M., Jiménez-Brenes, F.M., Csillik, O., López-Granados, F., 2018. An Automatic Random Forest-OBIA Algorithm for Early Weed Mapping between and within Crop Rows Using UAV Imagery. Remote Sensing 10, 285.

Epinat, V., Stein, A., de Jong, S.M., Bouma, J., 2001. A wavelet characterization of high-resolution NDVI patterns for precision agriculture. IJAEO 3, 121–132. https://doi.org/10.1016/S0303-2434(01)85003-0

Fassnacht, K.S., Gower, S.T., MacKenzie, M.D., Nordheim, E.V., Lillesand, T.M., 1997. Estimating the leaf area index of North Central Wisconsin forests using the landsat thematic mapper. Remote Sensing of Environment 61, 229–245. https://doi.org/10.1016/S0034-4257(97)00005-9

François, C., 2015. Keras: The python deep learning library. keras. io.

Gao, J., French, A.P., Pound, M.P., He, Y., Pridmore, T.P., Pieters, J.G., 2020. Deep convolutional neural networks for image-based Convolvulus sepium detection in sugar beet fields. Plant Methods 16, 29. https://doi.org/10.1186/s13007-020-00570-z

Gao, J., Liao, W., Nuyttens, D., Lootens, P., Vangeyte, J., Pižurica, A., He, Y., Pieters, J.G., 2018. Fusion of pixel and object-based features for weed mapping using unmanned aerial vehicle imagery. IJAEO 67, 43–53. https://doi.org/10.1016/j.jag.2017.12.012

Gašparović, M., Zrinjski, M., Barković, Đ., Radočaj, D., 2020. An automatic method for weed mapping in oat fields based on UAV imagery. Computer and Electronics in Agriculture 173, 105385. https://doi.org/10.1016/j.compag.2020.105385

Gitelson, A.A., Kaufman, Y.J., Stark, R., Rundquist, D., 2002. Novel algorithms for remote estimation of vegetation fraction. Remote Sensing Environment 80, 76–87. https://doi.org/10.1016/S0034-4257(01)00289-9

Golzarian, M.R., Frick, R.A., 2011. Classification of images of wheat, ryegrass and brome grass species at early growth stages using principal component analysis. Plant Methods 7, 28. https://doi.org/10.1186/1746-4811-7-28

Gómez-Casero, M.T., Castillejo-González, I.L., García-Ferrer, A., Peña-Barragán, J.M., Jurado-Expósito, M., García-Torres, L., López-Granados, F., 2010. Spectral discrimination of wild oat and canary grass in wheat fields for less herbicide application. Agronomy for Sustainable Development 30, 689–699. https://doi.org/10.1051/agro/2009052

Goodfellow, I., Bengio, Y., Courville, A., 2016. Deep learning. MIT press.

Gulli, A., Pal, S., 2017. Deep learning with Keras. Packt Publishing Ltd.

Gutiérrez, P.A., López-Granados, F., Peña-Barragán, J.M., Jurado-Expósito, M., Hervás-Martínez, C., 2008. Logistic regression product-unit neural networks for mapping Ridolfia segetum infestations in sunflower crop using multitemporal remote sensed data. Computer and Electronics in Agriculture 64, 293–306. https://doi.org/10.1016/j.compag.2008.06.001

Heather, J.G., Bennett, K.A., Ralph, B.B., Tardif, F.J., 2001. Evaluation of site-specific weed management using a direct-injection sprayer. Weed Science 49, 359–366.

Hemming, J., Rath, T., 2001. PA—Precision Agriculture: Computer-Vision-based weed identification under field conditions using controlled lighting. JAER 78, 233–243. https://doi.org/10.1006/jaer.2000.0639

Huang, H., Deng, J., Lan, Y., Yang, A., Deng, X., Zhang, L., 2018. A fully convolutional network for weed mapping of unmanned aerial vehicle (UAV) imagery. PloS one 13, e0196302. https://doi.org/10.1371/journal.pone.0196302

Hunt Jr, E.R., Daughtry, C.S.T., Eitel, J.U.H., Long, D.S., 2011. Remote Sensing Leaf chlorophyll content using a visible band index. Agronomy Journal 103, 1090–1099. https://doi.org/10.2134/agronj2010.0395

Kanellopoulos, I., Wilkinson, G.G., 1997. Strategies and best practice for neural network image classification. International Journal of Remote Sensing 18, 711–725. https://doi.org/10.1080/014311697218719

Kodagoda, S., Zhang, Z., Ruiz, D., Dissanayake, G., 2008. Weed detection and classification for autonomous farming. Intelligent Production Machines and Systems.

Li, Z., An, Q., Ji, C., 2008. Classification of weed species using artificial neural networks based on color leaf texture feature. Presented at the International Conference on Computer and Computing Technologies in Agriculture, Springer, pp. 1217–1225.

Liebl, R., Worsham, A.D., 1987. Interference of Italian Ryegrass *(Lolium multiflorum*) in Wheat (Triticum aestivum). Weed Science 35, 819–823. https://doi.org/10.1017/S0043174500079406

Lópeez-Granados, F., PeÑA-BarragÁN, J.M., Jurado-ExpÓSito, M., Francisco-FernÁNdez, M., Cao, R., Alonso-Betanzos, A., Fontenla-Romero, O., 2008. Multispectral classification of grass weeds and wheat (Triticum durum) using linear and nonparametric functional discriminant analysis and neural networks. Weed Research 48, 28–37. https://doi.org/10.1111/j.1365-3180.2008.00598.x

López-Granados, F., Torres-Sánchez, J., Serrano-Pérez, A., de Castro, A.I., Mesas-Carrascosa, F.J., Peña, J.-M., 2016. Early season weed mapping in sunflower using UAV technology: variability of herbicide treatment maps against weed thresholds. Precision Agriculture 17, 183–199. https://doi.org/10.1007/s11119-015-9415-8

M. Woebbecke, D., E. Meyer, G., Von Bargen, K., A. Mortensen, D., 1995. Color indices for weed identification under various soil, residue, and lighting conditions. Trans. ASAE 38, 259–269. https://doi.org/10.13031/2013.27838

Meyer, G.E., Neto, J.C., 2008. Verification of color vegetation indices for automated crop imaging applications. Computer and Electronics in Agriculture 63, 282–293. https://doi.org/10.1016/j.compag.2008.03.009

Milas, A.S., Arend, K., Mayer, C., Simonson, M.A., Mackey, S., 2017. Different colours of shadows: classification of UAV images. International Journal of Remote Sensing 38, 3084–3100. https://doi.org/10.1080/01431161.2016.1274449

Mingyang, L., Andrew, G.H., Carol, M.-S., 2016. Characterization of multiple herbicide-resistant Italian Ryegrass (*Lolium perenne* ssp. *multiflorum*) populations from winter wheat fields in Oregon. Weed Science 64, 331–338. https://doi.org/10.1614/WS-D-15-00147.1

Pearson, K., 1901. On lines and planes of closest fit to systems of points in space. The London, Edinburgh, and Dublin Philosophical Magazine and Journal of Science 2, 559–572. https://doi.org/10.1080/14786440109462720

Pedregosa, F., Varoquaux, G., Gramfort, A., Michel, V., Thirion, B., Grisel, O., Blondel, M., Prettenhofer, P., Weiss, R., Dubourg, V., 2011. Scikit-learn: Machine learning in Python. the Journal of machine Learning research 12, 2825–2830.

Peña, J.M., Torres-Sánchez, J., de Castro, A.I., Kelly, M., López-Granados, F., 2013. Weed mapping in early-season maize fields using object-based analysis of unmanned aerial vehicle (UAV) images. PloS one 8.

Pérez, M., Agüera, F., Carvajal, F., 2013. Low cost surveying using an unmanned aerial vehicle. Int. Arch. Photogramm. Remote Sens. Spat. Inf. Sci 40, 311–315.

Prochazka, A., Kingsbury, N.G., Payner, P.J.W., Uhlir, J., 2013. Signal analysis and prediction. Springer Science & Business Media.

Raschka, S., 2018. MLxtend: Providing machine learning and data science utilities and extensions to Python's scientific computing stack. Journal of open source software 3, 638.

Rumelhart, D.E., Hinton, G.E., Williams, R.J., 1986. Learning representations by back-propagating errors. Nature 323, 533–536.

S. Sural, Gang, Q., S. Pramanik, 2002. Segmentation and histogram generation using the HSV color space for image retrieval. Presented at the Proceedings. International Conference on Image Processing, p. II–II. https://doi.org/10.1109/ICIP.2002.1040019

Sa, I., Popović, M., Khanna, R., Chen, Z., Lottes, P., Liebisch, F., Nieto, J., Stachniss, C., Walter, A., Siegwart, R., 2018. WeedMap: A large-scale semantic weed mapping framework using aerial multispectral imaging and deep neural network for precision farming. Remote Sensing 10, 1423.

Sapkota, B., Singh, V., Cope, D., Valasek, J., Bagavathiannan, M., 2020. Mapping and estimating weeds in cotton using unmanned aerial systems-borne imagery. AgriEngineering 2, 350–366.

Sapkota, B.B., Liang, L., 2020. High-resolution mapping of ash (Fraxinus spp.) in bottomland hardwoods to slow Emerald Ash Borer infestation. Science of Remote Sensing 1, 100004. https://doi.org/10.1016/j.srs.2020.100004

Shanahan, J.F., Schepers, J.S., Francis, D.D., Varvel, G.E., Wilhelm, W.W., Tringe, J.M., Schlemmer, M.R., Major, D.J., 2001. Use of remote-sensing imagery to estimate corn grain yield. Agronomy Journal 93, 583–589. https://doi.org/10.2134/agronj2001.933583x

Shaner, D.L., Beckie, H.J., 2014. The future for weed control and technology. Pest Manage. Sci. 70, 1329–1339. https://doi.org/10.1002/ps.3706

Shapiro, L., Stockman, G., 2001. Computer vision prentice hall. Inc., New Jersey.

Singh, V., Rana, A., Bishop, M., Filippi, A.M., Cope, D., Rajan, N., Bagavathiannan, M., 2020. Chapter Three - Unmanned aircraft systems for precision weed detection and management: Prospects and challenges, in: Sparks, D.L. (Ed.), Advances in Agronomy. Academic Press, pp. 93–134.

Slafer, G.A., Calderini, D.F., Miralles, D.J., 1996. Yield components and compensation in wheat: opportunities for further increasing yield potential. Increasing yield potential in wheat: breaking the barriers 101–133.

Stanković, R.S., Falkowski, B.J., 2003. The Haar wavelet transform: its status and achievements. Computers & Electrical Engineering 29, 25–44. https://doi.org/10.1016/S0045-7906(01)00011-8

Stone, M.J., Cralle, H.T., Chandler, J.M., Miller, T.D., Bovey, R.W., Carson, K.H., 1998. Above- and belowground interference of wheat (*Triticum aestivum*) by Italian ryegrass (*Lolium multiflorum*). Weed Science. 46, 438–441. https://doi.org/10.1017/S004317450009086X

Subasi, A., 2007. EEG signal classification using wavelet feature extraction and a mixture of expert model. Expert Systems with Applications 32, 1084–1093. https://doi.org/10.1016/j.eswa.2006.02.005

Swanton, C.J., Weaver, S., Cowan, P., Acker, R.V., Deen, W., Shreshta, A., 1999. Weed Thresholds. Journal of Crop Production. 2, 9–29. https://doi.org/10.1300/9785529

Tamouridou, A.A., Alexandridis, T.K., Pantazi, X.E., Lagopodi, A.L., Kashefi, J., Moshou, D., 2017. Evaluation of UAV imagery for mapping Silybum marianum weed patches. International Journal of Remote Sensing 38, 2246–2259.

Thompson, J.F., Stafford, J.V., Miller, P.C.H., 1991. Potential for automatic weed detection and selective herbicide application. Crop Protection 10, 254–259. https://doi.org/10.1016/0261-2194(91)90002-9

Tucker, K.P., Morgan, G.D., Senseman, S.A., Miller, T.D., Baumann, P.A., 2006. Identification, distribution, and control of Italian Ryegrass (*Lolium multiflorum*) ecotypes with varying levels of sensitivity to triasulfuron in Texas. Weed Technology 20, 745–750. https://doi.org/10.1614/WT-04-316R1.1

Turner, D.P., Cohen, W.B., Kennedy, R.E., Fassnacht, K.S., Briggs, J.M., 1999. Relationships between Leaf Area Index and Landsat TM Spectral Vegetation Indices across Three Temperate Zone Sites. Remote Sensing of Environment 70, 52–68. https://doi.org/10.1016/S0034-4257(99)00057-7

Welsh, J.P., Bulson, H.A.J., Stopes, C.E., Froud-Williams, R.J., Murdoch, A.J., 1999. The critical weed-free period in organically-grown winter wheat. Annals of Applied Biology 134, 315–320. https://doi.org/10.1111/j.1744-7348.1999.tb05270.x

Xue, L.-H., Cao, W.-X., Yang, L.-Z., 2007. Predicting grain yield and protein content in winter wheat at different N supply levels using canopy reflectance spectra. Pedosphere 17, 646–653. https://doi.org/10.1016/S1002-0160(07)60077-0

Yagbasanlar, T., Özkan, H., Genç, I., 1995. Relationships of growth periods, harvest index and grain yield in common wheat under Mediterranean climatic conditions. Cereal Research Communications 59–62.

Yang, C.-C., Prasher, S.O., Landry, J.-A., Ramaswamy, H.S., 2003. Development of a herbicide application map using artificial neural networks and fuzzy logic. Agricultural Systems 76, 561–574. https://doi.org/10.1016/S0308-521X(01)00106-8

Yang, M.-D., Huang, K.-S., Kuo, Y.-H., Tsai, H.P., Lin, L.-M., 2017. Spatial and spectral hybrid image classification for rice lodging assessment through UAV Imagery. Remote Sensing 9. https://doi.org/10.3390/rs9060583

Yang, W., Wang, S., Zhao, X., Zhang, J., Feng, J., 2015. Greenness identification based on HSV decision tree. Information Processing in Agriculture 2, 149–160. https://doi.org/10.1016/j.inpa.2015.07.003

Zhou, X., Zheng, H.B., Xu, X.Q., He, J.Y., Ge, X.K., Yao, X., Cheng, T., Zhu, Y., Cao, W.X., Tian, Y.C., 2017. Predicting grain yield in rice using multi-temporal vegetation indices from UAV-based multispectral and digital imagery. ISPRS Journal of Photogrammetry and Remote Sensing 130, 246–255. https://doi.org/10.1016/j.isprsjprs.2017.05.003

3.8. Table and Figures

Table 3.1. Details of various features extracted and/or computed for image classification, through several computational procedures on the pixel value of imageries. The value in parenthesis indicates number of features belonging to the feature category.

Category	Features	Description/Formula **	Reference
Original bands (3)	Blue	-	
	Green		-
	Red		
Vegetation indices (3)	Excess Green Index (ExG)	$2\times \frac{G-R-B}{R+G+B}$	Woebeccke et al. (1995)
	Triangular Greenness Index (TGI)	$-\frac{190\,(R-G)-120(R-B)}{2}$	Hunt et al. (2011)
	Visible Atmospheric Resistant Index (VARI)	$\frac{G-R}{G+R-B}$	Gitelson et al. (2002)
Color space transformed features (3)	Hue	A gradation or variety of a color	Shapiro (2001)
	Saturation	Depth, purity, or shades of the color	
	Value	Brightness intensity of the color tone	
Wavelet transformed coefficients (2)	Wavelet coefficient mean	Mean value calculated for a pixel using discrete wavelet transformation	Stanković and Falkowski (2003)
	Wavelet coefficient standard deviation	Standard deviation calculated for a pixel using discrete wavelet transformation	
Principal components (1)	Principal component 1	Principal component analysis-derived component accounting maximum amount of variance	Pearson (1901)

**Abbreviations: R, G, and B represent Red, Green, and Blue bands, respectively

Table 3.2. Various hyperparameters and several potential values for corresponding hyperparameters tested for the best performance of the custom deep neural network system using the grid search cross validation method. A total of 150 trials were conducted to obtain the best set of values.

Hyperparameter	Values	Selected Value(s)
Number of hidden layers	1,2,3,4,5	5
Nodes in hidden layers*	(20) (40, 20) (60, 40, 20) (80, 60, 40, 20) (100, 80, 60, 40, 20)	(100, 80, 60, 40, 20)
Activation function	"Rectified linear unit" "Sigmoid function"	"Rectified linear unit"
Batch size	10, 20, 30, 40, 50	20
Number of epochs	100, 300, 500	100

* The values for hyperparameter "nodes in hidden layers" were assigned with respect to "number of hidden layers".

Table 3.3. Validation samples-based accuracy statistics for 10 best feature models used for detecting Italian ryegrass in wheat. The 10 best feature models were determined through the exhaustive feature selection process. The accuracy statistics for each feature model were based on 250 samples for each user-defined class.

Feature Model #	Features Used**	Precision (%)*	Recall (%)*	F-score (%)*
1	Green, Blue, Hue, Sat, Value, TGI, ExG, PC-1	94.28 ± 4.86	94.28 ± 5.24	94.27 ± 4.96
2	Hue, Value, VARI, ExG	94.28 ± 4.50	94.28 ± 7.94	94.27 ± 5.26
3	Red, Hue, Sat, VARI, ExG, Wavelet_Mean	94.95 ± 4.58	94.91 ± 4.98	94.91 ± 4.43
4	Hue, VARI, TGI, ExG	91.53 ± 6.75	90.63 + 8.93	90.54 + 2.29
5	Green, Blue, Hue, Sat, Value, ExG, Wavelet_Mean, PC-1	95.33 ± 4.23	95.38 ± 5.07	95.36 ± 4.14
6	Red, Green, Hue, Sat, ExG, Wavelet_Std	94.45 ± 4.67	94.44 ± 5.83	94.41 ± 4.98
7	Red, Green, Hue, Sat, TGI, Wavelet_Std	95.01 ± 4.31	94.94 ± 5.5	94.91 ± 4.25
8	Sat, Value, VARI, ExG	91.74 ± 8.14	91.59 ± 9.48	91.54 ± 8.21
9	Red, Blue, Sat, VARI, ExG, Wavelet_Mean	95.01 ± 4.71	94.97 ± 5.36	94.96 ± 4.67
10	Hue, Sat, VARI, ExG	95.34 ± 4.27	95.68 ± 5.05	95.56 ± 4.11

*A single mean value calculated by averaging the values of all the user-defined classes, and standard deviation value calculated among the accuracies for each user-defined class for each feature model.

** Abbreviations: ExG-Excess Greenness Index, PC-Principal component, Sat-Saturation, TGI-Triangular Greenness Index, VARI-Visible Atmospheric Resistant Index, Wavelet_mean-Wavelet transformed coefficient mean value, Wavelet_std-Standard deviation of Wavelet transformed coefficients mean value.

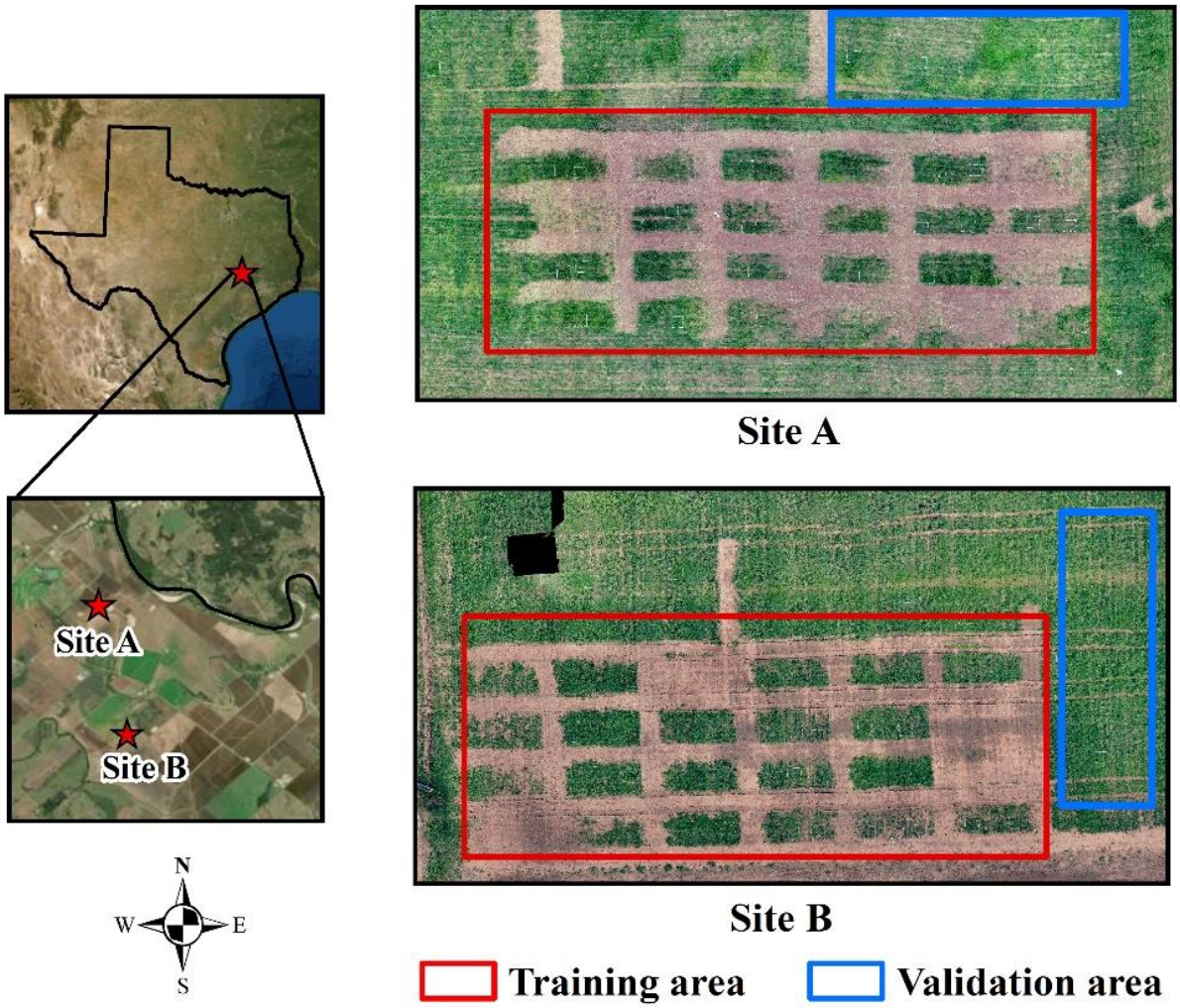

Figure 3.1. Study locations (Burleson county, Texas, U.S.) and experimental setup for detecting Italian ryegrass and evaluating the competitive response with wheat using unmanned aerial vehicle (UAV)-based aerial true color imagery (spatial resolution 3 mm/pixel). The study locations are located approximately 4 km apart and are unique in edaphic characteristics. Training area includes all the experimental units that would be used for building predictive models and validation area includes the area that would be subjected to validate the accuracy of the model.

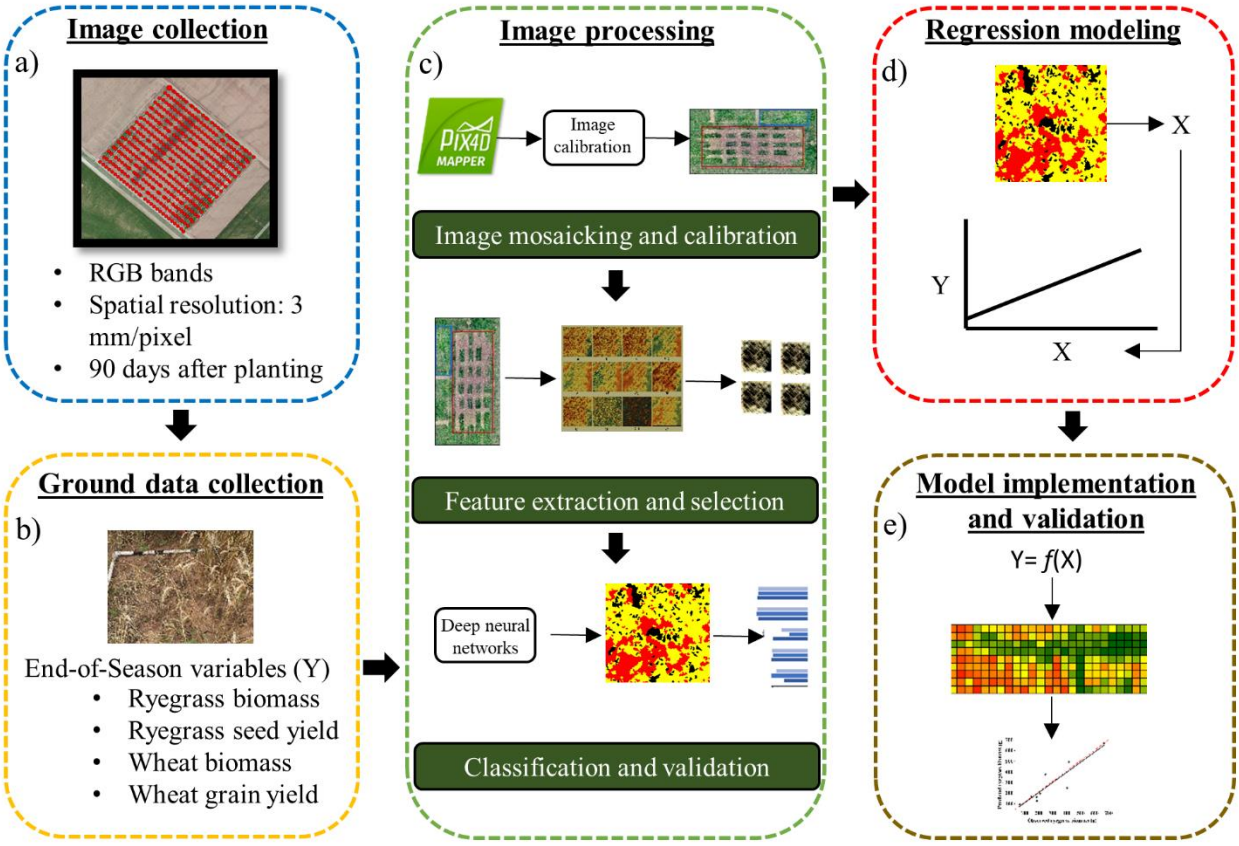

Figure 3.2. Flowchart for the overall methodology followed in this research for detecting Italian ryegrass in wheat and prediction of competitive interactions. The specific steps included (shown in dashed boxes) are: (a) image collection, (b) ground data collection, (c) image processing, (d) regression modeling, (e) model implementation and validation.

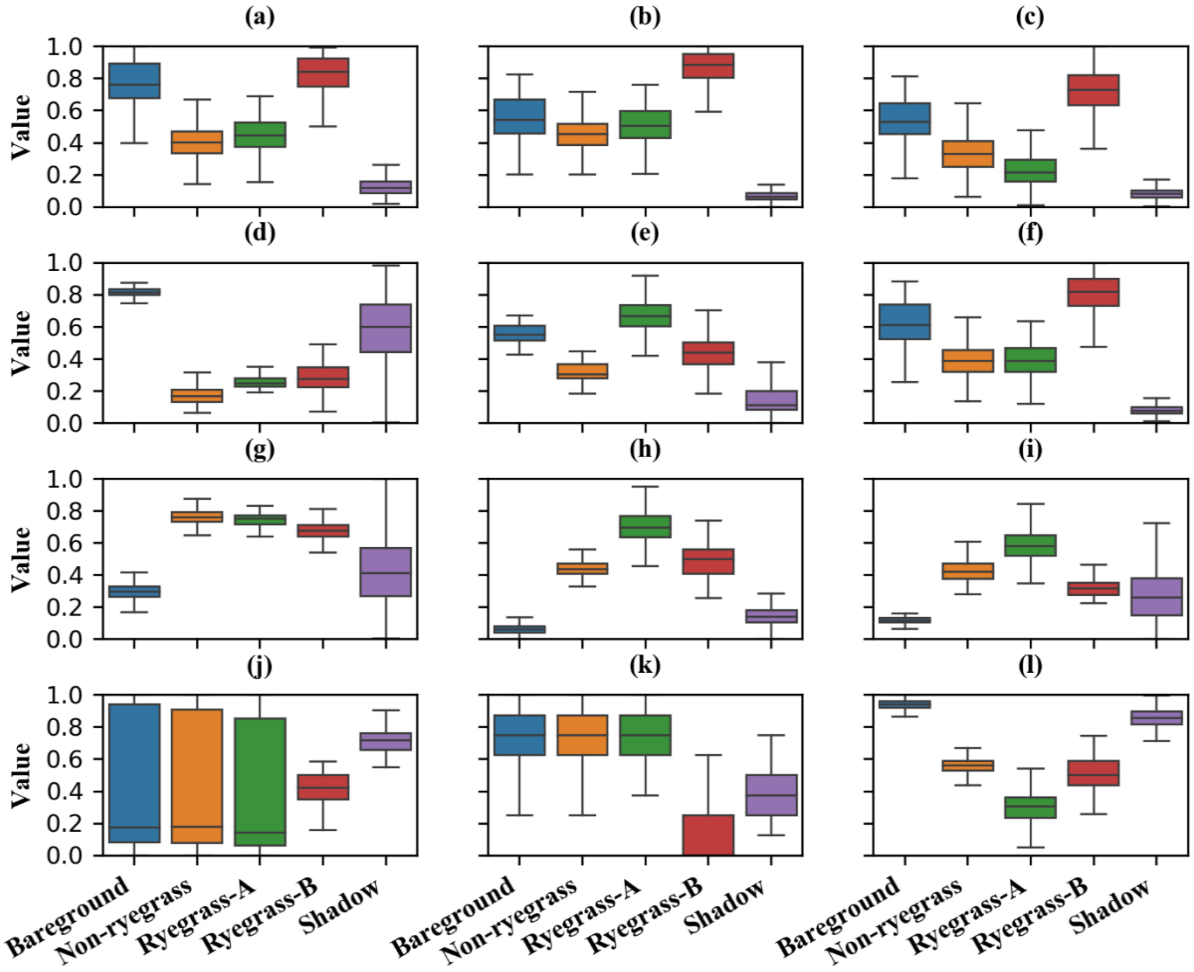

Figure 3.3. Boxplots showing the distribution of features for each of the user-defined classes, with X- and Y-axis being the user-defined classes and corresponding normalized values, respectively. The colored portion of boxplots shows inter-quartile range of the red band (a), green band (b), blue band (c), hue (d), saturation (e), value (f), Visible Atmospheric Resistant Index (g), Triangular Greenness Index (h), Excess Greenness Index (i), wavelet transformed coefficients mean (j), wavelet transformed coefficients standard deviation (k), and principal component 1 (l).

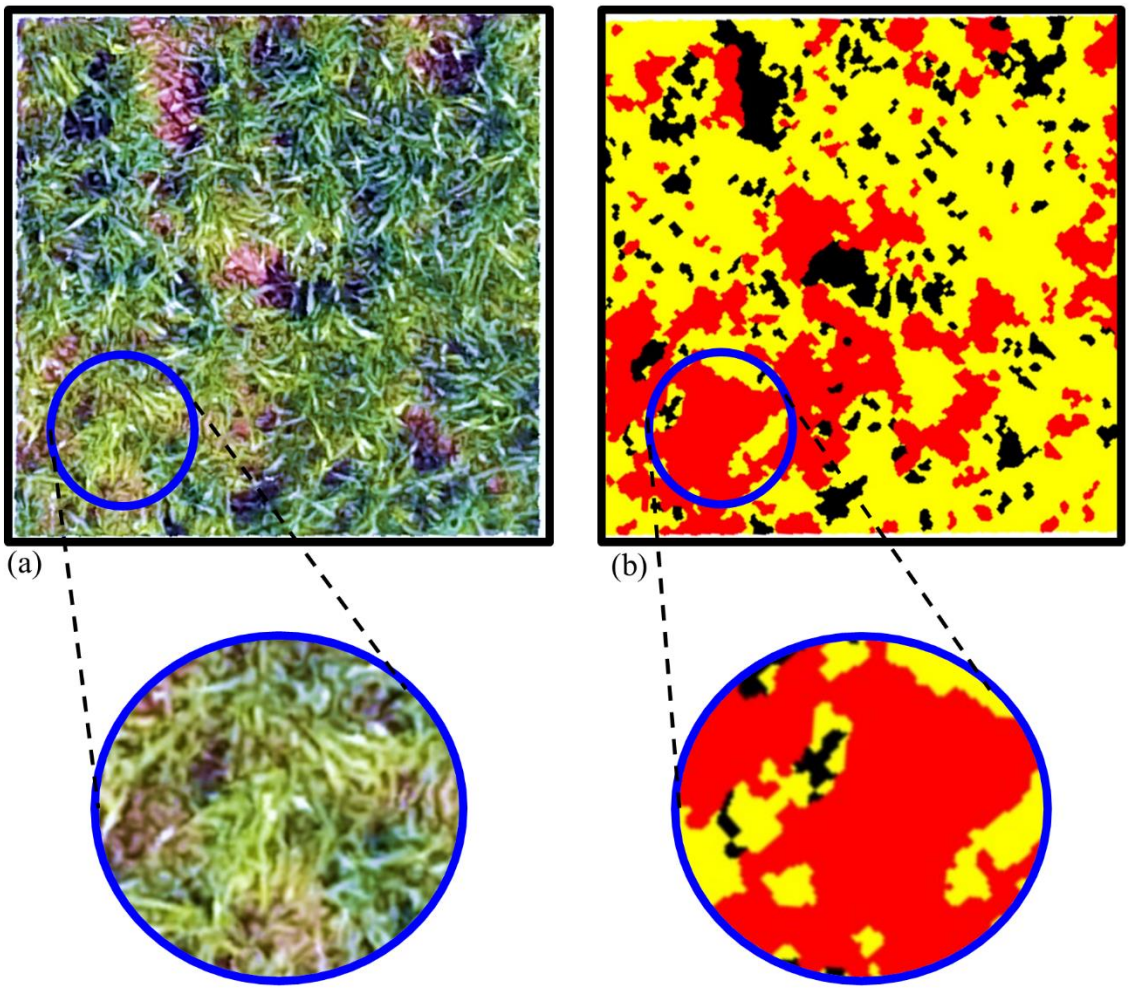

Figure 3.4. An example imagery showing Italian ryegrass coverage in wheat in a moderate density experimental unit (i.e., 1 m x 1 m quadrat) established in this study (a) and its corresponding classified map (b). The imagery for the experimental unit was classified using the best feature model determined in the study. The zoomed circles beneath the panels *a* and *b* represent a specific section of the imagery and its corresponding map. The red, yellow, and black colors in the map represent ryegrass coverage area, non-ryegrass vegetation, and baregound and shadow areas, respectively.

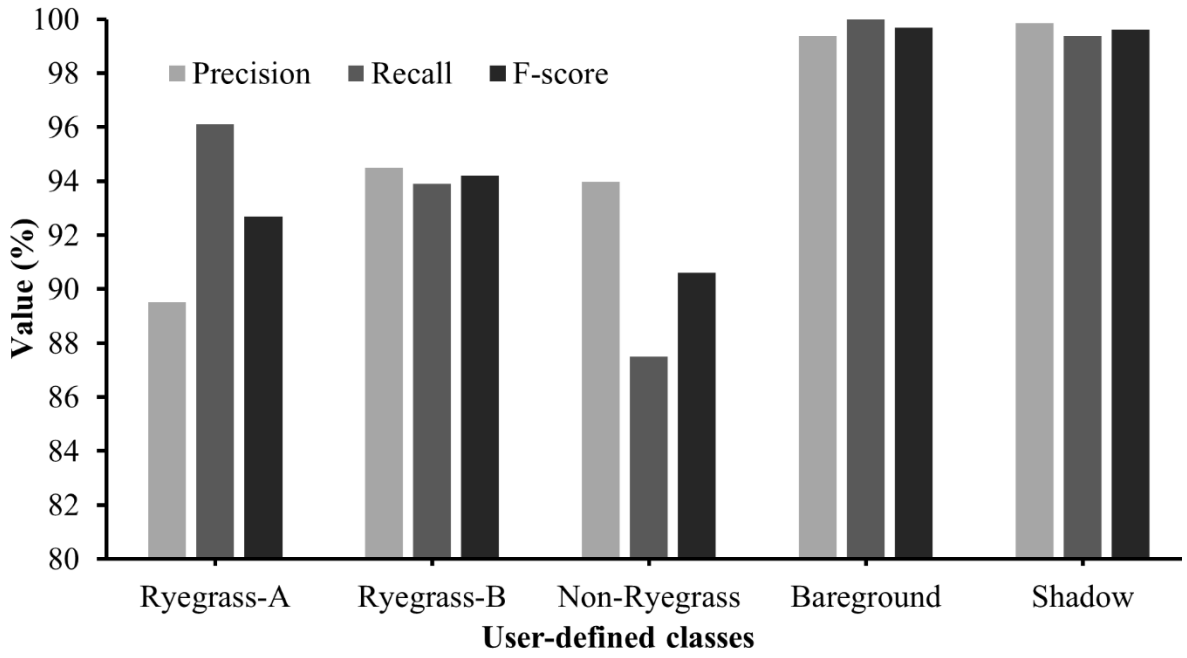

Figure 3.5. Accuracy statistics for the best model used for detecting Italian ryegrass in wheat, which combined color transformed features with vegetation indices. Precision, recall, and F-score values (%) (Y-axis) are shown for each of the five user defined class (X-axis).

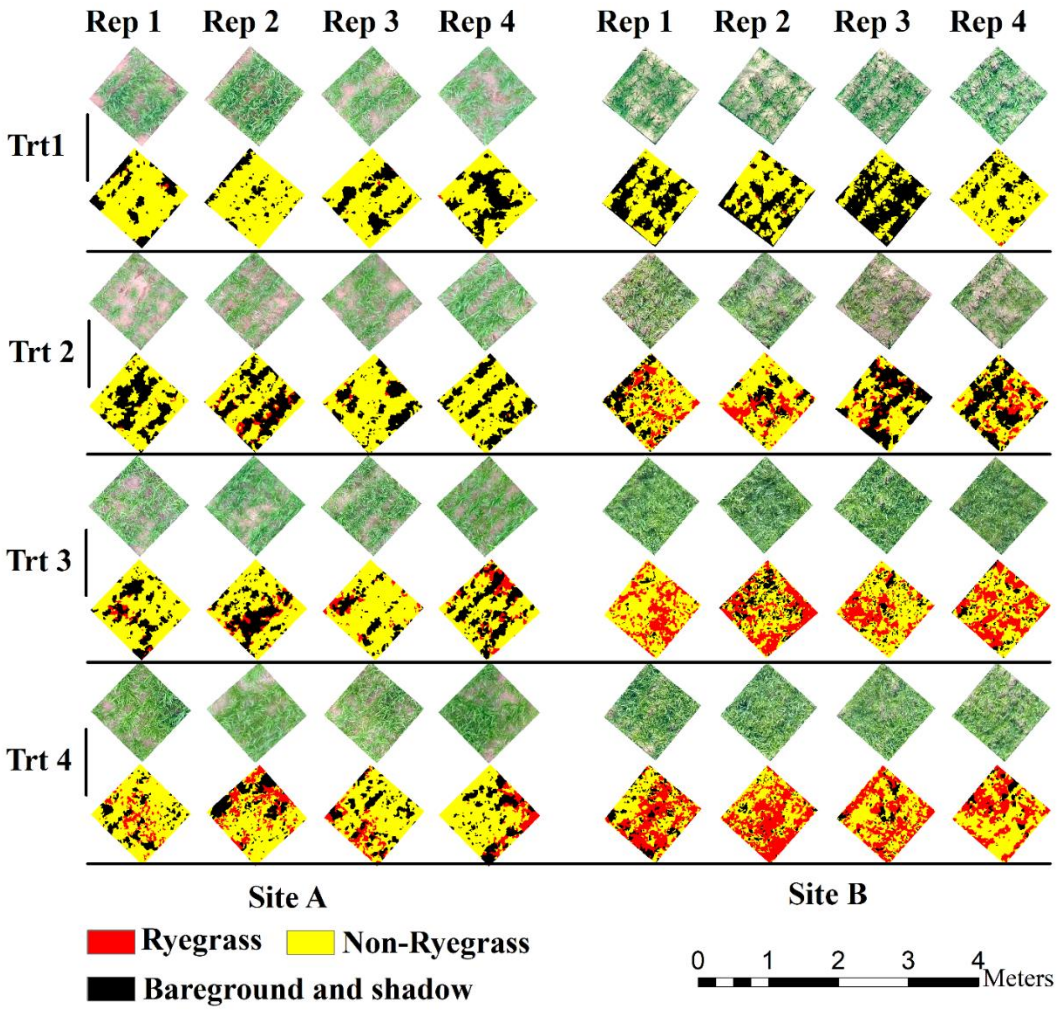

Figure 3.6. Implementation of the best model, that utilized color transformed features and vegetation indices, over training experimental units (1 m x 1 m quadrats) in both study sites (A and B) to detect and map Italian ryegrass in wheat. The figure consists of true color imagery and corresponding classified maps for the experimental units for weed-free check (Trt 1), low (Trt 2), moderate (Trt 3), and high (Trt 4) density treatments (red pixels: Italian ryegrass; yellow pixels: vegetation other than Italian ryegrass; and black pixels: bareground and shadow). Abbreviations: trt-treatments; rep-replications. Note: since each experimental unit was clipped based on the quadrat's boundary visible in the imagery and because the imagery was not perfectly ortho-rectified, the size of the clipped units may range between 1 ± 0.05 m. However, this may not affect the analysis as ryegrass canopy coverage (%) was calculated based on the total size of the unit.

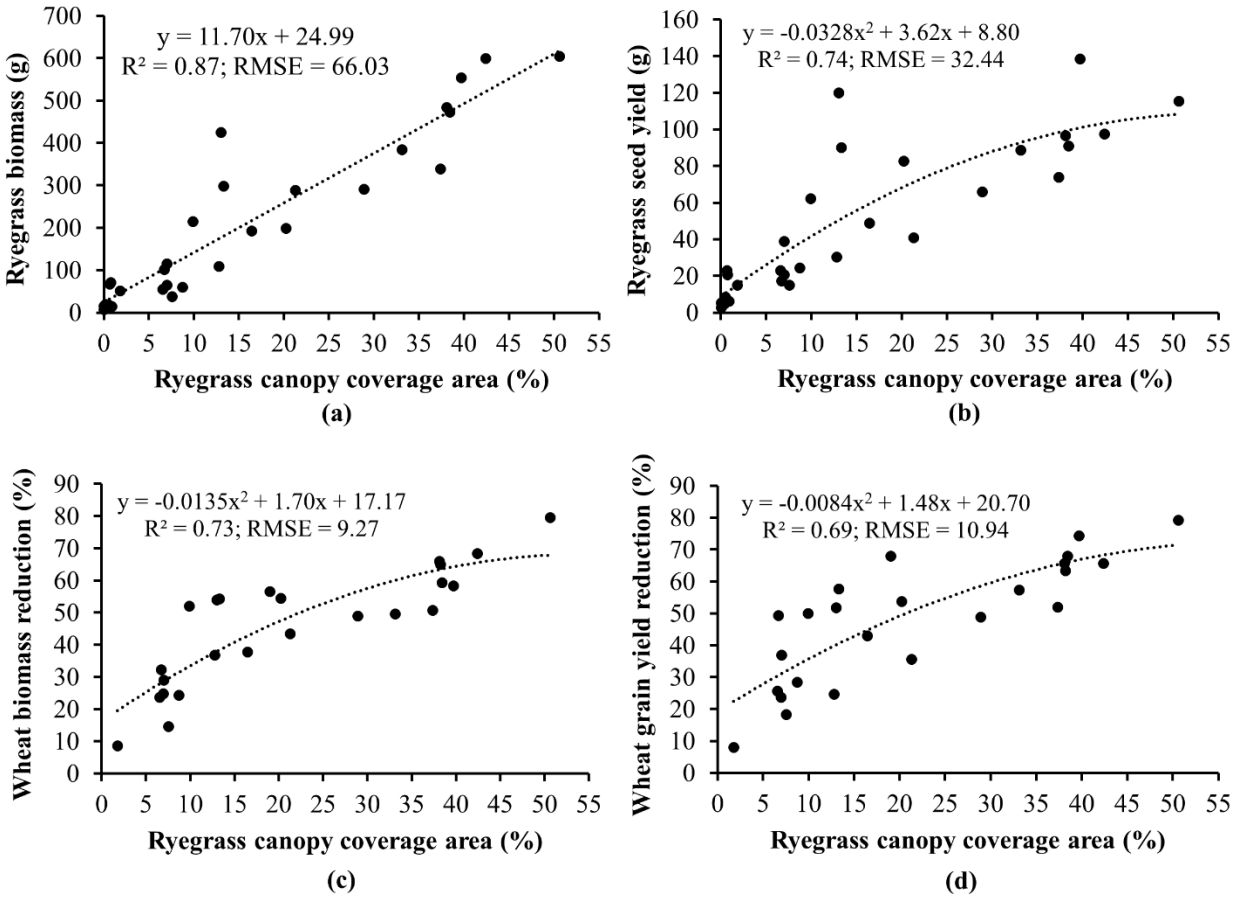

Figure 3.7. Regression analysis between Italian ryegrass canopy coverage area (%) determined using image analysis and ground truth Italian ryegrass biomass (a), Italian ryegrass seed yield (b), wheat biomass reduction (%) (c), and wheat grain yield reduction (%) (c), and wheat grain yield reduction (%) (d). The canopy coverage area (%) was derived from the classified images for experimental units (1 m × 1 m), whereas predicted variables (y-variables) were ground/field-based data.

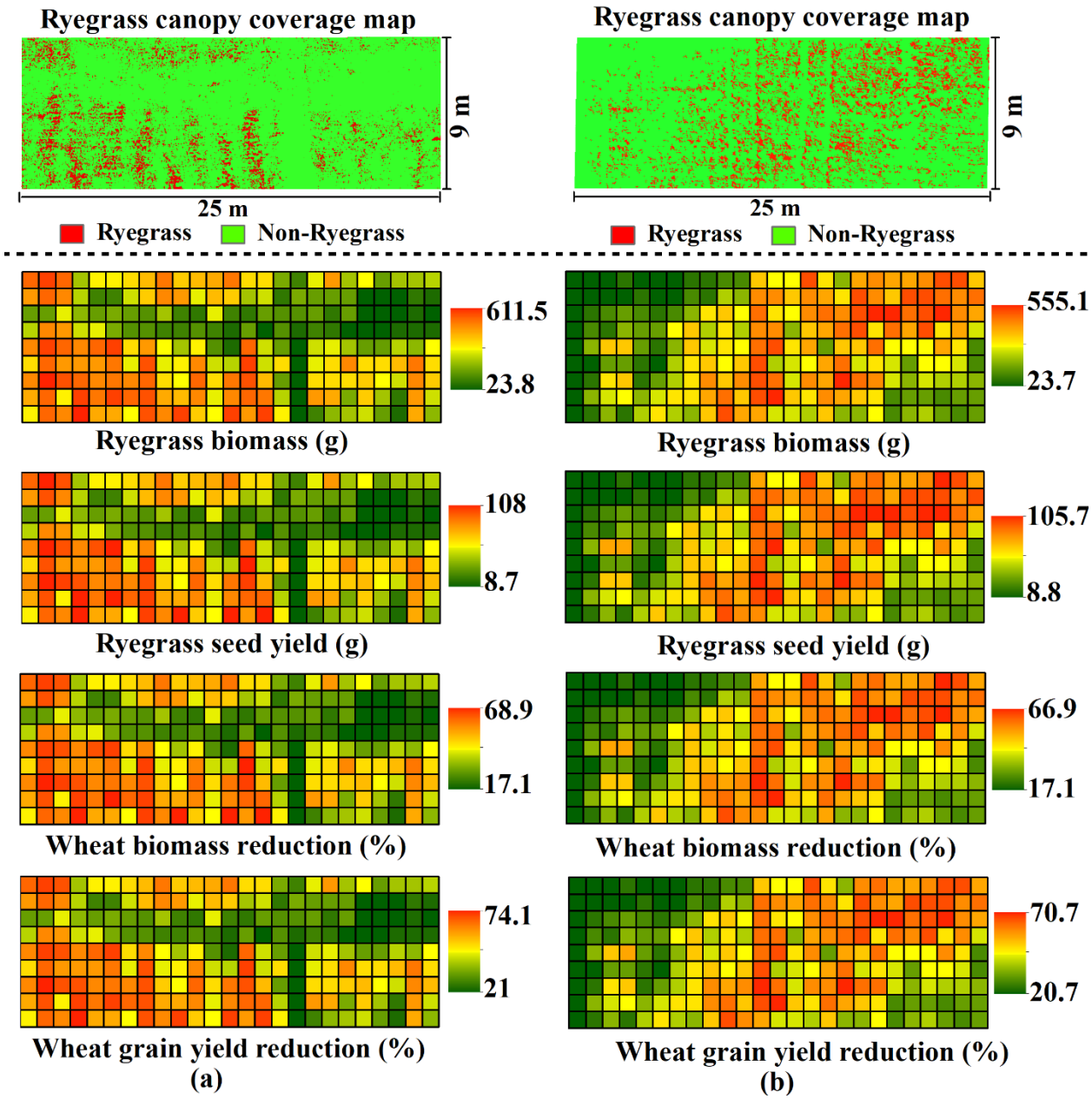

Figure 3.8. Implementation of predictive models over two validation sites (a and b). Predictions were done on 1 m × 1 m spatial grids created over the ryegrass canopy coverage map developed during early season (layers above the dashed line in the figure). The maps below the dashed line show the gradient of model predicted end-of-season estimates for different variables in each 1 m × 1 m grid.

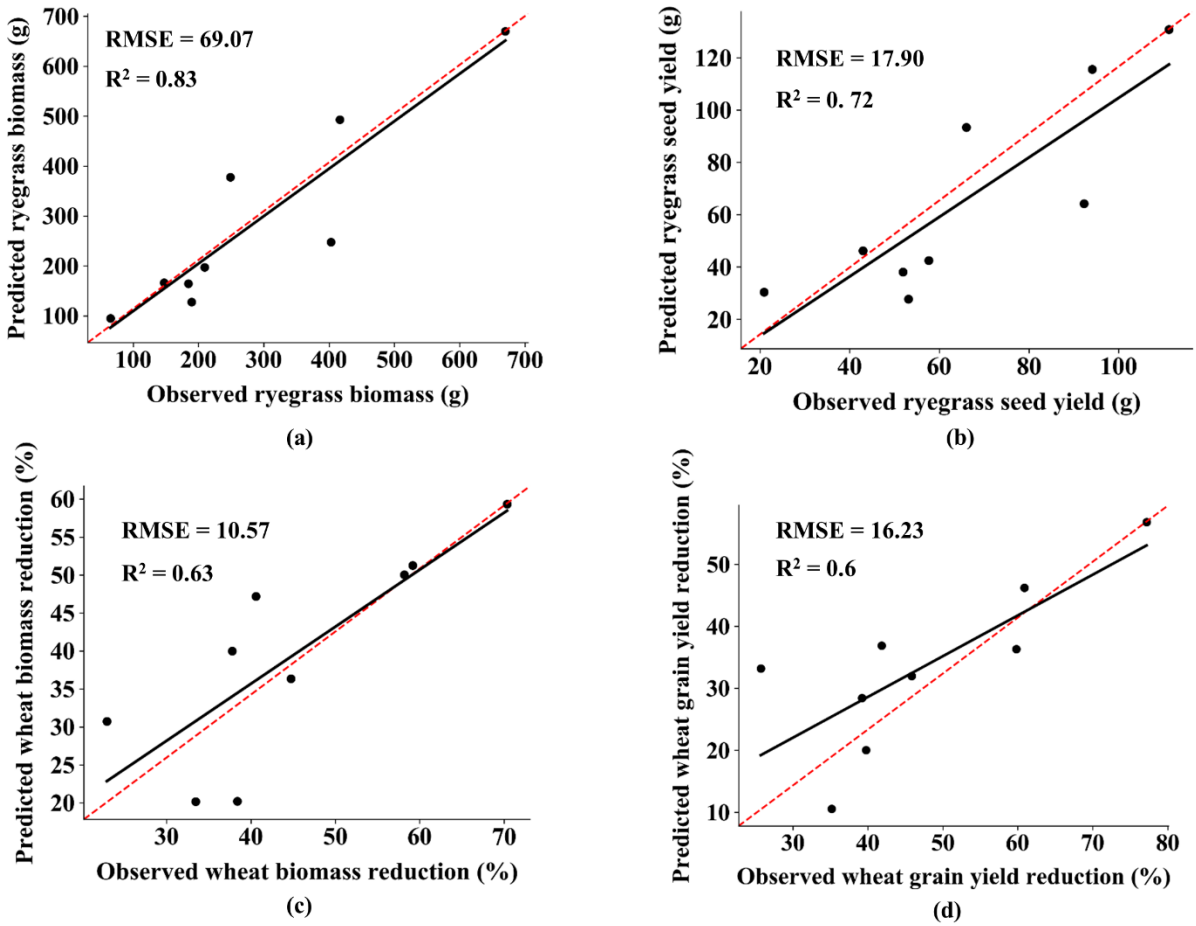

Figure 3.9. Predicted vs observed values in the validation experiment for different competition models pertaining to Italian ryegrass biomass (a), Italian ryegrass seed yield (b), wheat biomass reduction (%) (c), and wheat grain yield reduction (%) (d). The red-dashed line represents 1:1 slope line or reference diagonal line (expected values) and the black solid line represents the observed slope line between the predicted and observed datasets. The units of root mean square error (RMSE) values correspond to the units of respective predictor/observed values.

4. EVALUATING CROSS-APPLICABILITY OF WEED DETECTION MODELS ACROSS DIFFERENT CROPS IN SIMILAR PRODUCTION ENVIRONMENTS

4.1. Abstract

Convolutional neural networks (CNNs) have revolutionized the weed detection process with tremendous improvements in precision and accuracy. However, training these models is time-consuming and computationally demanding; thus, training weed detection models for every crop-weed environment may not be feasible. It is imperative to evaluate how a CNN-based weed detection model trained for a specific crop may perform in other crops. In this study, a CNN model was trained to detect morningglories and grasses in cotton at early-mid growth stage. Assessments were made to gauge the potential of the very model in detecting the same weed species in soybean and corn under two levels of detection complexity (level 1 and 2). Two popular object detection frameworks, YOLOv4 and Faster R-CNN were trained to detect weeds under two schemes: Detect_Weed (detecting at weed/crop level) and Detect_Species (detecting at weed species level). In addition, the main cotton dataset was supplemented with different amounts of non-cotton crop images to see if cross-crop applicability can be improved. Both frameworks achieved reasonably high accuracy levels for the cotton test datasets under both schemes (Average Precision: 0.83-0.88 and Mean Average Precision: 0.65-0.79). The same models performed differently over other crops under both frameworks (Average Precision: 0.33-0.83 and Mean Average Precision: 0.40-0.85). In particular, relatively higher accuracies were observed for soybean than for corn, and also for complexity level 1 than for level 2. Significant improvements in cross-crop applicability were further observed when additional corn and soybean images were added to the model training. These findings provide valuable insights into improving global applicability of weed detection models.

Keywords: deep learning, CNNs, digital technologies, precision weed control, site-specific weed control

4.2. Introduction

Weeds are major pests in agricultural landscapes that can cause serious crop yield losses (Buchanan and Burns, 1970; Nave and Wax, 1971). A multi-tactic approach to weed management has become vital to thwart herbicide-resistant weed issues in cropping systems globally (Bagavathiannan and Davis, 2018). Injudicious use of agrochemicals has been linked to negative effects on non-target organisms and the broader environment (Liu and Bruch, 2020). Under the conventional broadcast approach, weed control tactics are applied without any regard to weed distribution and densities in the field. Weeds that escape the pre-emergent herbicides or mechanical tillage typically occur sparsely across the field. In such situations, weed control tactics can instead be strictly focused on areas of weed occurrence to save resources (Berge et al., 2012). Site-specific management is expected to improve control outcomes and conserve management inputs (Beckie et al., 2019). In recent years, great efforts have been placed for developing and utilizing ground robots (Aravind et al., 2015; Kargar and Shirzadifar, 2013; Lottes et al., 2019; Sujaritha et al., 2017) and unmanned aerial systems (UAS) for site-specific weed control (Ahmad et al., 2020; Martin et al., 2020).

The precision weed control platforms ranging from ground robots to UAS-based selective spraying systems depend greatly on weed detection using computer vision techniques (Liu and Bruch, 2020; Machleb et al., 2020). The overall approach is to detect weeds in digital images and use the global positioning system coordinates of the detected objects for site-specific control operations (López-Granados, 2011). In addition to weed control, these techniques offer

tremendous opportunities for advancing weed ecology and biology research. Several image-based weed detection techniques have been proposed and implemented. Based on developments made so far, these techniques can be broadly categorized into two main groups: 1) traditional segmentation and machine learning-based techniques (Ahmed et al., 2012; García-Santillán and Pajares, 2018; Rumpf et al., 2012; Sabzi et al., 2018; Sapkota et al., 2020; Wu et al., 2011) and 2) advanced computer vision using convolution neural networks (CNNs) (Adhikari et al., 2019; Hu et al., 2021; Ma et al., 2019; Sharpe et al., 2020; Xie et al., 2021).

The CNNs are a specialized type of neural networks that are designed to extract multi-scale features and merge semantically similar features for better prediction and/or detection (LeCun et al., 2015). The use of CNNs in weed detection tasks has gained great attention lately due to their ability to learn complex features through dense and rigorous feature representations (e.g. Xie et al., 2021). The attention has been fostered by the transfer learning concept in CNN that allows sharing of common model weights from pre-trained models across different tasks (Abdalla et al., 2019; Fawakherji et al., 2019). The CNN-based object detection models have witnessed remarkable breakthroughs recently, and some of the detectors that have been widely used today for various detection tasks are Fast R-CNN (Girshick, 2015), Single-Shot Detector (Liu et al., 2016), Faster R-CNN (Ren et al., 2017), You Only Look Once (YOLO) (Redmon et al., 2016), YOLOv3 (Redmon and Farhadi, 2018), YOLOv4 (Bochkovskiy et al., 2020.), and more recently YOLOv5.

With respect to weed detection, different CNN-based detection frameworks have been successfully applied for various tasks. Gao et al. (2020) used YOLOv3 and Tiny YOLO models for detection of *Convolvulus sepium* (hedge bindweed) in *Beta vulgaris* (sugar beets) using field-collected and synthetic images. Using the same models, Jiang et al. (2020) also detected both

grass and broadleaf weed species in UAS-based Red-Green-Blue (RGB) imageries. Sharpe et al. (2020) detected goosegrass (*Eleusine indica* (L.) Gaertn.) in handheld digital camera-derived images obtained from two different horticultural crops, strawberry (*Fragaria × ananassa)* and tomato (*Solanum lycopersicum*), using YOLOv3-tiny model. Using YOLOv3, Partel et al. (2019) detected *Portulaca* spp. in pepper (*Capsicum annum*) for a precision spraying system. Yu et al. (2019a) employed DetectNet to detect dandelion (*Taraxacum officinale*), ground ivy (*Glechoma hederacea*), and spotted spurge (*Euphorbia maculata*) in perennial ryegrass (*Lolium perenne*). Hu et al. (2021) tested Faster R-CNN, DeepLabv3, and Mask R-CNN for broadleaf and grass weed detection in cotton (*Gossypium hirsutum*) and soybean (*Glycine max*) using UAS-borne high-resolution images.

Cross-applicability of the deep learning models for weed detection across different crops is vital for two important reasons. First, several weed species continuously occur in the rotational crops in a given production field (e.g. *Amaranthus palmeri* [Palmer amaranth] occurring in both soybean and corn (*Zea mays*) grown in rotation), and computer vision models should be able to detect these weeds in all crops in the production system. Secondly, it is likely that the dominant weed species might be similar across production fields within a locality, and the ability to use these models across multiple production fields might be beneficial from efficiency and economic standpoint. This is because CNN models usually require a large set of annotated training images for better performance (Gao et al., 2020; Oquab et al., 2014), which can be daunting.

When only the weeds are annotated in the images and trained for detection, the model considers crops in the same images as part of the background during the training process. Therefore, during inference, different crops may mimic different backgrounds for the same trained weeds in the images. It is therefore unclear how changes in the background (crop species

in our case) may affect weed detection accuracies for different object detection frameworks under various detection scenarios. To the best of our knowledge, no study has looked at the cross-applicability of weed detection models across three of the most popular row crops in the United States: cotton, corn, and soybean. Such an investigation can further advance our understanding of weed detection models and help unleash their full potential.

The main goal of the study was to build a model for weed detection in cotton and investigate the use of the same model for detection of the same weed spectrum in corn and soybean. This study has two specific objectives: 1) build and evaluate models for weed detection in cotton under two weed detection schemes (detection of weeds at the meta-level, and detection at the individual weed species level), and b) evaluate the performance of the cotton-based model on corn and soybean at different levels of detection complexity.

4.3. Materials and Methods

4.3.1. Study area and experimental setup

The study was conducted in 2020 and 2021 at the Texas A&M AgriLife Research farm (30°32′15″N, 96°25′35″W; elevation: 60 m). The location is characterized by a sub-tropical climate, with an average monthly maximum and minimum air temperatures during the study period (May – June) of 32.3°C and 21.3°C, respectively. Glyphosate-resistant (Roundup Ready®) cotton and glufosinate-resistant (Liberty Link®) soybean were planted in two separate strips (Figure 4.1) adjacent to each other on May 1, 2020 (for both crops), and April 20, 2021, at the seeding rates of 100,000 and 312,500 per hectare, respectively. Each crop was planted using a 4-row seed drill (row spacing: 1 m), with strip sizes of 16 m x 30 m (2020) or 8 m x 40 m (2021). In 2021, corn (Roundup Ready®) was also planted (8 m x 40 m) adjacent to these crops at a

seeding rate of 150,000 ha^{-1}. The fields were irrigated and fertilized as needed. The crops were grown following the recommended production practices for the region.

In this study, weeds that escaped preemergence and early-post emergence herbicide applications were targeted for building and testing models. To this effect, postemergence applications of appropriate herbicides were made in all three crops following standard application procedures, resulting in random escapes at sufficient densities for imaging (Table 4.1). The dominant weed species in the study area were a mix of morningglories (*Ipomoea* spp.) that composed of tall morningglory (*Ipomoea purpurea*) and ivyleaf morningglory (*Ipomoea hederacea*), Texas millet (*Urochloa texana*), and johnsongrass (*Sorghum halepense)*. Some other weed species occurred at low frequencies, including Palmer amaranth (*Amaranthus palmeri*), prostrate spurge (*Euphorbia humistrata*), and browntop panicum (*Panicum fasiculatum*). At the time of image collection, these weed species occurred at different growth stages, from cotyledon to about five true leaves.

4.3.2. Workflow

The methodological workflow for this study involved three major steps: Data collection and management, model training, and model performance evaluation on different test datasets. See Figure 4.2 for a schematic diagram showing the workflow followed in this research. The following sections describe these three steps in more detail.

4.3.3. High-resolution digital image collection

A 100-megapixel FUJIFILM GFX100 medium format mirrorless RGB imaging camera was integrated with a multi-copter drone, Hylio AG-110 (Hylio Inc., TX, USA) to capture high-resolution aerial images of the crop fields (Figure 4.1). The images were captured by the drone operating at 4.9 m aboveground level and a speed of 0.61 m/s. The FUJIFILM GF 32-64 mm f/4

R LM WR lens was set at a focal length of 64 mm, shutter speed at 1/4000s, ISO at 1250, and f-stop at 8, which resulted in high-quality images with a spatial resolution of 0.274 mm/pixel at the given flying height. Under such configurations, image resolution and quality were sufficient for young grass seedlings to be recognized in the images. However, the wind thrust (i.e. downwash) from the drone operation impacted some plants, causing them to look unreal in the images. They were excluded from the dataset before further analysis. All the images were stored in standard PNG format at 16-bit depth. Table 4.1 describes the details of the different image datasets collected in the study.

A total of three flights were made to capture images for all the crops in 2020 and 2021. Two image datasets for each crop (Cotton 1 & Cotton 2, Soybean 1 & Soybean 2, and Corn 1 & Corn 2) were acquired (Table 4.1). For each crop, the second image dataset (e.g. Cotton 2) differed from the first dataset with respect to crop growth stage, weed density, and image acquisition conditions. Cotton 1 was the prime dataset for this study as this consisted of cotton-weed images that were used for building the main model. This dataset was split into training (hereafter referred to as "Train100"), validation, and test datasets. Soybean 1 and Corn 1 datasets were also partitioned similarly to supplement training and validation images to Train100 during cross-applicability improvements later on. All images in Cotton 2, Soybean 2, and Corn 2 were used for testing purposes. Hereafter, these test datasets are referred to as "Cot1", "Cot2", "Soy1", "Soy2", "Corn1", and "Corn2" for respective crops.

4.3.4. Weed detection

4.3.4.1. Image annotations

For this study, the images were annotated and recorded in COCO format as this format is inter-changeable to several formats quickly and easily. The VGG VIA image annotator (Datta

and Zisserman, 2019) was used to annotate the weeds with bounding boxes in each image. The annotations were recorded for three categories: morningglories (MG), grasses (Grass), and other weed species (Other). Both Texas millet and johnsongrass seedlings were labeled as "Grass" during annotation as classifying them was not the scope of this study.

4.3.4.2. Weed detection in cotton

With respect to the first objective, i.e. develop and evaluate models for weed detection in cotton, the detection frameworks were trained with Train100. Train100 comprised of 8,580 annotations altogether, out of which MG, Grass, and Other represented 19.3, 79.5, and 1.2%, respectively (Table 4.2). Two popular object detection frameworks, YOLOv4 and Faster R-CNN, were used in this study. YOLOv4 is the 4th subsequent version of the YOLO (Redmon et al., 2016), developed recently by Bochkovskiy et al. (2020). This framework is a one-stage object detector that divides images into several grids and calculates the probabilities that the cell grids belong to a certain class by computing several feature maps. The bounding boxes are then predicted based on grids with the highest probability for the respective classes. The detector sees the entire image during training and inferences for encoding contextual information about classes. Faster R-CNN is the subsequent version of Fast R-CNN (Girshick, 2015) developed by Ren et al. (2017). In contrast to the YOLO frameworks, Faster R-CNN is a two-stage object detector composed of two modules working together. The first module is a Region Proposal Network (RPN) that proposes several candidate regions in the image. The second module is the detector that first extracts features from dense feature maps for the regions selected during RPN and then calculates the confidence score for each region that contains the object of interest (Girshick, 2015).

On-the-fly augmentation of data was carried out for both the frameworks. The 'mosaic' augmentation (Bochkovskiy et al., 2020) was enabled for YOLOv4, whereas the 'flip and resize' augmentation was performed with the default data loader when training Faster R-CNN. Pre-trained models as provided by the github sources (https://github.com/facebookresearch/detectron2 for Faster R-CNN and https://github.com/AlexeyAB/darknet for YOLOV4 for YOLOv4) were used for model initialization. A mini-batch Stochastic Gradient Descent method was used for model loss optimization for both frameworks. Faster R-CNN was trained for 50,000 iterations whereas YOLOv4 was trained for 6,000 epochs. The definition for *iterations* and *epochs* for these frameworks implies different meanings and are explained in their respective github documentation resource. The model weights were saved after every certain number of iterations or epochs so that the weight resulting in the highest validation accuracy can be chosen at the end for further analysis. Because of the differences in their detection mechanisms, these two frameworks could provide different results for the same detection problem. Hence, evaluation of these two frameworks can provide valuable insights into what level of accuracy can be expected for the given detection problem.

Hereafter, the model trained with Train100 is referred to as the "main cotton model". Two different schemes were designed for weed detection. In the first scheme, hereafter referred to as "Detect_Weed", frameworks were trained to detectweeds at the meta-level irrespective of the species. The label names for MG, Grass, and Other were merged and labeled as "Weed" while training under this scheme. However, in the second scheme, hereafter referred to as "Detect_Species", frameworks were trained to detect weeds at the species level. For training this scheme, the original annotation dataset that had separate labels for MG, Grass, and Other were

used. These schemes have different significance depending on how they are utilized for management. Currently, most of the mechanical platforms for real-time weed control employ "Detect_Weed" scheme for precision control actions (Gai et al., 2020). In most of the existing commercial platforms, detectors are trained to only detect weeds, but not required to classify them at the species level, as the weeds are pulled, zapped, or clipped regardless of species in these platforms. However, selective herbicide spray systems would require detection and classification of individual weeds for species-specific herbicide input. Hence, it may be informative to investigate how these two frameworks behave under these weed detection schemes.

4.3.4.3. Cross-crop applicability analysis

With respect to the second objective, i.e. assess the scope and prospects for applying the main cotton models to corn and soybean, the performance of the main cotton models was evaluated for each test dataset. In addition, the four non-cotton test datasets (i.e. Soy1, Soy2, Corn1, and Corn2) were grouped into two complexity levels based on their similarity in weed pressure conditions and image acquisition environment. It was assumed that these factors would have more influence than the similarity between crops. Thus, Soy1 and Corn1 were grouped under complexity level 1 while Soy2, and Corn2 under level 2. Cot2 was not grouped under any complexity level, but was rather considered as a replicate of Cot1. In the complexity level 1, the Soy1 and Corn1 differed from the Cotton 1 dataset only for the background crop species, whereas the weed density, growth stages of weeds, and image acquisition conditions were similar. In the complexity level 2, the datasets differed not only for the background crop species, but also for weed density, growth stages of weeds, and light conditions; these differences constitute a higher level of complexity to the weed detection process. Evaluations with these two

complexity levels advance our understanding of the model performances under various environments.

4.3.4.4. Cross-crop applicability improvement with training size expansion

The third objective was to test if supplementing Train100 with additional training images from Soybean 1 and Corn 1 image datasets improves prediction for corn and soybean. As the frameworks were trained to recognize only the weeds and consider crops as part of the background, changes in crop species might confuse the frameworks as to what comprises the background. This confusion intensifies when the frameworks infer upon crop species that were never seen before. Due to this situation, it was assumed that exposing these unseen crops to the frameworks might help boost the confidence score for background. It was more desirable to achieve considerable improvement in the performance with a minimal number of Soybean 1 and Corn 1 images. For this purpose, ten additional training datasets were prepared by randomly selecting an equal proportion of soybean and corn images and adding them to the main train dataset (i.e. Train100) such that the new dataset size didn't exceed 150% of the Train100 size (Table 4.2). Both frameworks were trained independently using ten different training datasets listed in Table 4.2 under the two detection schemes and were validated against test datasets. The same pre-trained models provided by the github source were used for model initialization for each training dataset. Moreover, configurations were also kept the same for these two frameworks.

4.3.4.5. Accuracy metrics for performance evaluation

The standard performance metric called Mean Average Precision (mAP) was calculated to assess the performance of weed detection under Detect_Species, whereas Average Precision (AP) was used as the performance metric for Detect_Weed. In recent years, these metrics have

been frequently used to assess the accuracy of object detection tasks. mAP is a mean of AP calculated for each class to be detected/predicted by the model. AP for each class is calculated as the area under a precision-recall curve. The area is determined in two stages. First, the recall values are evenly segmented to 11 parts starting from 0 to 1. Second, the maximum precision value is measured at each level of recall and averaged to determine AP (Equation 1).

$$\text{AP} = \frac{1}{11}\sum_{r \in \{0,0.1,0.2\ldots1\}} p_{max}(r) \qquad \text{(Equation 1)}$$

where p_{max} represents maximum precision measured at respective recall (r) level.

Precision and recall values are in turn calculated using the Equations 2 and 3, respectively.

$$\text{Precision} = \frac{TP}{TP + FP} \qquad \text{(Equation 2)}$$

$$\text{Recall} = \frac{TP}{TP + FN} \qquad \text{(Equation 3)}$$

where TP, FP, and FN denote true positive, false positive, and false negative samples, respectively.

True positives, false positives, and false negatives are identified with the help of the Intersection over Union (IoU) ratio. This ratio is calculated by comparing the ground truth box with the model predicted box. If the ratio is above the user-defined threshold, the predicted box is labeled as TP. In this study, the threshold for IoU was set to 0.5. The mAP value ranges between 0 to 1, with 0 indicating null accuracy and 1 indicating perfect accuracy. Only the AP for MG and Grass were averaged to calculate mAP under Detect_Species. AP for Other were found to be very low due to a very small test sample size during the evaluation which led to non-representative mAP values; thus, the accuracy for Other category was excluded during the evaluation process for both frameworks and schemes.

4.4. Results & Discussion

4.4.1. Performance of the main cotton model over cotton test datasets

Two popular object detection neural networks, YOLOv4 and Faster R-CNN were trained to detect weeds in cotton and non-cotton crops. Train100 was used to build two cotton-weed detection models under different detection schemes for each framework. Both YOLOv4 and Faster R-CNN provided reasonably fair accuracy levels under both detection schemes for Cot1 (Table 4.3). Under Detect_Species, AP was higher for MG compared to Grass. Although grasses were visible to naked eyes and also discernible in the images, the model failed to detect a few grass instances. On the contrary, the model led to over-detection (i.e. more plants were predicted than what was present) when these grasses had multiple tillers spread out. Lottes et al. (2018) also observed lower AP for grasses compared to broadleaves when they tested their weed detection model on UAV imageries. However, the opposite was true when they tested on images collected using a ground robot.

When the same models were tested over the second cotton dataset (i.e. Cot2) collected in 2021, the AP & mAP values declined by 12.5% & 14.5% and 11.7% & 22.5% for YOLOv4 and Faster R-CNN, respectively. Unlike Cot1, AP was higher for Grass than for MG for both frameworks under Detect_Species. It should be noted that Cot2 differed from Cot1 in three aspects: 1) Cot2 had a relatively higher density of weeds and the median size of MG and Grass differed from that of Cot1, 2) some of the cotton plants in Cot2 had slightly different visual appearance due to herbicide drift, and 3) the illumination conditions for Cot2 was slightly darker than that of Cot1. Hu et al. (2021) suggested that illumination conditions can affect weed detection accuracy. With respect to herbicide drift impact, Suarez et al. (2017) found in cotton that drift can lead to a significant change in the spectral behavior of the crop. All these reports

indicate that morphological, agronomical, and illumination differences can be attributed to the lower accuracy levels observed for Cot2.

Very few studies have looked at weed detection and mapping in cotton. Alchanatis et al. (2005) used rank order algorithms and neighborhood operations to detect broadleaves and grass weeds in cotton. With their approach, 86% of the true weed area was correctly identified, with only 14% misclassified as cotton. Lam et al. (2002) developed an early growth stage weed control system for cotton. Using morphological analysis such as binarization and erosion, their system was able to correctly identify and spray 88.8% of the weeds. On a different note, both frameworks used in this study have been already used in other weed detection studies. For example, Gao et al. (2020) employed YOLOv4 and Tiny YOLO to detect field bindweed (*Convolvulus sepium*) in sugar beet (*Beta vulgaris*) fields. They used synthetic images in addition to real images to train the framework and obtained an mAP_{50} value of 0.829 for field bindweed detection. Osorio et al. (2020) used YOLOv3 and other object detection frameworks for weed detection in commercial lettuce crops and obtained an overall accuracy of 89% with YOLOv3. Using the Faster R-CNN framework with the Inception_ResNet-V2 backbone, Le et al. (2020) achieved an $mAP_{0.50}$ value of 0.55 for detection of wild radish (*Raphanus raphanistrum*) and capeweed (*Arctotheca calendula*) in barley. The overall accuracy obtained in this study for weed detection compares well with reported accuracies by past studies.

4.4.2. Cross-crop applicability of main cotton models

The main cotton models were also applied over non-cotton test datasets (i.e. Soy1, Soy2, Corn1, and Corn2) under both detection schemes. The main goal was to see if one crop-based weed detection model can be used to detect the same weeds in other crop species under similar or different agronomic and image acquisition conditions. The detection results by both

frameworks for different test datasets under Detect_Species and Detect_Weed are shown in Figures 4.3 and 4.4, respectively for qualitative evaluation. The Detect_Species cotton model performed satisfactorily for Soy1 and Soy2 datasets, while not so effectively for Corn1 and Corn 2 datasets. The Detect_Weed model performed the same way except that AP was higher for Corn1 but not for Soy2. The significant difference in performance between Faster R-CNN and YOLOv4 for Soy2 under Detect_Weed is notable. In this regard, YOLOv4 predictions on Soy2 images were further investigated. Several MG were not detected by the model, resulting in many false negatives. AP/mAP for non-cotton test datasets was not better than that of Cot1 for both frameworks. Among non-cotton test datasets, the highest AP/mAP was obtained for Soy1 for both frameworks (Table 4.3). Further, in general, the model performed relatively better on complexity level 1 than level 2 (Figure 4.5). The difference in performance was more obvious under Detect_Weed for both frameworks.

It was notable that Soy1 yielded higher AP/mAP values than Cot2 for both frameworks under both schemes. The authors could think of two reasons for this outcome: Soy1 had similar weed density and sizes to that of Train100; further, Soy1 and Train100 datasets were acquired at the same time, and hence illumination conditions were exactly the same. Here, higher accuracy for Soy1 suggests that illumination conditions and weed density can impose more influence on the detection accuracy. In general, higher accuracies were obtained for soybean datasets compared to corn datasets. The main reason could be the confusion between Grass and corn plants. A few instances of corn plants were detected as Grass by the model as they looked similar during early growth stages. Such misclassification was also observed when corn was distinctively larger than grasses. This suggests that the model may have focused more on the canopy structure than canopy size. Further, the detection performances between complexity

levels were in line with our expectations. The primary reason for higher accuracy with complexity level 1 was the similar illumination conditions and weed density to the training dataset, i.e. Train100 as compared to the level 2 test datasets.

4.4.3. Cross-crop applicability improvement with additional non-cotton image datasets

Train100 was supplemented with different amounts of training images from Soy1 and Corn1 to generate various training datasets. These datasets were used to train new models under two detection schemes and finally, the built models were tested over cotton and non-cotton test datasets. Both frameworks showed general increments in accuracy with the addition of non-cotton crop images under both detection schemes (Figure 4.6). The rate of increment, however, varied across test datasets, frameworks, and detection schemes (Table 4.4). The trend was relatively smoother for Faster R-CNN compared to YOLOv4 for all test datasets. The increment was the highest for Corn2 and the lowest for either of the cotton test datasets for both frameworks and detection schemes. AP/mAP for test datasets under each complexity level were averaged along with Cot1 values to calculate average AP/mAP (Figure 4.7). The trend was smoother for Faster R-CNN compared to YOLOv4 for all complexity levels.

4.4.4. Scope and limitations of the study

Cross-crop applicability assessments conducted in this study provides useful insights into how models can be generalized for broad application. Such generalization could save enormous efforts and resources and help make rapid progress towards effective site-specific weed management. Cross-applicability has become an absolute necessity owing to the huge data requirements by the CNN models for a given crop-weed environment. Often, a significant amount of data resources is used to train a weed detection model for a single crop environment. For example, Yu et al. (2019) used a total of 29,000 images to train a model that could detect

multiple weeds in perennial ryegrass. Czymmek et al. (2019) trained a model to detect weeds in organic carrot farms using 2500 images. It is increasingly important to focus on how these data resources can be exploited strategically for maximizing efficiency and productivity. By testing the approach of data supplementation, this study demonstrated that cross-crop applicability can be improved with such tactics.

It should be noted that this study evaluated CNN model cross-applicability for crops that had similar weed compositions. The cross-crop applicability findings from this study do not apply to crops differing in weed species composition. In other words, the models would fail to perform if applied over soybean and corn infested with other weed species. A single crop-based model may not be effectively applied at regional scales where weed composition differs. Furthermore, not all the hyperparameters for both frameworks used in the study were tuned, but rather used as defaults in the settings. The reported accuracies may change if parameters are tuned.

4.5. Conclusions

The study explored two popular object detection frameworks under two useful detection schemes for weed detection in cotton. The study also evaluated the feasibility of cross-crop applicability of the cotton model and experimented with several amounts of non-cotton images to improve cross-applicability. Based on the results, the following main conclusions could be derived:

a. The cotton model achieved reasonably high weed detection accuracy in cotton test datasets.

b. The cotton model achieved a fair level of accuracy on non-cotton crops infested with similar weed compositions. On average, the performance was better for soybean than for corn.

c. The cross-crop applicability was improved (AP/mAP: + 3.61% to 127.27%) when Train100 was supplemented with non-cotton images.

The outcomes of this study are expected to advance our understanding of cross-crop applicability of weed detection models. Such understanding will guide our efforts towards optimal use of data resources and accelerate weed detection, mapping, and site-specific management in agricultural systems. In the future, CNN model cross-applicability will be assessed for additional crops and different levels of complexities.

4.6. References

Abdalla, A., Cen, H., Wan, L., Rashid, R., Weng, H., Zhou, W., He, Y., 2019. Fine-tuning convolutional neural network with transfer learning for semantic segmentation of ground-level oilseed rape images in a field with high weed pressure. Computers and Electronics in Agriculture 167, 105091. https://doi.org/10.1016/j.compag.2019.105091

Adhikari, S.P., Yang, H., Kim, H., 2019. Learning semantic graphics using convolutional encoder–decoder network for autonomous weeding in paddy. Frontiers in Plant Science 10. https://doi.org/10.3389/fpls.2019.01404

Ahmad, F., Qiu, B., Dong, X., Ma, J., Huang, X., Ahmed, S., Ali Chandio, F., 2020. Effect of operational parameters of UAV sprayer on spray deposition pattern in target and off-target zones during outer field weed control application. Computers and Electronics in Agriculture 172, 105350. https://doi.org/10.1016/j.compag.2020.105350

Ahmed, F., Al-Mamun, H.A., Bari, A.S.M.H., Hossain, E., Kwan, P., 2012. Classification of crops and weeds from digital images: A support vector machine approach. Crop Protection 40, 98–104. https://doi.org/10.1016/j.cropro.2012.04.024

Alchanatis, V., Ridel, L., Hetzroni, A., Yaroslavsky, L., 2005. Weed detection in multi-spectral images of cotton fields. Computers and Electronics in Agriculture 47, 243–260. https://doi.org/10.1016/j.compag.2004.11.019

Aravind, R., Daman, M., Kariyappa, B.S., 2015. Design and development of automatic weed detection and smart herbicide sprayer robot, in: 2015 IEEE Recent Advances in Intelligent Computational Systems (RAICS). Presented at the 2015 IEEE Recent Advances in Intelligent Computational Systems (RAICS), pp. 257–261. https://doi.org/10.1109/RAICS.2015.7488424

Bagavathiannan, M.V., Davis, A.S., 2018. An ecological perspective on managing weeds during the great selection for herbicide resistance. Pest Management Science 74, 2277–2286. https://doi.org/10.1002/ps.4920

Beckie, H.J., Ashworth, M.B., Flower, K.C., 2019. Herbicide resistance management: recent developments and trends. Plants 8, 161. https://doi.org/10.3390/plants8060161

Berge, T.W., Goldberg, S., Kaspersen, K., Netland, J., 2012. Towards machine vision based site-specific weed management in cereals. Computers and Electronics in Agriculture 81, 79–86. https://doi.org/10.1016/j.compag.2011.11.004

Bochkovskiy, A., Wang, C.-Y., Liao, H.-Y.M., 2020. YOLOv4: Optimal speed and accuracy of object detection. arXiv:2004.10934 [cs, eess].

Buchanan, G.A., Burns, E.R., 1970. Influence of weed competition on cotton. Weed Science 18, 149–154. https://doi.org/10.1017/S0043174500077560

Czymmek, V., Harders, L.O., Knoll, F.J., Hussmann, S., 2019. Vision-based deep learning approach for real-time detection of weeds in organic farming, in: 2019 IEEE International Instrumentation and Measurement Technology Conference (I2MTC). Presented at the 2019 IEEE International Instrumentation and Measurement Technology Conference (I2MTC), pp. 1–5. https://doi.org/10.1109/I2MTC.2019.8826921

Dutta, A., Zisserman, A., 2019. The VIA annotation software for images, audio and video. Proceedings of the 27th ACM International Conference on Multimedia 2276–2279. https://doi.org/10.1145/3343031.3350535

Fawakherji, M., Youssef, A., Bloisi, D., Pretto, A., Nardi, D., 2019. Crop and weeds classification for precision agriculture using context-independent pixel-wise segmentation, in: 2019 Third IEEE International Conference on Robotic Computing (IRC). Presented at the 2019 Third IEEE International Conference on Robotic Computing (IRC), pp. 146–152. https://doi.org/10.1109/IRC.2019.00029

Gai, J., Tang, L., Steward, B.L., 2020. Automated crop plant detection based on the fusion of color and depth images for robotic weed control. Journal of Field Robotics 37, 35–52. https://doi.org/10.1002/rob.21897

Gao, J., French, A.P., Pound, M.P., He, Y., Pridmore, T.P., Pieters, J.G., 2020. Deep convolutional neural networks for image-based *Convolvulus sepium* detection in sugar beet fields. Plant Methods 16, 29. https://doi.org/10.1186/s13007-020-00570-z

García-Santillán, I.D., Pajares, G., 2018. On-line crop/weed discrimination through the Mahalanobis distance from images in maize fields. Biosystems Engineering 166, 28–43. https://doi.org/10.1016/j.biosystemseng.2017.11.003

Girshick, R., 2015. Fast R-CNN. Presented at the Proceedings of the IEEE International Conference on Computer Vision, pp. 1440–1448.

Hu, C., Sapkota, B.B., Thomasson, J.A., Bagavathiannan, M.V., 2021. Influence of image quality and light consistency on the performance of convolutional neural networks for weed mapping. Remote Sensing 13, 2140. https://doi.org/10.3390/rs13112140

Jiang, H., Zhang, C., Qiao, Y., Zhang, Z., Zhang, W., Song, C., 2020. CNN feature based graph convolutional network for weed and crop recognition in smart farming. Computers and Electronics in Agriculture 174, 105450. https://doi.org/10.1016/j.compag.2020.105450

Kargar B., A.H., Shirzadifar, A.M., 2013. Automatic weed detection system and smart herbicide sprayer robot for corn fields, in: 2013 First RSI/ISM International Conference on Robotics and Mechatronics (ICRoM). Presented at the 2013 First RSI/ISM International Conference on Robotics and Mechatronics (ICRoM), pp. 468–473. https://doi.org/10.1109/ICRoM.2013.6510152

Lamm, R.D., Slaughter, D.C., Giles, D.K., 2002. Precision weed control system for cotton. Transactions of the ASAE 45, 231.

Le, V.N.T., Ahderom, S., Alameh, K., 2020. Performances of the LBP based algorithm over CNN models for detecting crops and weeds with similar morphologies. Sensors 20, 2193. https://doi.org/10.3390/s20082193

LeCun, Y., Bengio, Y., Hinton, G., 2015. Deep learning. Nature 521, 436–444. https://doi.org/10.1038/nature14539

Liu, B., Bruch, R., 2020. Weed detection for selective spraying: a review. Current Robotic Report 1, 19–26. https://doi.org/10.1007/s43154-020-00001-w

Liu, W., Anguelov, D., Erhan, D., Szegedy, C., Reed, S., Fu, C.-Y., Berg, A.C., 2016. SSD: Single Shot MultiBox Detector, in: Leibe, B., Matas, J., Sebe, N., Welling, M. (Eds.), Computer Vision – ECCV 2016, Lecture Notes in Computer Science. Springer International Publishing, Cham, pp. 21–37. https://doi.org/10.1007/978-3-319-46448-0_2

López-Granados, F., 2011. Weed detection for site-specific weed management: mapping and real-time approaches. Weed Research 51, 1–11. https://doi.org/10.1111/j.1365-3180.2010.00829.x

Lottes, P., Behley, J., Chebrolu, N., Milioto, A., Stachniss, C., 2019. Robust joint stem detection and crop-weed classification using image sequences for plant-specific treatment in precision farming. Journal of Field Robotics 37, 20–34. https://doi.org/10.1002/rob.21901

Lottes, P., Behley, J., Chebrolu, N., Milioto, A., Stachniss, C., 2018. Joint stem detection and crop-weed classification for plant-specific treatment in precision farming, in: 2018 IEEE/RSJ International Conference on Intelligent Robots and Systems (IROS). Presented at the 2018 IEEE/RSJ International Conference on Intelligent Robots and Systems (IROS), pp. 8233–8238. https://doi.org/10.1109/IROS.2018.8593678

Ma, X., Deng, X., Qi, L., Jiang, Y., Li, H., Wang, Y., Xing, X., 2019. Fully convolutional network for rice seedling and weed image segmentation at the seedling stage in paddy fields. PLOS ONE 14, e0215676. https://doi.org/10.1371/journal.pone.0215676

Machleb, J., Peteinatos, G.G., Kollenda, B.L., Andújar, D., Gerhards, R., 2020. Sensor-based mechanical weed control: present state and prospects. Computers and Electronics in Agriculture 176, 105638. https://doi.org/10.1016/j.compag.2020.105638

Martin, D., Singh, V., Latheef, M.A., Bagavathiannan, M., 2020. Spray deposition on weeds (Palmer amaranth and Morningglory) from a remotely piloted aerial application system and backpack sprayer. Drones 4, 59. https://doi.org/10.3390/drones4030059

Nave, W.R., Wax, L.M., 1971. Effect of weeds on soybean yield and harvesting efficiency. Weed Science 19, 533–535. https://doi.org/10.1017/S0043174500050608

Oquab, M., Bottou, L., Laptev, I., Sivic, J., 2014. Learning and transferring mid-level image representations using convolutional neural networks. Presented at the Proceedings of the IEEE Conference on Computer Vision and Pattern Recognition, pp. 1717–1724.

Osorio, K., Puerto, A., Pedraza, C., Jamaica, D., Rodríguez, L., 2020. A deep learning approach for weed detection in lettuce crops using multispectral images. AgriEngineering 2, 471–488. https://doi.org/10.3390/agriengineering2030032

Partel, V., Charan Kakarla, S., Ampatzidis, Y., 2019. Development and evaluation of a low-cost and smart technology for precision weed management utilizing artificial intelligence. Computers and Electronics in Agriculture 157, 339–350. https://doi.org/10.1016/j.compag.2018.12.048

Redmon, J., Divvala, S., Girshick, R., Farhadi, A., 2016. You Only Look Once: Unified, real-time object detection. Presented at the Proceedings of the IEEE Conference on Computer Vision and Pattern Recognition, pp. 779–788.

Redmon, J., Farhadi, A., 2018. YOLOv3: An incremental improvement. arXiv:1804.02767 [cs].

Ren, S., He, K., Girshick, R., Sun, J., 2017. Faster R-CNN: Towards real-time object detection with region proposal networks. IEEE Trans. Pattern Analysis and Machine Intelligence. 39, 1137–1149. https://doi.org/10.1109/TPAMI.2016.2577031

Rumpf, T., Römer, C., Weis, M., Sökefeld, M., Gerhards, R., Plümer, L., 2012. Sequential support vector machine classification for small-grain weed species discrimination with special regard to *Cirsium arvense* and *Galium aparine*. Computers and Electronics in Agriculture 80, 89–96. https://doi.org/10.1016/j.compag.2011.10.018

Sabzi, S., Abbaspour-Gilandeh, Y., García-Mateos, G., 2018. A fast and accurate expert system for weed identification in potato crops using metaheuristic algorithms. Computers in Industry 98, 80–89. https://doi.org/10.1016/j.compind.2018.03.001

Sapkota, B., Singh, V., Neely, C., Rajan, N., Bagavathiannan, M., 2020. Detection of Italian ryegrass in wheat and prediction of competitive interactions using remote-sensing and machine-learning techniques. Remote Sensing 12, 2977. https://doi.org/10.3390/rs12182977

Sharpe, S.M., Schumann, A.W., Boyd, N.S., 2020. Goosegrass detection in strawberry and tomato using a convolutional neural network. Scientific Reports 10, 9548. https://doi.org/10.1038/s41598-020-66505-9

Suarez, L.A., Apan, A., Werth, J., 2017. Detection of phenoxy herbicide dosage in cotton crops through the analysis of hyperspectral data. International Journal of Remote Sensing 38, 6528–6553. https://doi.org/10.1080/01431161.2017.1362128

Sujaritha, M., Annadurai, S., Satheeshkumar, J., Kowshik Sharan, S., Mahesh, L., 2017. Weed detecting robot in sugarcane fields using fuzzy real time classifier. Computers and Electronics in Agriculture 134, 160–171. https://doi.org/10.1016/j.compag.2017.01.008

Wu, X., Xu, W., Song, Y., Cai, M., 2011. A detection method of weed in wheat field on machine vision. Procedia Engineering, CEIS 2011 15, 1998–2003. https://doi.org/10.1016/j.proeng.2011.08.373

Xie, S., Hu, C., Bagavathiannan, M., Song, D., 2021. Toward robotic weed control: detection of nutsedge weed in bermudagrass turf using inaccurate and insufficient training data. IEEE Robotics and Automation Letters. https://doi.org/10.1109/LRA.2021.3098012

Yu, J., Schumann, A.W., Cao, Z., Sharpe, S.M., Boyd, N.S., 2019. Weed detection in perennial ryegrass with deep learning convolutional neural network. Frontiers in Plant Science. https://doi.org/10.3389/fpls.2019.01422

4.7. Tables and Figures

Table 4.1. Various datasets used in the study.

	Image dataset name	Acquisition Date	Crop/growth stage	Weed composition/growth stage	Weed density (plants m^{-2})	Image acquisition conditions	Train/Val/Test [images, annotations]	Annotation composition[a] [MG, Grass, Other]
1	Cotton 1 (Test data referred to as Cot1)	May 06, 2020	Cotton: 4-5 leaves	MG: cotyledon-4 leaves JG: 2-3 leaves TM: 2-3 leaves	18	Sunny	Train: [460, 8580] Val: [100, 721] Test: [100, 848]	[19.3, 79.5, 1.2] [22.4, 74.2, 3.4] [51.8, 48.1, 1.1]
2	Cotton 2 (referred to as Cot2)	June 13, 2021	Cotton: 2-4 leaves	MG: cotyledon-6 leaves TM: 2-4 leaves	21	Partially cloudy	Test: [95, 600]	[36, 63.8, 0.2]
3	Soybean 1 (Test data referred to as Soy1)	May 06, 2020	Soybean: 6-7 leaves	MG: cotyledon-4 leaves JG: 2-3 leaves TM: 2-3 leaves	17	Sunny	Train: [115, 990] Val: [25, 200] Test: [100, 848]	[46.4, 53.48, 0.07] [48.4, 50.8, 0.8] [54.22, 43.22, 2.56]
4	Soybean 2 (referred to as Soy2)	May 14, 2021	Soybean: 1-3 leaves	MG: cotyledon-6 leaves TM: 2-4 true leaves	21	Cloudy	Test: [97, 547]	[63.07, 35.4, 1.53]
5	Corn 1 (Test data referred to as Corn1)	May 07, 2021	Corn: 2-3 leaves	MG: cotyledon-3 leaves JG: 2-3 leaves TM: 2-3 leaves	18	Sunny	Train: [115, 1010] Val: [25, 215] Test: [100, 890]	[81.16, 16.75, 2.1] [95.2, 4.1, 0.7] [94.62, 4.9, 0.48]
6	Corn 2 (referred to as Corn2)	May 14, 2021	Corn: 3-4 leaves	MG: cotyledon-6 leaves TM: 2-4 true leaves	23	Cloudy	Test: [95, 559]	[80.5, 17.5, 2]

Abbreviation: Train- Training; Val-Validation; MG-Morningglores; TM-Texas millet; JG- Johnsongrass
a- The annotations statistics shown within the brackets are given in %.

Table 4.2. Various training datasets evaluated in the study for training YOLOv4 and Faster R-CNN and annotations record for each training dataset.

Training dataset	Non-cotton Images (%)[a]	Annotations			
		MG (%)	Grass (%)	Other (%)	Total
Train100[b]	0	19.3	79.5	1.20	8,580
Train105	5	20.0	78.8	1.25	8,775
Train110	10	20.7	78.0	1.23	8,915
Train115	15	21.7	77.1	1.21	9,072
Train120	20	22.9	75.9	1.19	9,234
Train125	25	23.0	75.7	1.33	9,480
Train130	30	23.9	74.7	1.32	9,689
Train135	35	24.3	74.4	1.34	9,827
Train140	40	25.0	73.7	1.32	9,970
Train145	45	25.5	73.2	1.31	10,113
Train150	50	25.7	73.0	1.29	10,198

Abbreviation: MG- Morningglories; Grass- Grass weeds; Other – Weeds other than MG and Grass

[a]The numerical figures in this column indicate the percentage of images added to Train100 (i.e. 460 images).

[b]Train100 had a total of 460 cotton images and 0 non-cotton images.

"Train100" represents the dataset with cotton images only, i.e. no non-cotton images. The last two digits of training dataset names represent the percentage of non-cotton images added to Train100 randomly for building the respective training dataset. The percentage was with respect to Train100.

Table 4.3. Accuracy obtained for various test datasets with YOLOv4 and Faster R-CNN under Detect_Weed and Detect_Species using the main cotton model.

	Detect_Weed		Detect_Species					
	YOLOv4	Faster R-CNN	YOLOv4			Faster R-CNN		
	AP	AP	AP (MG)	AP(Grass)	mAP	AP (MG)	AP(Grass)	mAP
Cot_1	0.88	0.87	0.88	0.83	0.85	0.86	0.79	0.83
Cot_2	0.79	0.74	0.71	0.79	0.75	0.60	0.70	0.65
Soy_1	0.83	0.76	0.83	0.75	0.79	0.72	0.70	0.71
Soy_2	0.35	0.60	0.63	0.64	0.64	0.72	0.49	0.61
Corn_1	0.72	0.62	0.88	0.15	0.52	0.78	0.15	0.47
Corn_2	0.33	0.39	0.65	0.15	0.40	0.54	0.03	0.29

Abbreviations: MG- Morningglories; Grass- Grass weeds; AP – Average Precision; mAP- Mean Average Precision
AP and mAP values were computed to assess the performance of the main cotton model over the test datasets. mAP was calculated by averaging AP for MG and Grass. AP was calculated as a function of precision and recall values obtained when Intersection Over Union was set to 0.5.

Table 4.4. The maximum rate of increment in accuracy for various test datasets with the addition of non-cotton images.

	Detect_Weed (AP%)		Detect_Species (mAP%)	
	YOLOv4	Faster R-CNN	YOLOv4	Faster R-CNN
Cot1	2.27	2.29	5.89	2.42
Cot2	7.60	2.70	2.00	7.70
Soy1	3.61	5.26	6.32	7.74
Soy2	122.8	16.00	11.90	8.27
Corn1	31.9	53.22	12.62	34.40
Corn2	127.27	69.23	28.75	58.62

Abbreviations: AP-Average Precision; mAP- Mean Average Precision
The rate was determined by subtracting the accuracy obtained with Train100 (no non-cotton images) from the highest accuracy obtained among all training datasets for the respective test dataset.

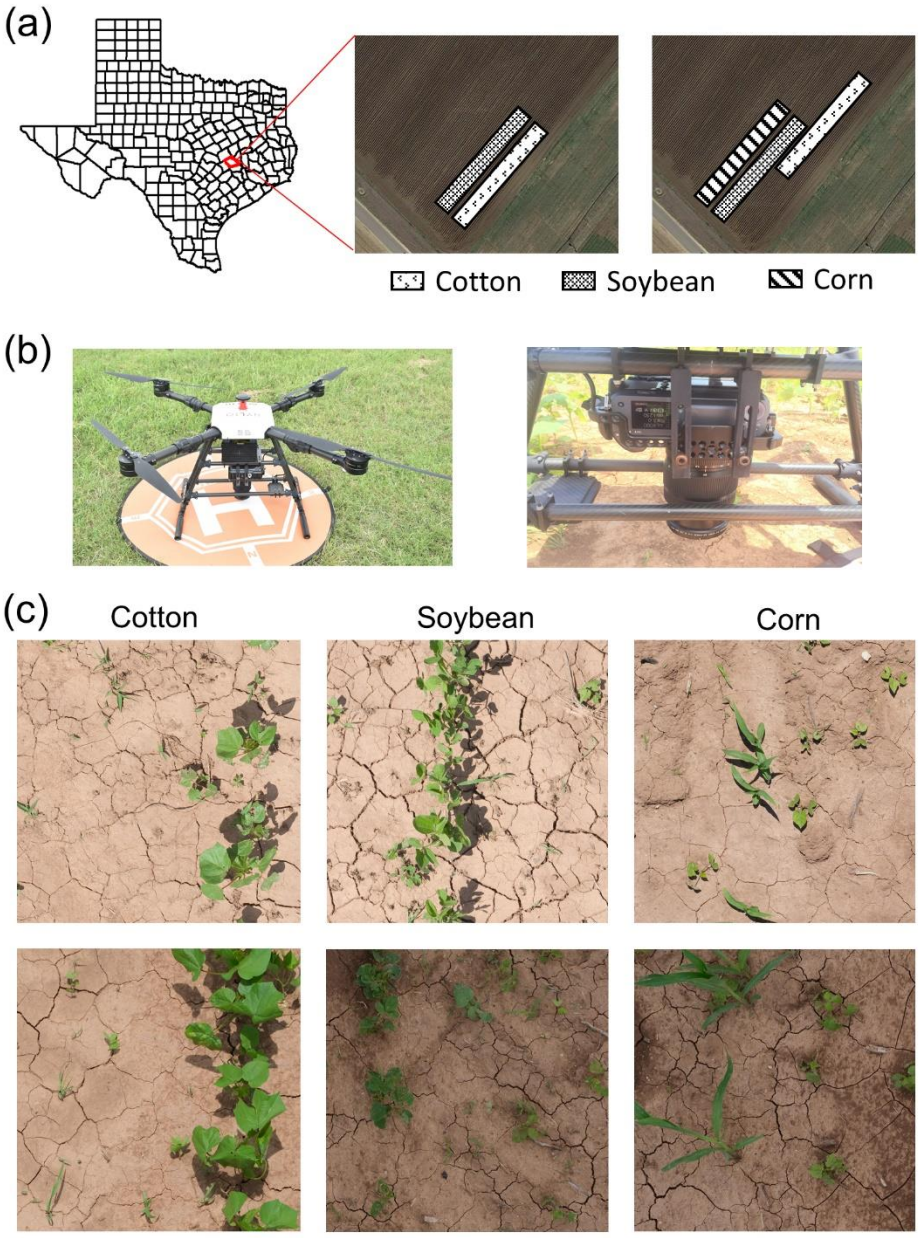

Figure 4.1. a) Study area (Texas A&M AgriLife Research Farm, Burleson County, TX) and field setup for the two experimental years; b) a multi-copter drone (Hylio Inc., Houston, TX, USA) attached with Fujifilm GFX100 (100 MP) camera; and c) image datasets (top and bottom rows) collected under two different environmental conditions for cotton, soybean, and corn.

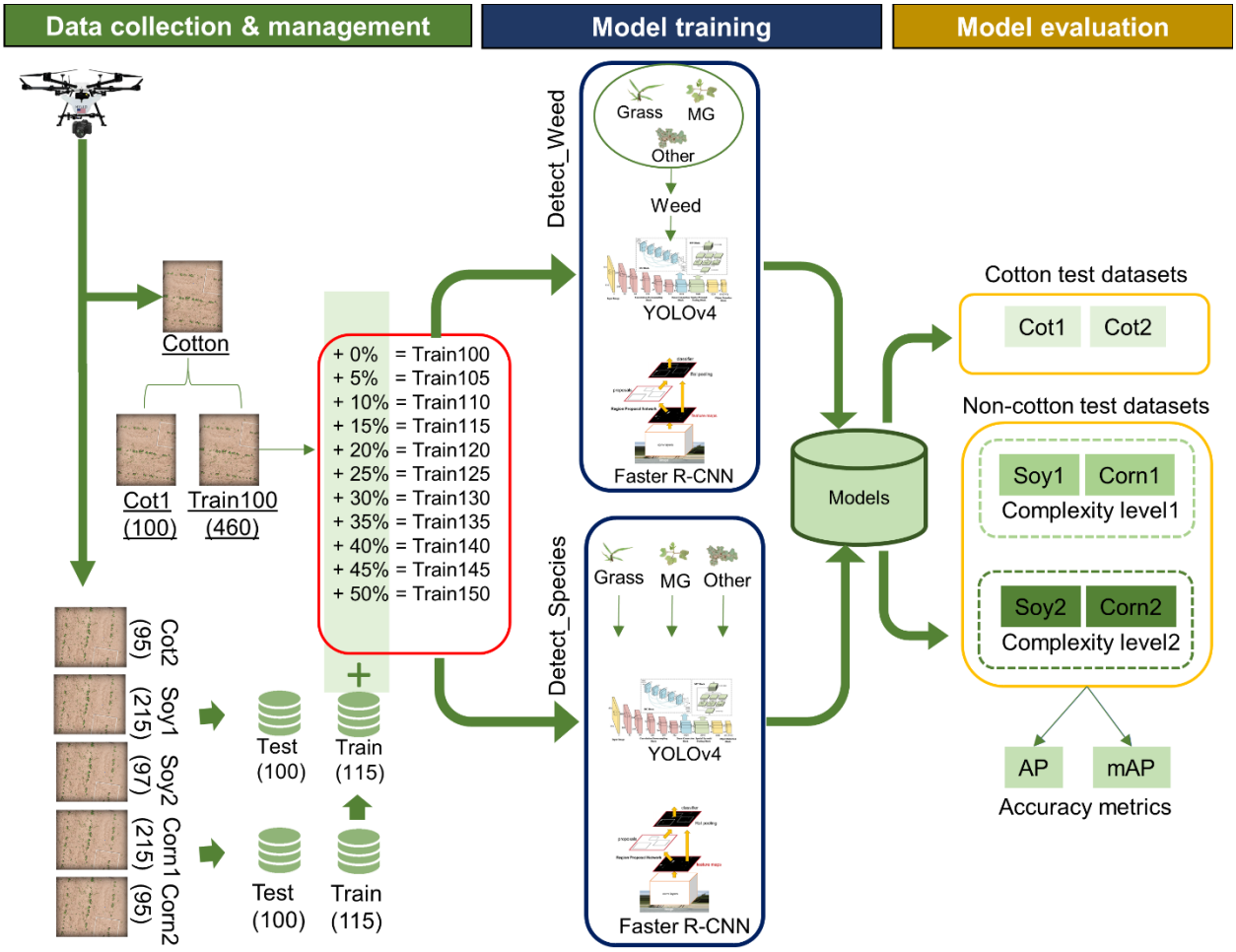

Figure 4.2. Schematic showing the workflow used in the study. The study began with data collection using an UAV and the collected data were distributed for training and test datasets. Data management was followed by model training under two detection schemes: Detect_Weed (detecting at weed/crop level) and Detect_Species (detecting at weed species level). After the models were trained, they were evaluated on the test datasets (Other was excluded during the calculation of accuracy metrics). Average Precision (AP) and mAP (Mean Average Precision) was used as the metrics for performance evaluation.

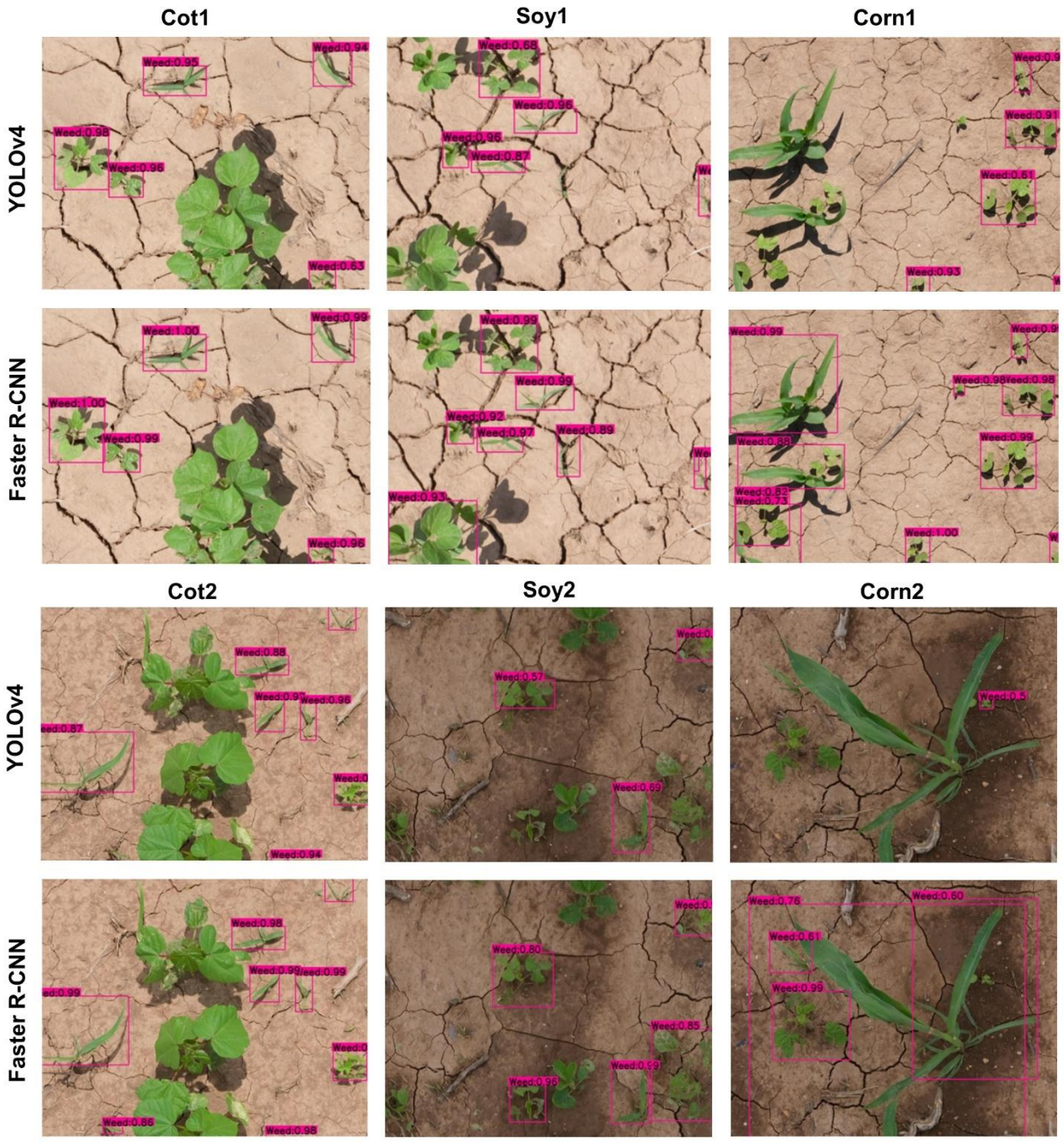

Figure 4.3. Weed detection using bounding boxes by the main cotton models under "Detect_Weed" scheme for various test datasets used in the study. YOLOv4 and Faster R-CNN were trained with the Train100 dataset (i.e. dataset containing cotton images only) to develop the main cotton models. Under this scheme, MG, Grass, and Other were combined into "Weed" category while training the model.

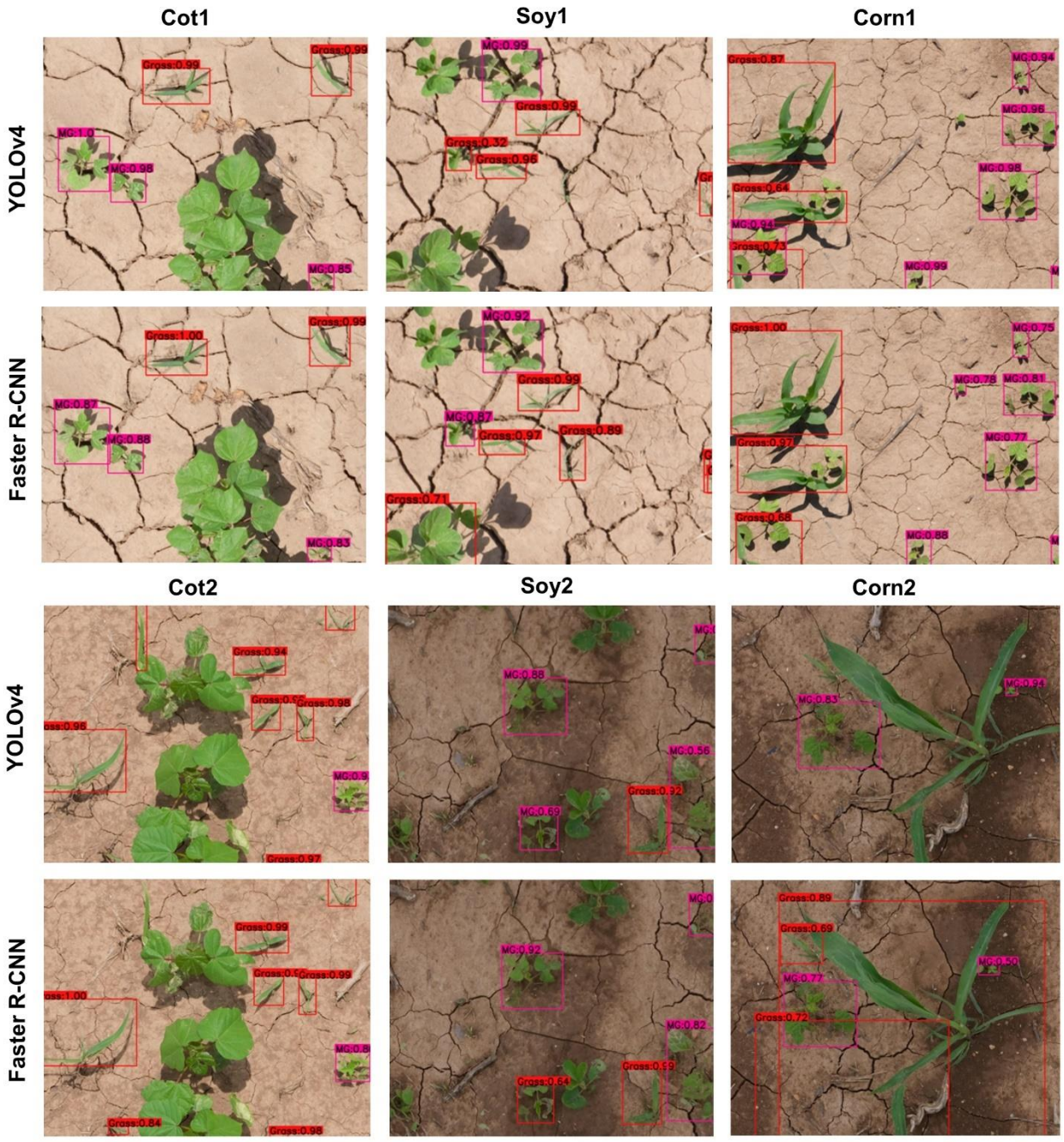

Figure 4.4. Bounding boxes generated for MG and Grass by the main cotton models under "Detect_Species" scheme for various test datasets used in the study. YOLOv4 and Faster R-CNN were trained with the Train100 dataset (i.e., dataset containing cotton images only) to develop the main cotton models. Under this scheme, MG, Grass, and Other were trained as separate categories.

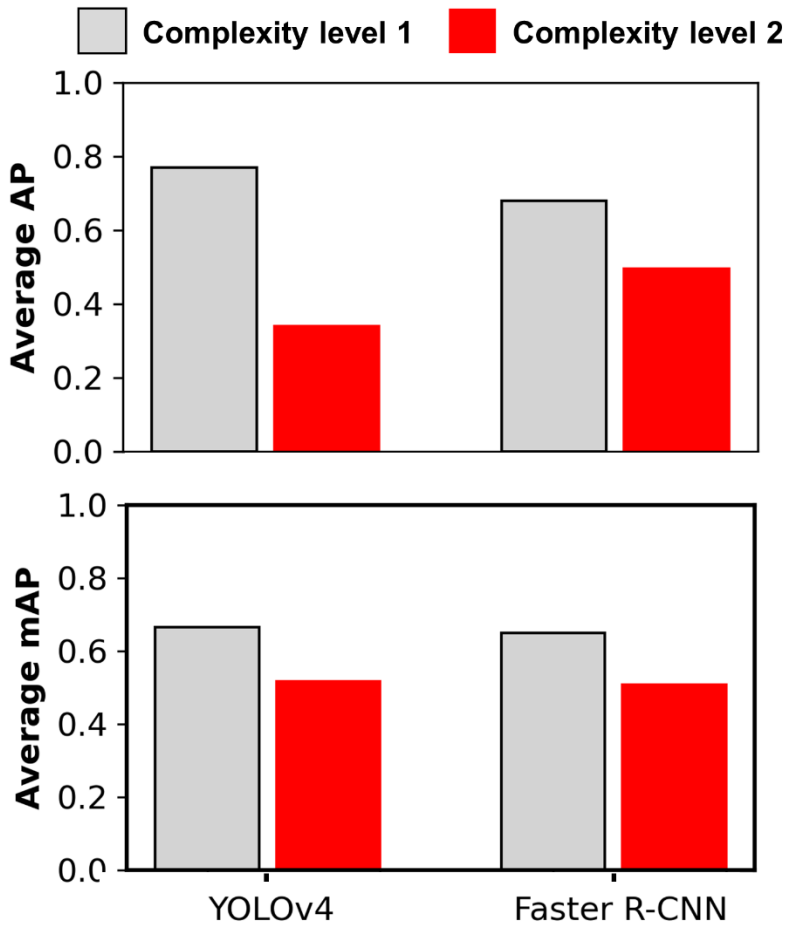

Figure 4.5. Average Precision (AP) and Mean Average Precision (mAP) achieved for different complexity level datasets with main cotton models. Complexity level 1 datasets include Soy1 and Corn1 whereas level 2 include Soy2 and Corn2. The main cotton models were derived by training the detection frameworks (YOLOv4 and Faster R-CNN) with Train100 (i.e. dataset containing cotton images only). The AP/mAP for datasets under each complexity level were averaged to derive average AP and mAP.

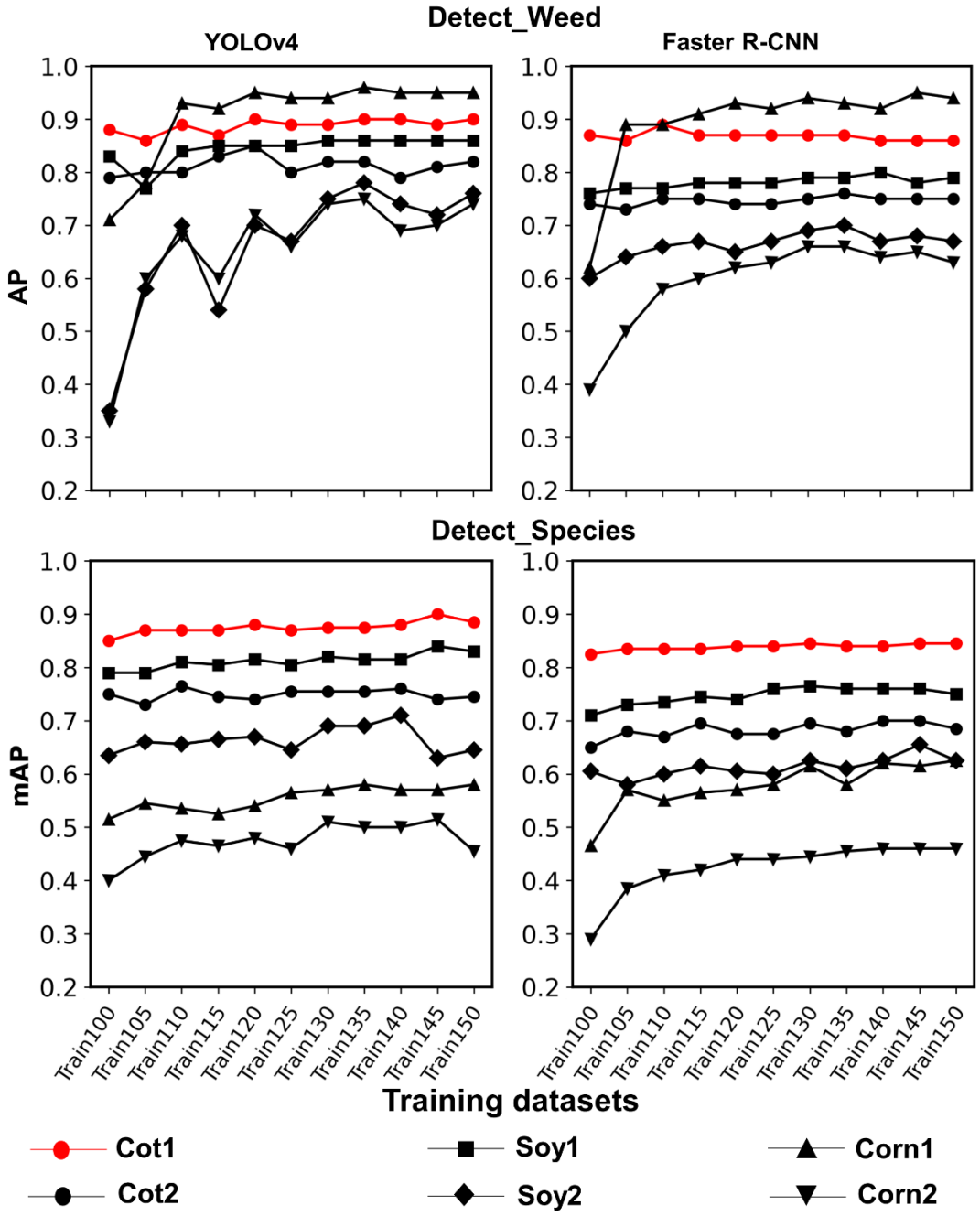

Figure 4.6. Line plots showing Average Precision (AP) and Mean Average Precision (mAP) achieved with various training datasets for each test dataset used in the study for both frameworks and detection schemes. Various training datasets were created by adding Soy1 and Corn1 training images to the original dataset, i.e. Train100. These non-cotton crop images were added 5% at a time until they amounted to 50% of Train100. The last two digits in the training dataset name denote the % of images added to Train100.

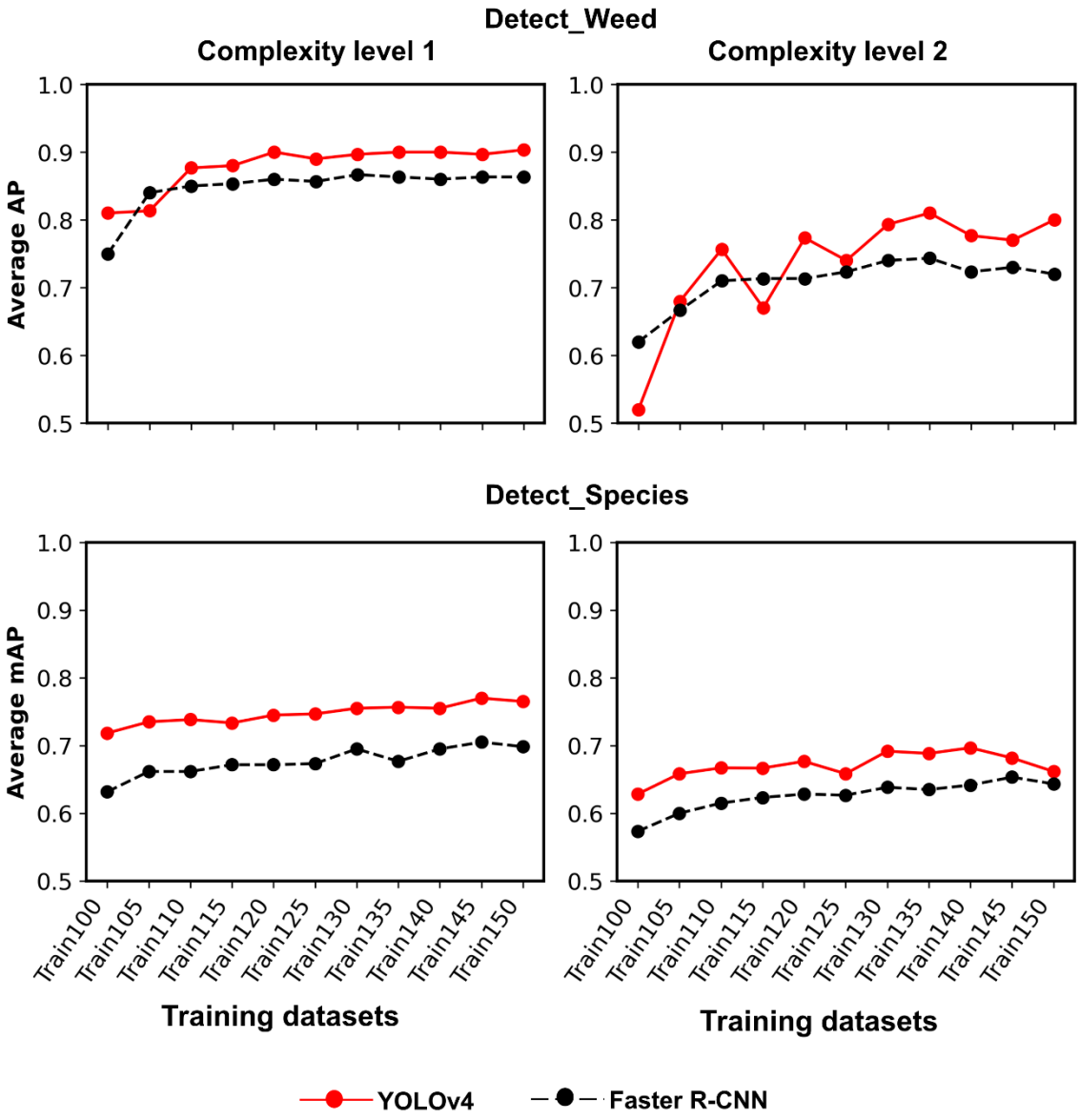

Figure 4.7. Line plots showing Average Precision (AP) and Mean Average Precision (mAP) achieved for each complexity level with YOLOv4 and Faster R-CNN. Complexity level 1 datasets include Soy1 and Corn1, whereas level 2 include Soy2 and Corn2. AP and mAP for Cot1 dataset were also included in the averaging process of each complexity level to understand how well the models perform with both cotton and non-cotton datasets.

5. EVALUATING IMAGE SYNTHESIS TECHNIQUES FOR TRAINING A DEEP LEARNING MODEL TO DETECT WEEDS AND ESTIMATE BIOMASS IN FIELD CROPS

5.1. Abstract

Site-specific treatment of weeds in agricultural landscapes has been gaining importance in recent years due to economic savings and minimal impact on the environment. Over the years, advanced precision systems have been developed for site-specific weed treatment; weed detection is usually the most crucial component of these systems. Different detection methods have been developed and tested, but recent developments in neural networks have offered great prospects. However, a major limitation with the neural network models is the requirement of high volumes of data for training. The current study aims at exploring an alternative approach to real images to address this issue. In this study, synthetic images were generated with various strategies using plant instances clipped from UAV-borne real images to train a powerful convolutional neural network (CNN) known as "Mask R-CNN" for weed detection and segmentation. The study was conducted on morningglories (MG) and grass weeds (Grass) infested in cotton. The biomass for individual weeds was also collected in the field for biomass modeling using detection and segmentation results. Results showed comparable performance between the synthetic and real images. Around 40-50 plant instances were sufficient for generating synthetic images that resulted in optimal performance. Row-orientation of cotton in the synthetic images was beneficial compared to random-orientation. Synthetic images generated with automatically-clipped plant instances performed similar to the ones generated with manually-clipped instances. Generative Adversarial Networks-derived fake plant instances-based synthetic images did not perform as effective as real plant instance-based images. The canopy

mask area predicted weed biomass with R^2 values of 0.66 and 0.46 for MG and Grass, respectively. The findings of this study offer valuable insights for guiding future endeavors oriented towards using synthetic images for weed detection and segmentation, and biomass estimation in row crops.

Key words: Precision weed management, digital agriculture, computer vision, synthetic images, Mask R-CNN

5.2. Introduction

Weeds cause severe crop yield loss and therefore timely and effective management is key to increased agricultural productivity. The conventional weed control approach may provide effective weed control but is often inefficient and expensive. The precision weed management approach can improve resource use efficiency and economics by restricting the inputs to only where needed. This approach, however, can be complex as it comprises several components including weed detection and actuation systems. The weed detection system is an important component since it guides the actuation systems. Several detection models have been designed and tested so far (Ahmed et al., 2012; Rumpf et al., 2012; Sapkota et al., 2020) but the convolutional neural network (CNN)-based models have revolutionized this domain.

CNN is a class of artificial neural networks that create numerous feature maps from input images to learn the semantic pattern of the object (LeCunn et al., 2015). Their ability to self-optimize the parameters to improve the pattern recognition process allows for complex object detection. CNNs are increasingly used for weed detection, owing to their great accuracy and less human supervision requirements. Liu and Bruch (2020) used the You Only Look Once (YOLOv2), a lightweight CNN framework, to detect weeds in romaine lettuce in digital RGB

images and achieved the highest mean average precision (mAP) value of 0.91. Yu et al. (2019a) detected dandelion (*Taraxacum officinale*), ground ivy (*Glechoma hederacea*), and spotted spurge (*Euphorbia maculata*) in perennial ryegrass using DetectNet frameworks with an F-score >0.92. Lottes et al. (2018) employed CNN with an encoder-decoder structure to detect weeds in sugar beet and achieved an average F-score of 0.92.

CNNs usually require a large number of training samples for better training. Manual data annotations for large training sample sets can be tedious and laborious (Hu et al., 2021). Additionally, it is at times difficult to obtain large image datasets specific to the needs. One way to deal with these problems would be to create real-looking artificial images. An increasingly common approach of image synthesis is to clip the real plants in the imagery, apply modifications to clipped plants, and finally paste over the background images to create synthetic images (Dwibedi et al., 2017; Georgakis et al., 2017). Few studies have already embraced this concept for weed detection tasks. For example, Gao et al. (2020) created 2271 synthetic images using this approach to train the YOLOv3 and tiny YOLO models in combination with 452 real field images. They applied three types of modifications (zoom, flip, and rotation) to automatically clipped individual instances and pasted them at a random position within the image. Hu et al. (2021) also used the same approach to create a synthetic image dataset to train weed detection models. They used manually-clipped, instead of automatically-clipped, plants in the image synthesis procedure. Skovsen et al. (2021) also implemented the same concept to generate huge amounts of synthetic images for grass-clover mixtures. While automating the plant clipping process can speed up image synthesis, it is unknown whether it can yield the same levels of accuracy as manually-clipped plants. It is also unknown whether crop positions in the synthetic images affect the performance of detection and segmentation. To the best of our

knowledge, no study has evaluated the image synthesis concept for training an instance segmentation model.

It can at times be difficult to obtain real plant images and therefore fake plants can be great alternatives to real plant instances for generating synthetic images. One of the promising techniques for creating fake images of object of interest available today is Generative Adversarial Networks (GANs). GANs have been successfully used for various image processing and computer vision tasks ranging from fashion design to video games. Recently, GANs have been utilized for various predictive tasks in the agricultural domain, including weed detection/classification in digital images (Espejo-Garcia et al., 2021; Fawakherji et al., 2020; Kerdegari et al., 2019). Espejo-Garcia et al. (2021) tested several architectures and configurations of GANs for creating artificial images of tomatoes and black nightshade. The models trained with these images were able to distinguish between these two plant species with very high accuracy. For example, Wang et al. (2020) used Wasserstein GANs for enhancing RGB images to train semantic segmentation models that could perform pixel-wise segmentation. Very few studies have utilized GANs for weed detection and segmentation.

In addition to weed localization, biomass information can also be useful for precision weed control systems. With this information, herbicide spray systems can be configured to deliver spray output optimized for plant biomass, thus saving resources. Previous studies have used various techniques for estimating plant biomass using digital technologies. For example, Harket et al. (2020) used LiDAR-derived 3D point clouds to estimate biomass for winter wheat, potato, and sugar beet. Using the depth and RGB image-based volume reconstruction method, Andújar et al. (2016) calculated 3D mesh volume for weeds to estimate weed biomass. Although these 3D techniques are proven to result in more accurate biomass estimation, they are

computationally more expensive and often inefficient compared to the 2D-image based techniques. A simple 2D approach that utilizes plant coverage information has been studied by Skovsen et al. (2020). However, these studies have investigated biomass estimation in a unit area, rather than that of individual plants, which is critical for precision management. The current study explores the feasibility of a simple 2D approach coupled with instance segmentation for estimating biomass at the individual plant level.

In this study, the main goal was to investigate various methods of generating synthetic images for training a Mask R-CNN model for weed detection and segmentation. The objectives of the study were:

1. Explore the potential of synthetic images in training and building a robust mask R-CNN model
    a. Evaluate the effect of crop row arrangement, instance diversity, and clipping method on synthetic image quality and performance
    b. Compare the performance of real plant-based vs fake plant-based synthetic images
    c. Evaluate performance gain with the mixed dataset (real + synthetic images)
2. Assess the potential of a deep learning model-based segmentation results in estimating above-ground biomass of weeds

5.3. Materials & Methods

5.3.1. Study area and experimental setup

The study was conducted in summers of 2020 & 2021 at the Texas A&M AgriLife Research farm (30°32′15″N, 96°25′35″W; elevation: 70 m). The location is characterized by a

sub-tropical climate, with an average monthly maximum and minimum temperature during the study period (May – June) of 32.3°C and 21.3°C, respectively. Cotton was chosen as the model row crop for this study. Glyphosate-resistant (Roundup Ready®) cotton was planted at the seeding rate of 100,000 per hectare on May 1, 2020 and April 20, 2021, respectively using a 4-row seed drill (row spacing: 1 m). Cotton was grown following the recommended production practices for the region. The dominant weed species in the study area were a mix of morningglories (*Ipomoea* spp.) that comprised of tall morningglory (*Ipomoea purpurea*) and ivyleaf morningglory (*Ipomoea hederacea*), Texas millet (*Urochloa texana*), and johnsongrass (*Sorghum halepense)*. Some other weed species occurred at low frequencies, including Palmer amaranth (*Amaranthus palmeri*), prostrate spurge (*Euphorbia humistrata*), and browntop panicum (*Panicum fasiculatum*). At the time of image collection, weed species occurred at different growth stages, from cotyledon to about five true leaves (Table 5.1).

5.3.2. Data collection

5.3.2.1. High resolution digital images

A 100-megapixel FUJIFILM GFX100 medium format mirrorless RGB imaging camera was integrated with a multi-copter drone, Hylio AG-110 (Hylio Inc., TX, USA) to capture high-resolution aerial images of the cotton in summer of 2020 and 2021, hereafter referred as Cotton 1 and Cotton 2 dataset, respectively. The images were captured by the drone operating at 4.9 m above the ground level and a speed of 0.61 m/s. The FUJIFILM GF 32-64 mm f/4 R LM WR lens was set at a focal length of 64 mm, shutter speed at 1/4000s, ISO at 1250, and f-stop at 8, which resulted in high-quality images with a spatial resolution of 0.0274 mm/pixel at the flying height specified above. All the images were stored in standard PNG format at 16-bit depth. Cotton 1 was the main dataset and comprised 560 images out of which 460 were reserved for

training and validation dataset and remaining 100 as hold-out test dataset. Whereas, Cotton 2 had 100 images for test purposes.

5.3.2.2. Above-ground weed biomass collection

A total of 15 quadrats (1 m^2) were randomly placed in a cotton field (0.12 ha) for weed biomass collection in 2020 and 2021. Each plant in the quadrat was clipped at the ground level and stored in separate paper bags. The location of each weed in the quadrat was physically mapped on a paper for later use during image analysis to identify and reference each individual. In total, 60 morningglories and 58 grass weed instances were clipped in 2020, and 44 and 41 respectively in 2021. The clipped plants were dried in an oven at 60°C for 48 hours for dry biomass measurement.

5.3.3. Methodology for objective 1

The general workflow for this experiment is shown in Figure 5.1. The workflow shows progression of major methodological steps undertaken for both the objectives.

5.3.3.1. Synthetic image generation pipeline

The synthetic image generation pipeline (SIGP) consisted of three main components (Figure 5.1). The first component included the instance pool (IP) which consisted of individual plants clipped either from real images or individual fake plants generated and stored in a 4-band (RBGA) PNG format. The second component included a random modifier (RM) algorithm that randomly obtained instances from the IP and applied several modifications to those instances. The modifications were made in three ways: a) rotating instances by a random angle between 0-180, b) transforming instances with a random size factor ranging between 0.6 and 1.2, and c) changing digital values for hue and saturation of instances by 0 - 10%. The third component included a paste operator (PO) algorithm that pasted modified instances at user-defined or

random locations in the soil background images to create synthetic images. Five representative soil background images of 2048 × 2048 pixels were clipped from real images acquired using the Fujifilm camera. The PO recorded information on the locations where instances were pasted as well as several other metadata such as instance id, instance category, image id, etc. to create annotation dictionary for each image. The PO finally merged the annotation directories for all the images to create an annotation file in the *.json* file format. The pipeline was programmed in such a way that each image would have 4 instances for each of the three categories: a) cotton, b) MG, and c) Grass.

Algorithm 1: Row-oriented synthetic image generation pipeline

---

Input: Instance pool P, background image templates $T = \{b_1, b_2, \ldots, b_m \mid m = 1 \ldots 5\}$, plant species $k = 4$, plant count per each species $d = 4$, target image width w, target image height h,

Output: Synthetic images I

For i = 1 to k **do**:

    For j = 1 to d **do**:

        Randomly select a background template b_m from T

        Randomly select a plant instance from P corresponding to $i^{th}\ species$

        Randomly rotate a plant instance with a rotation angle θ within $(0, 2\pi)$

        Randomly change color by magnitude in % ranging between $(0, 10\%)$

        Randomly scale the plant instance by factor between $(0.7, 1.3)$

        if j == cotton do:

9		Paste at location q where $q = \left(\frac{3w}{8}, b\right) where\ b\ \in \{0, \frac{h}{4}, \frac{h}{2}, \frac{3h}{4}\}$
10	**else**:	
11		Randomly paste at (x, y) location where $x\ \in\ [0, w]\ and\ y\ \in\ [0, h]$

5.3.3.2. Effect of crop row arrangement

The aim was to evaluate if the row arrangement of crops was important for row crops such as cotton in the synthetic images for better training results. To test this, two sets of synthetic images were generated: a) images with cotton lined-up in a row (row-oriented), and b) images with cotton pasted in random locations (randomly-pasted) (Figure 5.2a). First, real plants for cotton, MG, and Grass were clipped to canopy boundary from the real images to create an IP. Fifty instances were clipped for each class. Second, the SIGP was implemented with a slight change in the PO, which was programmed to paste the cotton instances coming from RM in two ways: a) following user-defined locations to line up in a row for row-oriented images, and b) following machine-generated random locations for random-oriented images. The synthetic image sets were then used for training the model separately. In order to evaluate how the results change with image resolution, another sets of synthetic images with reduced image resolution (512 × 512 pixels) for both arrangements. Assessments were made to compare the performance of the models.

5.3.3.3. Effect of instance diversity

The aim was to determine how the IP size influences the performance of the Mask R-CNN model. It was hypothesized that the more the number of plant instances used in SIGP, the

more the variance captured by the synthetic images, and thus better the training. Altogether, seven IPs with varying sizes were created that contained 1, 5, 10, 20, 30, 40, and 50 instances from each class. Seven different synthetic image and annotation datasets were created from respective IPs, which were then used to train and build detection models. Individual assessments were made to compare the performance of each model.

5.3.3.4. Effect of instance clipping method

The goal was to compare the performance between the models trained with synthetic images generated using plant instances clipped manually or automatically. The real images captured with the Fujifilm camera were subjected to automated plant clip pipeline (APCP) (Figure 5.2b). The algorithm logic used in APCP is shown in Algorithm 2. First, the excess greenness index (ExG) was calculated for selected real images using equation 1. Second, Otsu's method was employed to mask the bareground. Finally, an alpha channel was added to the resultant image to create a 4-band (RBGA) PNG image. The plant instances clipped automatically or manually were fed into SIGP to generate individual sets of synthetic images.

$$ExG = \frac{2*g - r - b}{r+g+b}$$

(Equation 1)

where $g, r, and\ b$ represent digital values for green, red, and blue channels, respectively.

Algorithm 2: Automated plant clipping pipeline

Input: RGB images

Output: Individual plant instances in RBGA format (PNG)

1 Generate an ExG layer using Equation 1

2 Determine Otsu's threshold for ExG layer $T = max\ (W_b W_f\ (\mu_b - \mu_f)^2$, where W_b, W_f , μ_b, μ_f represent weights (W) and mean values (μ) for the background and foreground, respectively

3 Generate a binary image *f* by applying T

4 Apply a dilation and erosion function to f using $3 \times 3\ kernel\ k$

$D_f = \left\{ \begin{matrix} (x,y) = 1 & if\ one\ pixel\ in\ k\ coincides\ with\ a\ foreground\ pixel\ in\ f \\ (x,y) = 0 & otherwise \end{matrix} \right\}$, where

D_f denotes dilution function; (x, y) represents the intersecting pixel between the center of k and f

$E_f = \left\{ \begin{matrix} (x,y) = 0 & if\ one\ pixel\ in\ \ k\ coincides\ with\ a\ foreground\ pixel\ in\ f \\ (x,y) = 1 & otherwise \end{matrix} \right\}$, where

E_f denotes erosion function; (x, y) represents the intersecting pixel between the center of k and f

5 Add an alpha channel to RGB for converting to RGBA

5.3.3.5. Performance of real plant instances Vs fake plant instances

The aim was to compare the performance of fake plant-based synthetic images with real plant-based synthetic images. An improved GAN framework called StyleGAN2 with adaptive discriminator augmentation (StyleGAN-ADA) developed by NVIDIA (Karras et al., 2020) was used in this study to generate fake plants. GANs are essentially composed of two main networks, a generator and a discriminator (Figure 5.3a). The generator deterministically generates samples from latent variables whereas the discriminator distinguishes samples from the real dataset and the generator. The model was trained with 50 instances of each class using the official

TensorFlow implementation code provided in (https://github.com/NVlabs/stylegan2-ada). The training samples were subjected to an on-the-fly augmentation process to increase the sample size. A pre-trained network model 'ffhq256' was used as the base model for transfer learning. After model training, approximately 50 fake plant instances in 3-band format were generated for each class, which were then passed through the APCP method to create a new IP comprised of 4-band PNG images (Figure 5.3b). The new IP was subjected to SIGP to create a unique set of synthetic images. The sample results obtained at different training phases of GAN is shown in Figure 5.3c. The algorithm logic for the GAN process is provided in Algorithm 3.

Algorithm 3: The GAN process for fake plant instance generation

---

Input: Instance pool for Cotton P_c , MG P_m, Grass P_g with size m; pretrained styleGAN-ADA model M; number of plant instances to be generated N

Output: Individual plant instance for each species in RBGA format

1. Train M with P_c, P_m, P_g individually to generate custom trained models $C_c, C_m, and\ C_g,$ respectively

$$L_D = \frac{1}{m}\sum_{i=1}^{m}[log\ \mathrm{D}\ (x^i) + log\ (1 - D(G(z^i)]$$

$$L_G = \frac{1}{m}\sum_{i=1}^{m} log\ (1 - D(G(z^i)$$

where $\mathrm{D}\ (x^i)$ denotes a label predicted by the discriminator for real image x^i, $D(G(z^i)$ denotes a label predicted by the discriminator for fake images produced by the generator, and $L_D\ and\ L_G$ denote loss functions for the discriminator and the generator, respectively.

2. **For** $i = 1\ to\ N$ ***do***:

Generate fake plant instances for Cotton C_f, MG M_f, and Grass G_f using respective trained models

3. Apply algorithm 2 with inputs as $C_f, M_f, and\ G_f$

5.3.3.6. Performance gain with mixed dataset

The idea was to compare the performance of a mixed dataset (real images + synthetic images) with just a synthetic image-derived dataset. For this, a total of 460 real images acquired using the Fujifilm camera sensor were manually annotated for Cotton, MG, and Grass individuals. The polygon annotations were drawn for each plant in all the images. The synthetic image dataset was combined with a real image dataset to create the mixed dataset. The synthetic dataset that yielded the highest accuracy in the earlier analysis was chosen for inclusion in the mixed dataset. The mixed dataset comprised a total of 1,210 images and 18,000 annotations that were separately used to train the Mask R-CNN model.

5.3.3.7. Model training and accuracy assessment

Mask R-CNN, an instance segmentation model (He et al., 2015), was used for weed detection and segmentation in this study. Mask R-CNN is similar to its predecessor "Faster R-CNN" framework except that it has an additional mask branch that results in an object mask in addition to the bounding box. Both Faster R-CNN and Mask R-CNN are two-stage object detectors composed of two modules. The first module is a Region Proposal Network (RPN) that proposes several object candidate regions in the image using anchors. The second module is a detector that works in two steps. First, it extracts features from dense feature maps for the regions selected during RPN and in the second step, it calculates the confidence score for each region that contains the object of interest (Girshick, 2015). Detectron2-a PyTorch-based modular

object detection library (https://github.com/facebookresearch/detectron2), was used to implement Mask R-CNN in this study. A pre-trained model provided by the repository was used for transfer learning. Mask R-CNN was trained, validated, and tested with different sets of images generated/acquired in real-world settings to evaluate the effects as discussed earlier in the manuscript (Table 5.2). The configurations set for the model are provided in Table 5.3. It should be noted that annotation proportion of real image training dataset was imbalanced between the species. To minimize the biasness due to imbalanced dataset in training, a data sampler known as "RepeatFactorTrainingSampler" was used instead of regular data sampler while training the model. This sampler first computes per-image repeat factors based on category frequency for the rarest category for the given image and creates a list of image indices that needs to be repeated while feeding into the model in each to use for one epoch (https://detectron2.readthedocs.io/en/latest/_modules/detectron2/data/samplers/distributed_sampler.html).

Cotton1 and Cotton2 test datasets were used for the assessment of all the models trained in this study. The standard performance metric called Mean Average Precision (mAP) was calculated to assess the performance of the Mask R-CNN model. mAP was calculated separately for both model results, bounding box (bbox) and mask. mAP for these results is hereafter referred as mAP_b and mAP_m, respectively. In recent years, these metrics have been frequently used to assess the accuracy of object detection and segmentation tasks (Gao et al., 2020; Hu et al., 2021). mAP is a mean of AP calculated for each class to be detected/predicted by the model. AP for each class is calculated as the area under a precision-recall curve. The area is determined in two stages. First, the recall values are evenly segmented to 11 parts starting from 0 to 1.

Second, the maximum precision value is measured at each level of recall and averaged to determine AP (Equation 2).

$$\text{AP} = \frac{1}{11}\sum_{r \in \{0,0.1,0.2\ldots1\}} p_{max}(r) \qquad \text{(Equation 2)}$$

where p_{max} represents maximum precision measured at respective recall (r) level.

Precision and recall values are in turn calculated using the Equations 3 and 4, respectively.

$$\text{Precision} = \frac{TP}{TP + FP} \qquad \text{(Equation 3)}$$

$$\text{Recall} = \frac{TP}{TP + FN} \qquad \text{(Equation 4)}$$

where TP, FP, and FN denote true positive, false positive, and false negative samples, respectively.

True positives, false positives, and false negatives are identified using the Intersection over Union (IoU) ratio criterion. This ratio is calculated by comparing the ground truth box/mask with the model predicted box/mask. If the ratio is above the user-defined threshold, the predicted box/mask is labeled as TP. In this study, the threshold for IoU was set to 0.5. The mAP value ranges between 0 and 1, with 0 indicating null accuracy and 1 representing perfect accuracy.

5.3.4. Methodology for objective 2

The second objective of the study was aimed at assessing the potential of detection results (i.e. weed canopy masks and bounding boxes) in estimating above-ground weed biomass. The best model evaluated among all the models developed earlier was chosen for this purpose. The model was applied over the test images that contained the weeds sampled for biomass measurements. Both the detected bounding box and segmented canopy mask area of respective weeds were calculated and regressed separately with above-ground biomass collected for each

species. The coefficient of determination was calculated to assess the biomass predictability of model outputs.

5.4. Results & Discussion

5.4.1. Effect of crop row arrangement

Two different sets of synthetic images were produced (row-oriented and randomly-oriented) to test the importance of crop row orientation in the images for model performance. The row-oriented dataset resulted in higher mAP_b and mAP_m for both cotton datasets compared to the randomly-oriented dataset. This was true when training the model at both the original size (2048 x 2048 pixels) and at a reduced resolution (512 × 512 pixels) (Figure 5.4). The accuracy was greater when training was performed on the original size images. The detection and segmentation results using both sets of images are shown in Figure 5.5. The discrepancy in performance was more obvious for Cotton2 than for Cotton1. The Mask R-CNN framework used the ResNet101 backbone for feature extraction. This backbone has 101 layers that is able to learn a multitude of patterns and complex features at various scales (He et al., 2015). It is likely that the row-arrangement of cotton was well- recognized by the edge detector filters at the shallow layers of ResNet, which may have contributed to efficient learning at higher levels. The higher-level feature map may have highlighted cotton row as a prominent feature as these maps are derived from a series of convolution operations from lower-level feature maps.

5.4.2. Effect of instance diversity

Seven different sets of synthetic images were generated with different IP sizes. The main goal was to evaluate the effect of IP size on the synthetic image quality and performance. As expected, the performance differed across different IP sizes (Figure 5.5a). In general, the mAP_b

and mAP_m showed an increasing trend with increases in IP from 1 to 50 for both the cotton datasets (Figure 5.5b). It is notable that an IP size of 1 resulted in a satisfactory mAP value of 0.55. The rate of increase flattened towards an IP size of 40, indicating that any further increase in IP size may not necessarily improve the performance significantly. Hu et al. (2021) also observed no significant improvements beyond an IP size of 68 when training a Faster R-CNN model with synthetic images. Overall, results indicate that quality synthetic images can be generated even with low IP sizes, given that the samples are truly representative of the objects of interest.

5.4.3. Effect of clipping methods

Models were trained using two different sets of synthetic images generated with the IP that comprised of manually-clipped and automatically-clipped plants. The overall results for Cotton1 and Cotton2 showed that automatically-clipped plants can perform comparably to the manual-clipping method (Figure 5.6). In particular, mAP_b and mAP_m were similar between the two clipping methods for both cotton datasets. In total, it took 170 minutes to manually clip 150 plant instances, whereas the same instances were clipped and sorted automatically just in 5 mins, a 34-fold faster rate. Gao et al. (2020) also successfully used automatically clipped plant instances to generate synthetic images for training a weed detection model. The present study provides a comparative evaluation of these two common methods by testing for a multi-class detection and mask generation problem.

5.4.4. Performance of GAN-derived fake plants Vs real plants

The performance of GAN-derived fake plant-based synthetic images and real plant-based synthetic images was evaluated to independently train the Mask R-CNN model. The real plant-based model resulted in a better accuracy compared to the GAN-based model for both cotton

datasets (Figure 5.7). In general, MG was misclassified as cotton and vice-versa whereas such errors were less common with Grass. Such similarity in appearance could be attributed to misclassification between cotton and MG. It is likely that the training sample size employed for styleGAN in our case (~50 plants per class) was not sufficient for generating high quality fake plants. However, the GAN approach is still promising for training the weed detection and segmentation model. Fawakherji et al. (2021) utilized a conditional GAN to generate realistic multi-spectral synthetic images and used them in combination with the original images in the training process. They observed improvements in the segmentation performance by the model.

5.4.5. Performance of the mixed dataset Vs real dataset

The mixed dataset did not result in a significant performance gain in this study. For both cotton datasets, the performance of the mixed dataset was generally comparable to the real dataset (Figure 5.8). This finding doesn't conform previous reports (e.g. Gao et al. 2020) that found considerable improvements in accuracy with the addition of synthetic images to real image dataset for training. The lack of improvements in accuracy in this study could be attributed to the fact that the real images utilized here contained sufficient variance for different objects of interest. In future, a subset of the real image dataset could be mixed with the synthetic images to gain more insights into the critical minimum number of real images required for training.

5.4.6. Assessing the biomass predictability of model outputs

The area of the bounding boxes and canopy masks resulting from Mask R-CNN were regressed independently with biomass of respective weeds to determine the biomass predictability of model outputs. The regression was performed separately for MG and Grass. For both groups, the canopy mask area was found to be a better estimator compared to the bounding box area. Further, biomass was estimated more accurately for MG (R^2=66) than for Grass

(R^2=0.40) with canopy mask area (Figure 5.9). The bounding boxes overestimate the leaf surface area, which is not systematic owing to varying canopy structure of plants. This problem is pronounced in the case of Grass due to the random orientation of Grass leaves, resulting in increased bounding box area. This could be the prime reason why the canopy mask area was more effective in estimating biomass than the bounding box area. The reason the authors could think of why biomass for MG were better predicted compared to Grass using mask area is that Grass had extremely low biomass and such biomass measurements were prone to errors. Vanamberg et al. (2007) utilized digital image analysis to estimate aboveground biomass of shortgrass prairie and obtained an R^2 value of 0.55. Albert et al. (2019) effectively used canopy coverage area to estimate weed dry biomass in a grass-clover mixture. Skovsen et al. (2019) also found a linear association between model predicted visual weed fraction in pixels and fractional weed biomass in kg. Both of these studies investigated weed biomass estimation in a unit area that included multiple plants. However, the current study explored the feasibility of biomass prediction at an individual plant level, which is crucial for site-specific weed management. The results indicate that canopy mask area can be a reliable predictor of biomass, especially for broadleaved weeds.

5.5. Conclusions

This study explored various strategies for generating synthetic images in training a Mask R-CNN model for weed detection and segmentation. The feasibility of biomass estimation with the Mask R-CNN model outputs was also assessed. The important take-aways from this study are:

- Synthetic images can be a great alternative to real images. In this study, real plant instance-based synthetic images provided ~80% of the accuracy that was achieved with original real images.
- Row-orientation of cotton in the synthetic images proved to be beneficial compared to random orientation. This calls for a careful selection of crop positions in the images while generating synthetic images.
- About 40-50 real plant instances were sufficient for generating synthetic images for optimal performance. This implies that the quality (i.e. variability) of plant instances can be prioritized over the number of plant instances.
- Synthetic images generated with automatically-clipped plant instances performed comparably to the ones generated with manual clipping. This suggests that enormous amounts of time and other resources could be saved by clipping plant instances automatically.
- The GAN-derived fake plant instance-based synthetic images did not provide accuracy levels comparable to that of the real plant instance-based synthetic images. However, it should be noted that a small training sample size was used in this study for training the GAN model, which may have resulted in low-quality synthesis.
- Weed segmentation output (i.e. canopy mask area) can be a good predictor for biomass, especially for broadleaved weeds.

There are several other benefits of synthetic images. For example, synthetic images as generated in this study can be greatly utilized temporal image analysis as classification models can be quickly trained. However, the findings presented in this study are not applicable to every single

situation, and they do have some practical limitations. For example, automatic clipping may be challenging under complex crop-weed background scenes, including occlusions. Further, the optimal IP size reported in this study may not be sufficient for other row-crops and weed species depending on the level of variability in the population. Future research should investigate these questions.

5.6. References

Ahmed, F., Al-Mamun, H.A., Bari, A.S.M.H., Hossain, E., Kwan, P., 2012. Classification of crops and weeds from digital images: A support vector machine approach. Crop Protection 40, 98–104. https://doi.org/10.1016/j.cropro.2012.04.024

Albert, P., Saadeldin, M., Narayanan, B., Mac Namee, B., Hennessy, D., O'Connor, A., O'Connor, N., McGuinness, K., 2021. Semi-supervised dry herbage mass estimation using automatic data and synthetic images. Presented at the Proceedings of the IEEE/CVF International Conference on Computer Vision, pp. 1284–1293.

Andújar, D., Dorado, J., Fernández-Quintanilla, C., Ribeiro, A., 2016. An approach to the use of depth cameras for weed volume estimation. Sensors 16, 972. https://doi.org/10.3390/s16070972

Dwibedi, D., Misra, I., Hebert, M., 2017. Cut, paste and learn: surprisingly easy synthesis for instance detection. Presented at the Proceedings of the IEEE International Conference on Computer Vision, pp. 1301–1310.

Espejo-Garcia, B., Mylonas, N., Athanasakos, L., Vali, E., Fountas, S., 2021. Combining generative adversarial networks and agricultural transfer learning for weeds

identification. Biosystems Engineering 204, 79–89. https://doi.org/10.1016/j.biosystemseng.2021.01.014

Fawakherji, M., Potena, C., Prevedello, I., Pretto, A., Bloisi, D.D., Nardi, D., 2020. Data augmentation using GANs for crop/weed segmentation in precision farming, in: 2020 IEEE Conference on Control Technology and Applications (CCTA). Presented at the 2020 IEEE Conference on Control Technology and Applications (CCTA), pp. 279–284. https://doi.org/10.1109/CCTA41146.2020.9206297

Gao, J., French, A.P., Pound, M.P., He, Y., Pridmore, T.P., Pieters, J.G., 2020. Deep convolutional neural networks for image-based Convolvulus sepium detection in sugar beet fields. Plant Methods 16, 29. https://doi.org/10.1186/s13007-020-00570-z

Georgakis, G., Mousavian, A., Berg, A.C., Kosecka, J., 2017. Synthesizing training data for object detection in indoor Scenes. arXiv:1702.07836 [cs].

Girshick, R., 2015. Fast R-CNN. Presented at the Proceedings of the IEEE International Conference on Computer Vision, pp. 1440–1448.

Harkel, J., Bartholomeus, H., Kooistra, L., 2020. Biomass and crop height estimation of different crops using UAV-Based lidar. Remote Sensing 12, 17. https://doi.org/10.3390/rs12010017

He, K., Gkioxari, G., Dollar, P., Girshick, R., 2017. Mask R-CNN. Presented at the Proceedings of the IEEE International Conference on Computer Vision, pp. 2961–2969.

He, K., Zhang, X., Ren, S., Sun, J., 2015. Deep residual learning for image recognition. arXiv:1512.03385 [cs].

Hu, C., Sapkota, B.B., Thomasson, J.A., Bagavathiannan, M.V., 2021. Influence of image quality and light consistency on the performance of convolutional neural networks for weed mapping. Remote Sensing 13, 2140. https://doi.org/10.3390/rs13112140

Kerdegari, H., Razaak, M., Argyriou, V., Remagnino, P., 2019. Smart monitoring of crops using generative adversarial networks, in: Vento, M., Percannella, G. (Eds.), Computer Analysis of Images and Patterns, Lecture Notes in Computer Science. Springer International Publishing, Cham, pp. 554–563. https://doi.org/10.1007/978-3-030-29888-3_45

LeCun, Y., Bengio, Y., Hinton, G., 2015. Deep learning. Nature 521, 436–444. https://doi.org/10.1038/nature14539

Liu, B., Bruch, R., 2020. Weed detection for selective spraying: a review. Current Robot Reports 1, 19–26. https://doi.org/10.1007/s43154-020-00001-w

Lottes, P., Behley, J., Milioto, A., Stachniss, C., 2018. Fully convolutional networks with sequential information for robust crop and weed detection in precision farming. IEEE Robotics and Automation Letters 3, 2870–2877. https://doi.org/10.1109/LRA.2018.2846289

Pearlstein, L., Kim, M., Seto, W., 2016. Convolutional neural network application to plant detection, based on synthetic imagery, in: 2016 IEEE Applied Imagery Pattern Recognition Workshop (AIPR). Presented at the 2016 IEEE Applied Imagery Pattern Recognition Workshop (AIPR), pp. 1–4. https://doi.org/10.1109/AIPR.2016.8010596

Rumpf, T., Römer, C., Weis, M., Sökefeld, M., Gerhards, R., Plümer, L., 2012. Sequential support vector machine classification for small-grain weed species discrimination with

special regard to Cirsium arvense and Galium aparine. Computers and Electronics in Agriculture 80, 89–96. https://doi.org/10.1016/j.compag.2011.10.018

Sapkota, B., Singh, V., Neely, C., Rajan, N., Bagavathiannan, M., 2020. Detection of Italian Ryegrass in Wheat and Prediction of Competitive Interactions Using Remote-Sensing and Machine-Learning Techniques. Remote Sensing 12, 2977. https://doi.org/10.3390/rs12182977

Skovsen, S., Dyrmann, M., Mortensen, A.K., Laursen, M.S., Gislum, R., Eriksen, J., Farkhani, S., Karstoft, H., Jorgensen, R.N., 2019. The grass-clover image dataset for semantic and hierarchical species understanding in agriculture, in: 2019 IEEE/CVF Conference on Computer Vision and Pattern Recognition Workshops (CVPRW). Presented at the 2019 IEEE/CVF Conference on Computer Vision and Pattern Recognition Workshops (CVPRW), IEEE, Long Beach, CA, USA, pp. 2676–2684. https://doi.org/10.1109/CVPRW.2019.00325

Vanamburg, L.K., Trlica, M.J., Hoffer, R.M., Weltz, M.A. 2006. Ground based digital imagery for grassland biomass estimation, International Journal of Remote Sensing, 27, 939-950, https://doi.org/10.1080/01431160500114789.

Wang, A., Xu, Y., Wei, X., Cui, B., 2020. Semantic segmentation of crop and weed using an encoder-decoder network and image enhancement method under uncontrolled outdoor illumination. IEEE Access 8, 81724–81734. https://doi.org/10.1109/ACCESS.2020.2991354

Yu, J., Schumann, A.W., Cao, Z., Sharpe, S.M., Boyd, N.S., 2019. Weed detection in perennial ryegrass with deep learning convolutional neural network. Frontiers in Plant Science. https://doi.org/10.3389/fpls.2019.01422

5.7. Tables and Figures

Table 5.1. Crop-weed conditions during real image dataset acquisition in 2020 and 2021 using a Fujifilm camera.

Image dataset name	Acquisition Date	Cotton growth stage	Weed composition/growth stage	Weed density (plants m^{-2})
Cotton1	May 06, 2020	4-5 leaves	MG: cotyledon-4 leaves JG: 2-3 leaves TM: 2-3 leaves	18
Cotton2	June 13, 2021	2-4 leaves	MG: cotyledon-6 leaves TM: 2-4 leaves	21

Table 5.2. Details on training, validation, and test datasets used in this study.

Image dataset	# of images	# of annotations	Annotation composition
Real_training_image_dataset	460	9115	Cotton: 7.65% MG: 17.8% Grass: 75.01%
Synthetic_training_image_dataset	770	9237	Cotton: 33.34% MG: 33.32% Grass: 33.34%
Real_validation_image dataset	100		Cotton: 7.65% MG: 17.8% Grass: 75.01%
Real_test_image_dataset (Cotton1)	100	848	Cotton: 12.66% MG: 45.31% Grass: 42.01%
Real_test_image_dataset (Cotton2)	50	976	Cotton: 10.04% MG: 7.4% Grass: 82.01%

Table 5.3. Major hyperparameters and values used with Mask R-CNN training.

Major hyperparameters	Values
BACKBONE	ResNet101
EPOCH*	50000
BASE_LEARNING_RATE	0.001
LEARNING_RATE_SCHEDULER_NAME	WarmupMultiStepLR
MOMENTUM	0.9
WEIGHT DECAY	0.0001
RPN_BATCH_SIZE_PER_IMAGE	256
RPN_NMS_THRESHOLD	0.7
ANCHOR_SIZES	[32, 64, 128, 256, 512]
NUMBER OF CLASSES*	3
CHECKPOINT_PERIOD*	5000
TEST_EVAL_PERIOD*	1000

[1]Hyperparameters with * were used with custom values whereas hyperparameters (without *) were used in default values. The description of the hyperparameters can be found at https://detectron2.readthedocs.io/en/latest/modules/index.html.

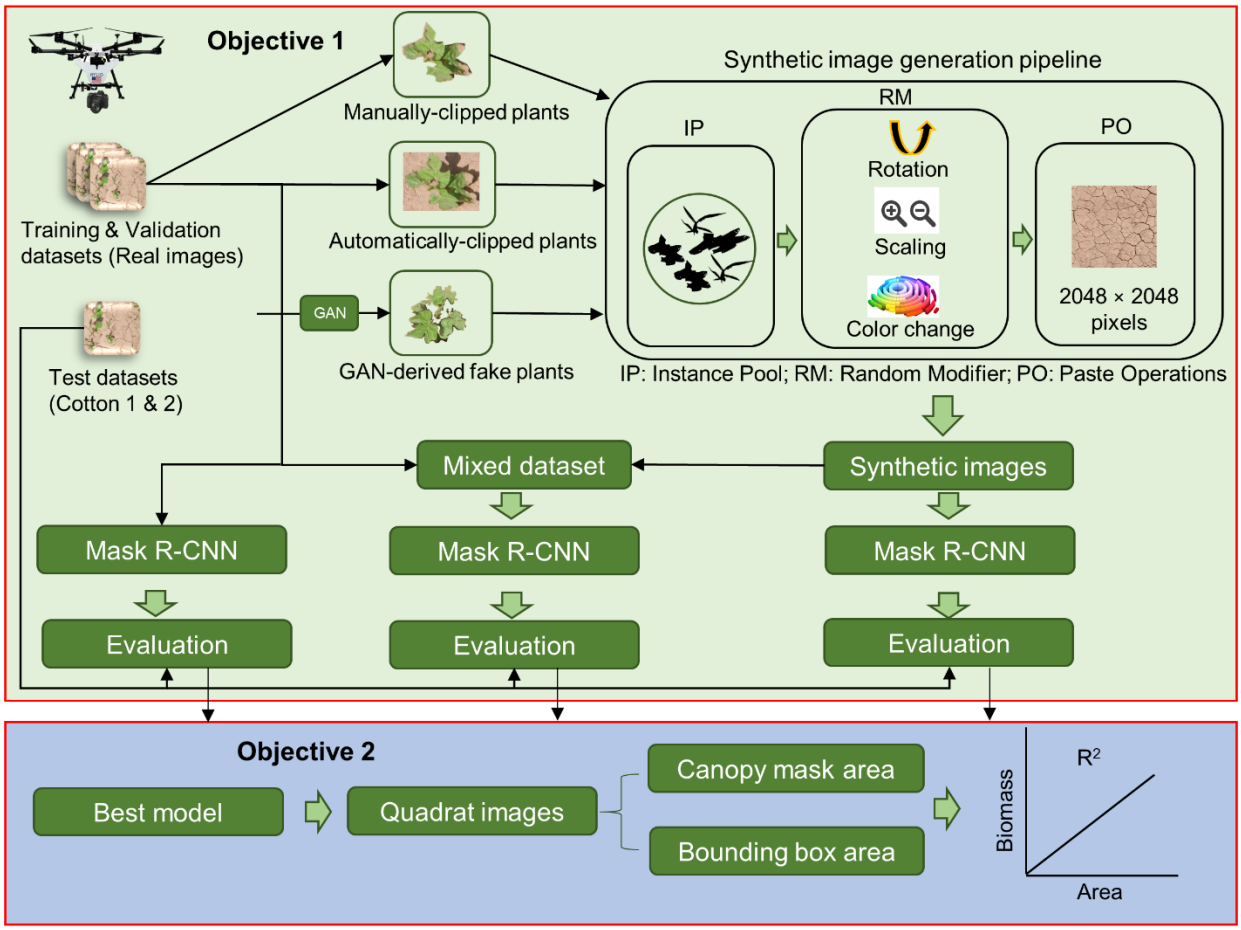

Figure 5.1. Workflow diagram for the methodology implemented in this study. The pale green and blue sections show the schematic for objectives 1 and 2, respectively. The objective 1 is aimed at testing several models with different-source input images, whereas the objective 2 determines the predictability of model results to estimate above-ground biomass of weeds

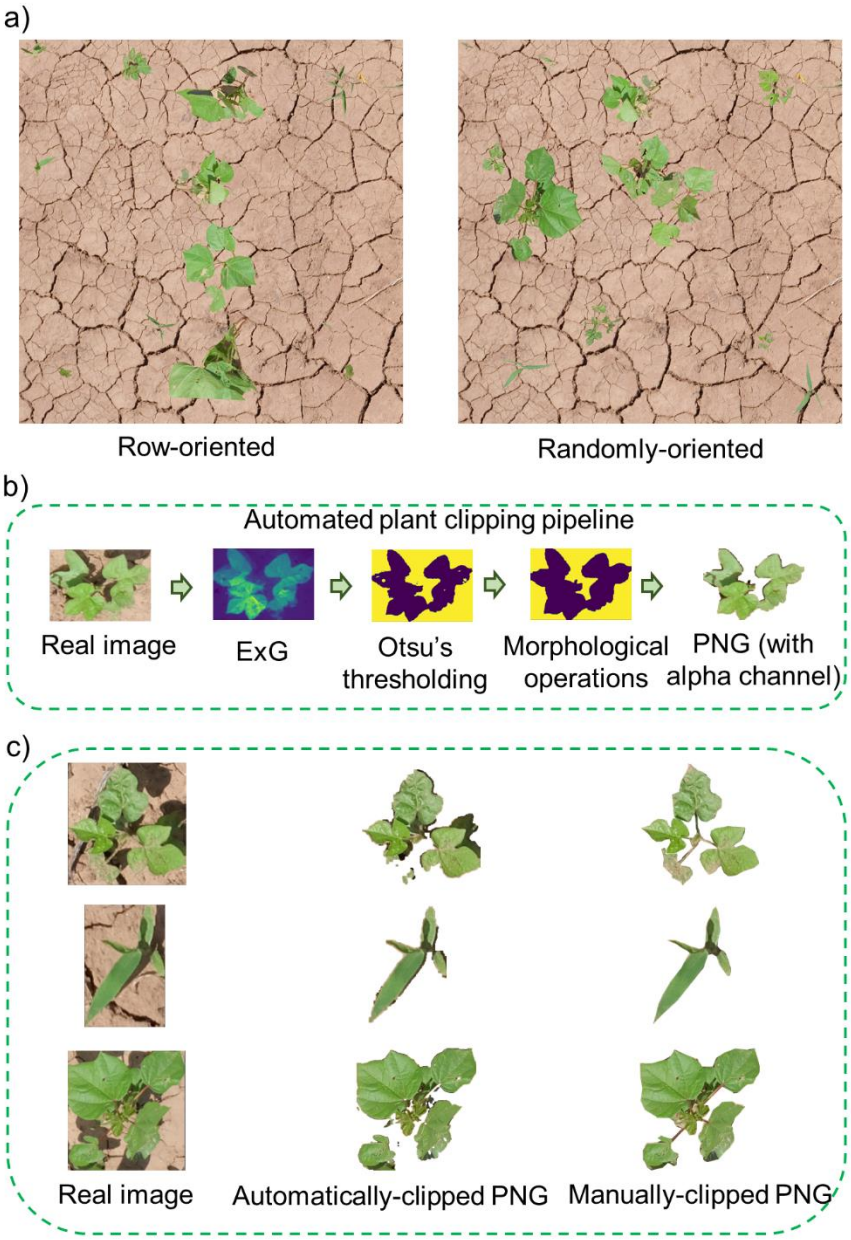

Figure 5.2. a) A representative sample for row-oriented and randomly-oriented images produced with the synthetic image generation pipeline, b) The automated plant clipping pipeline to derive PNG images with alpha channel, and c) Comparison of automatically-clipped and manually-clipped PNG instances for the given real plant images.

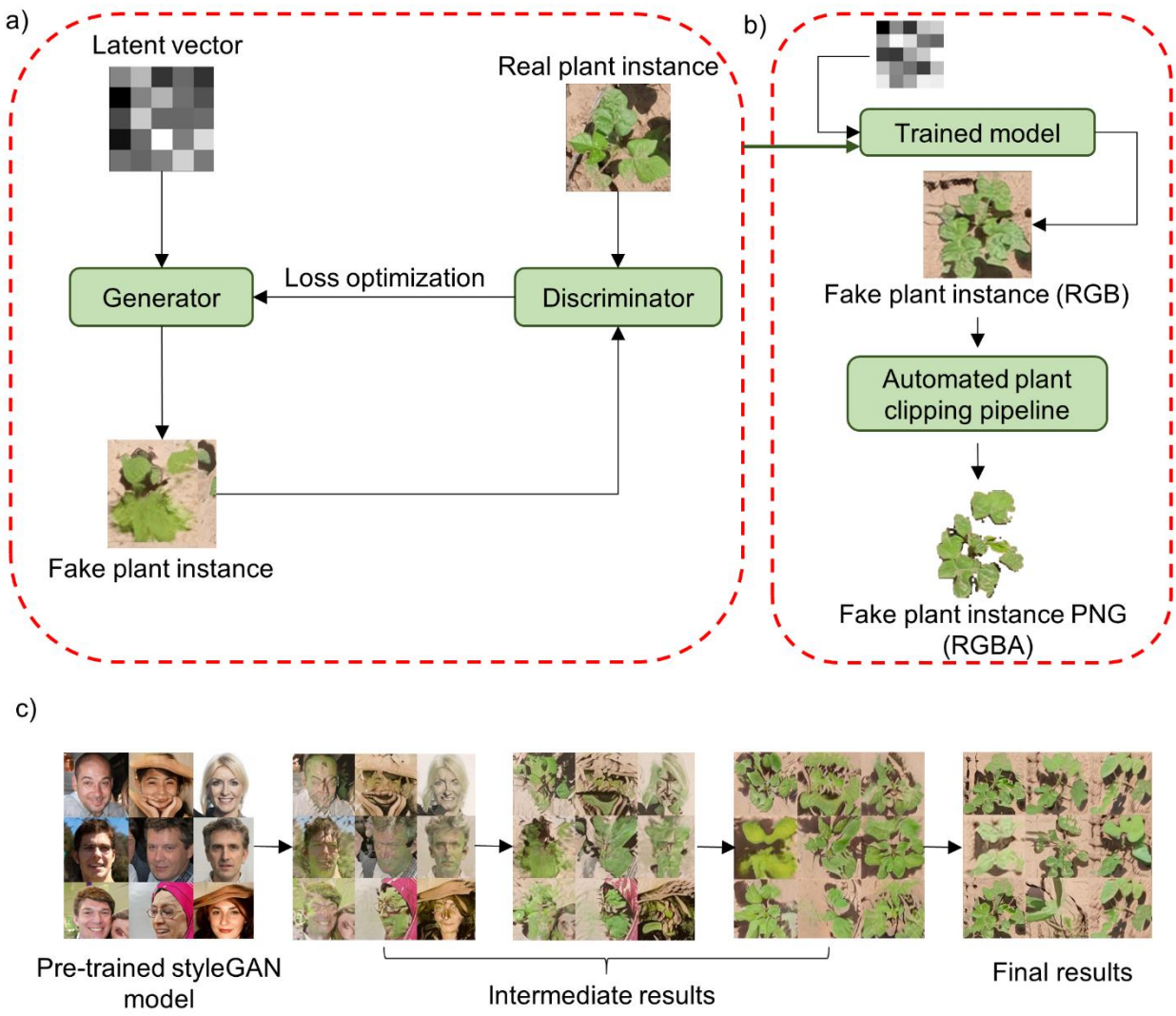

Figure 5.3. a) Schematic showing the general workflow for a simple generative adversarial network (GAN) model, b) Additional post-processing step for generating new fake plant PNGs using the custom trained styleGAN model, and c) sample results obtained with the custom styleGAN model at various stages of the training process.

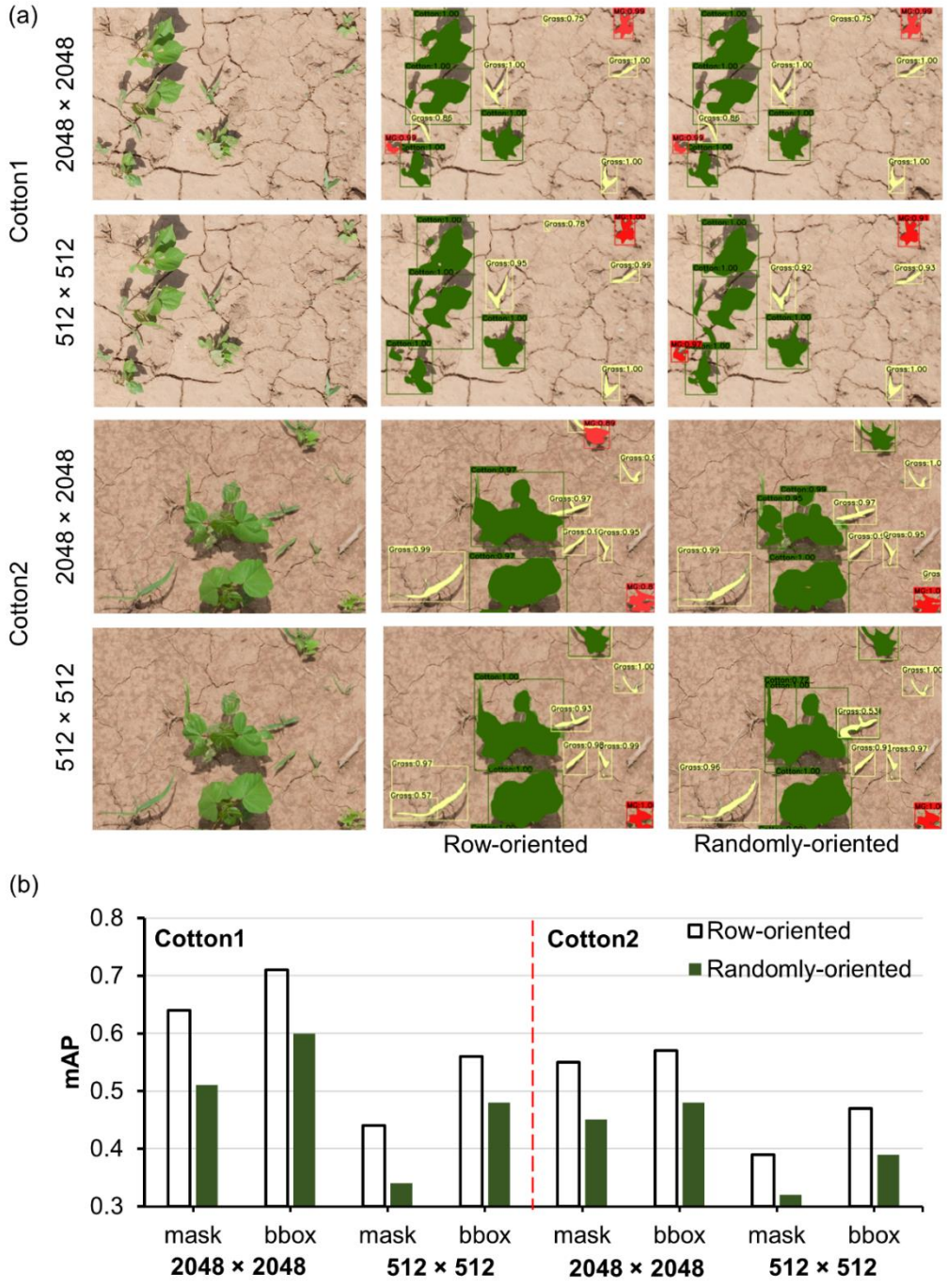

Figure 5.4. Results obtained from models trained with row-oriented and randomly-oriented synthetic images: a) Detection and segmentation results obtained for both test datasets (Cotton1 and Cotton2) with the original image size (2048 x 2048) and reduced image size (512 × 512), and b) mAP values (mask and bbox) obtained for Cotton1 and Cotton2.

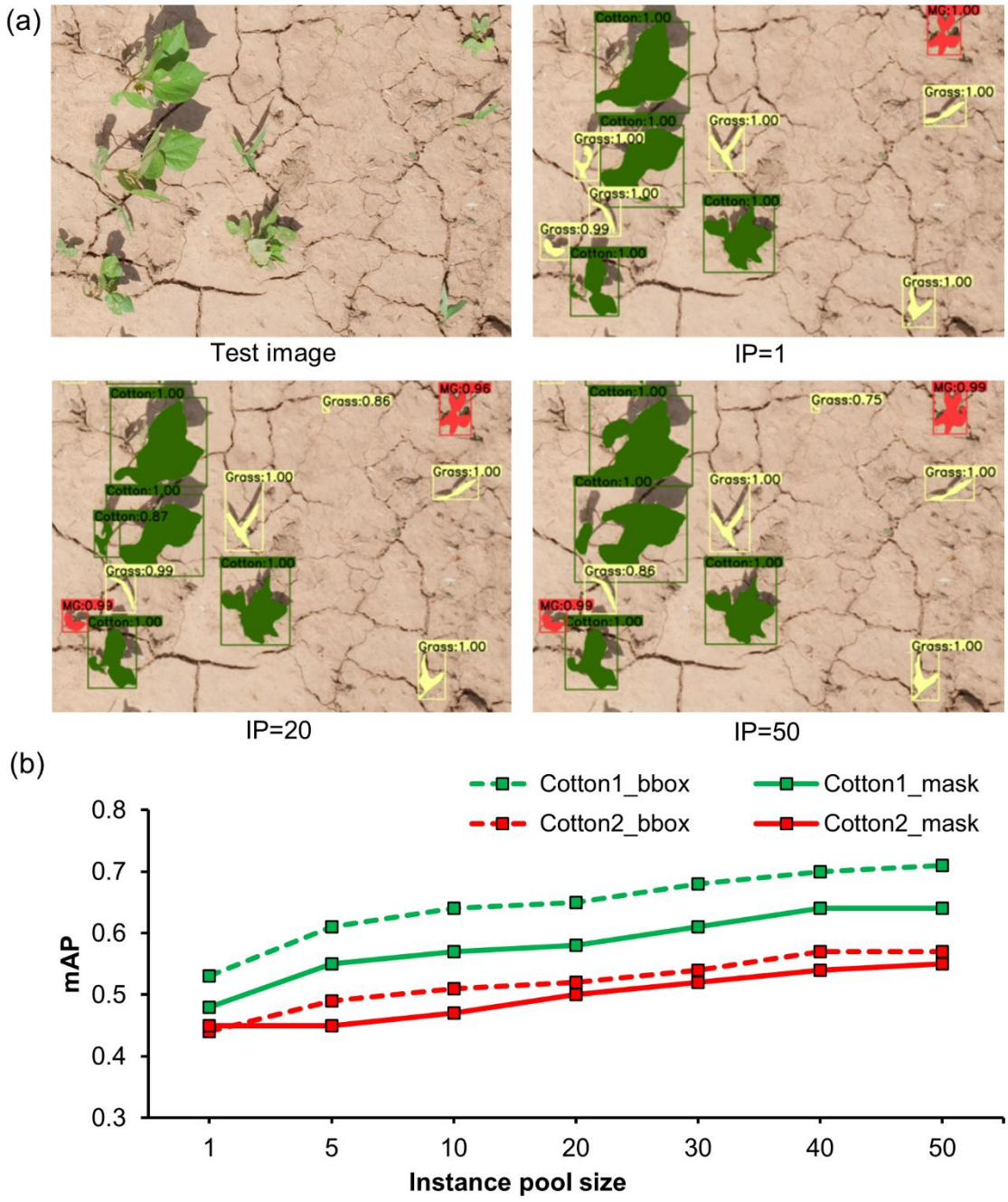

Figure 5.5. Results obtained from models trained with synthetic images generated using various instance pool (IP) sizes: a) Detection and segmentation results obtained for Cotton1 with IP=1, IP=20, and IP=50, and b) Mean average precision (mAP) values compared for bounding box (bbox) and mask results for Cotton1 and Cotton2, obtained for IP sizes ranging from 1 to 50.

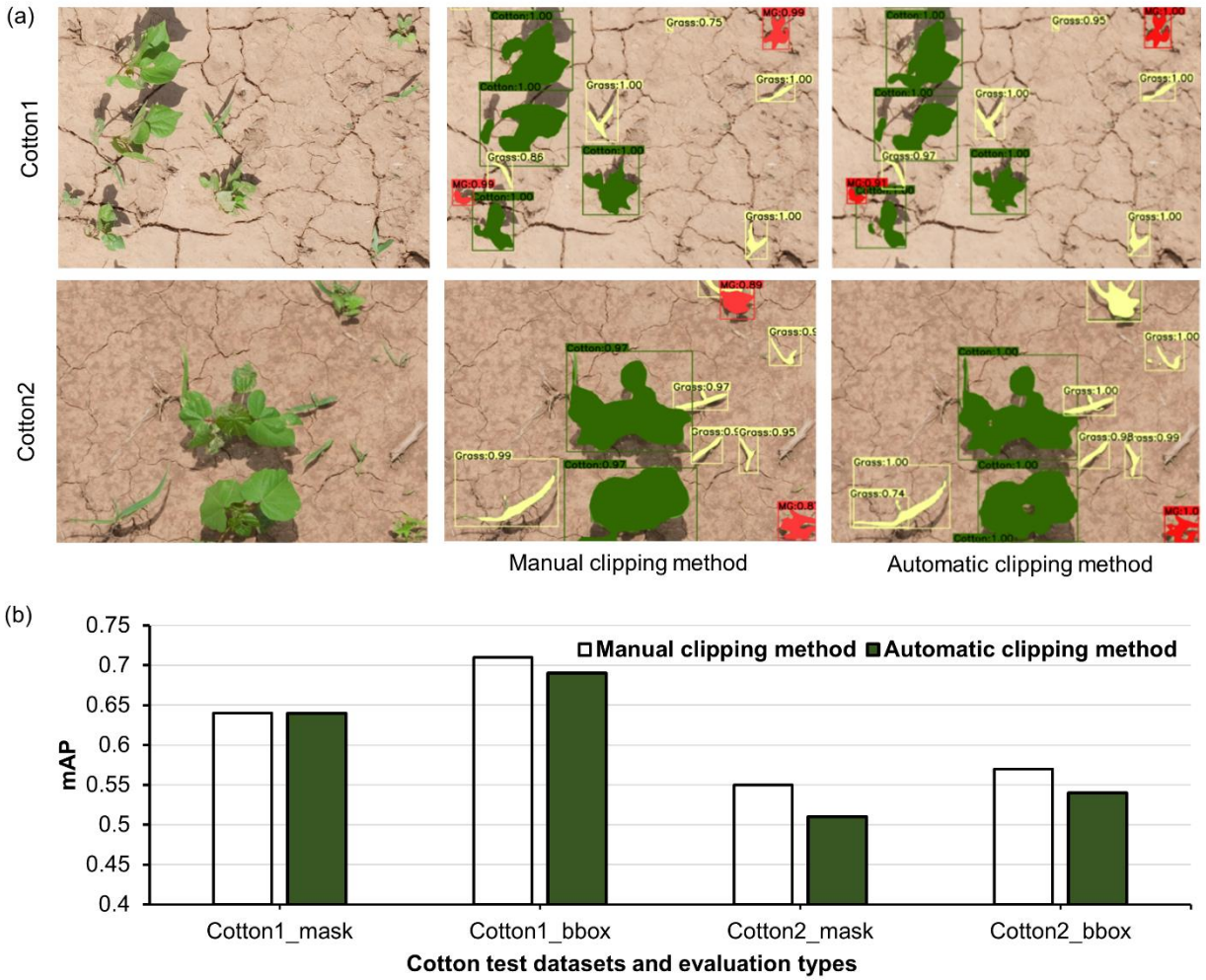

Figure 5.6. Results obtained with models trained with synthetic images generated using manual clip and automatic clip method: a) Detection and segmentation results obtained for both test datasets (Cotton1 and Cotton2), and b) Mean average precision (mAP) values for bounding box (bbox) and mask results obtained for Cotton1 and Cotton2

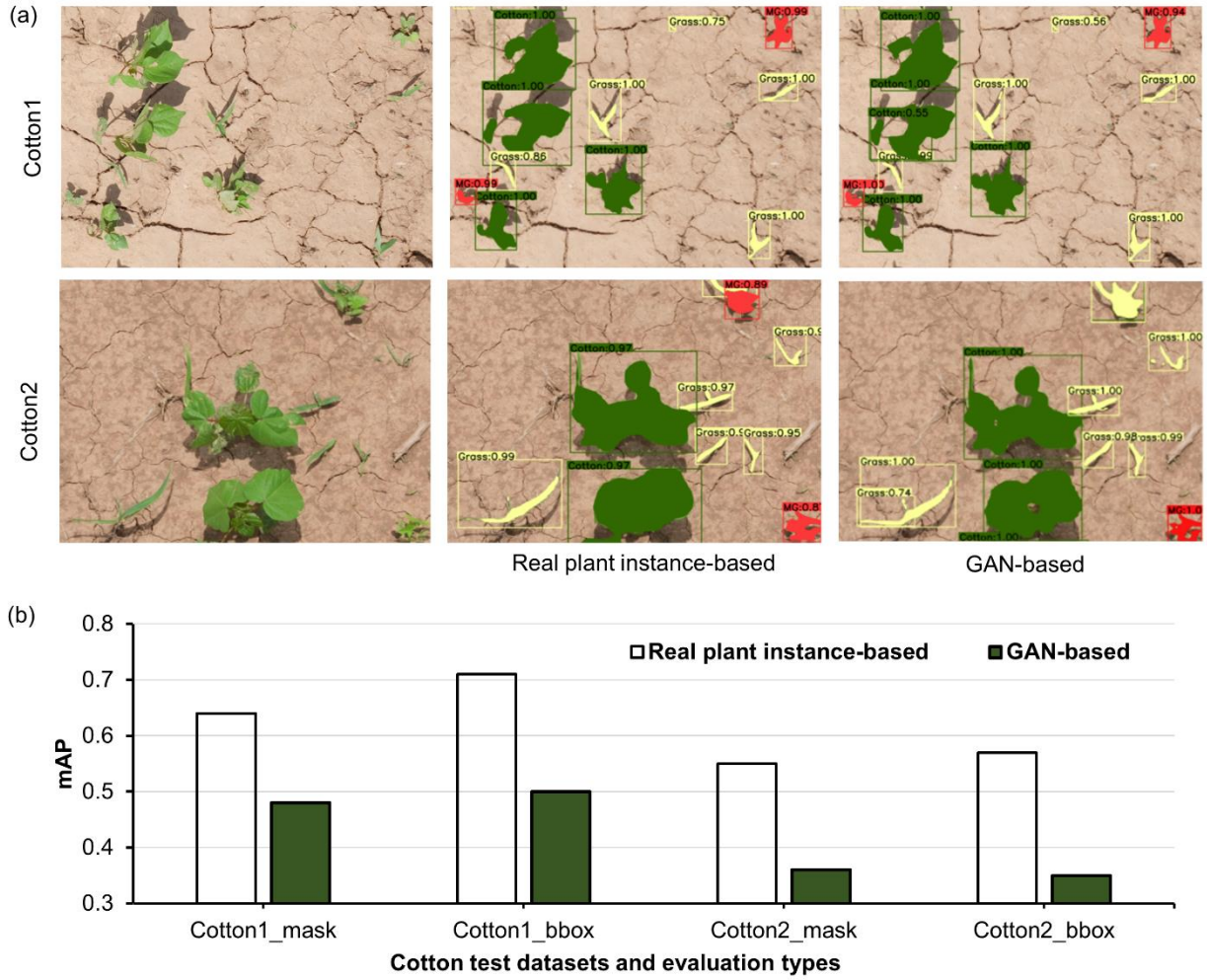

Figure 5.7. Results obtained from models trained with synthetic images generated using real plant instances and generative adversarial network (GAN)-derived fake plants: a) Detection and segmentation results obtained for the test datasets Cotton1 and Cotton2, and b) Mean average precision (mAP) values for bounding box (bbox) and mask results obtained for Cotton1 and Cotton2.

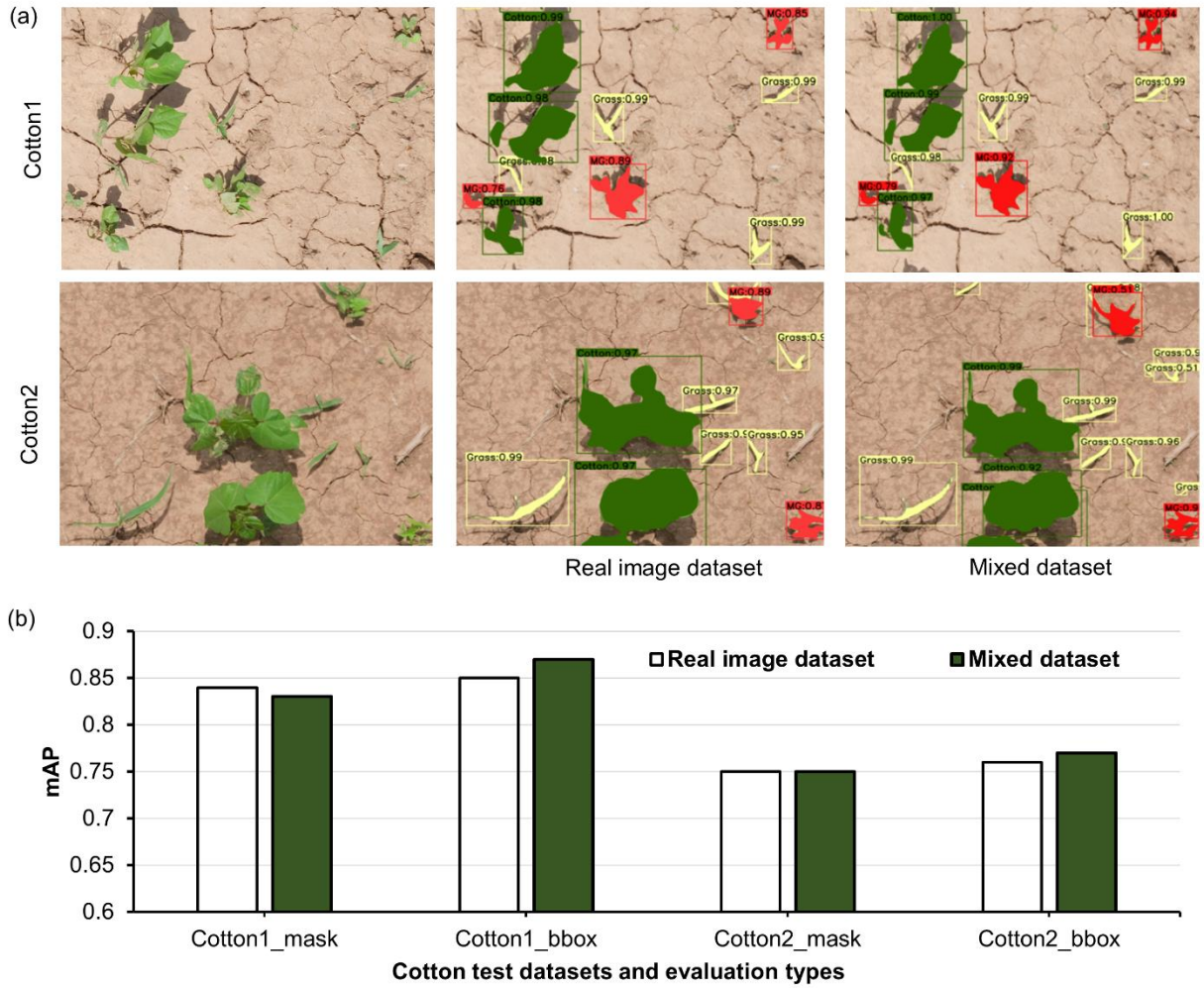

Figure 5.8. Results obtained from models trained with real image dataset and mixed dataset (original real images + real plant-based synthetic images): a) Detection and segmentation results obtained for the test datasets Cotton1 and Cotton2, and b) Mean average precision (mAP) values for bounding box (bbox) and mask results obtained for Cotton1 and Cotton2.

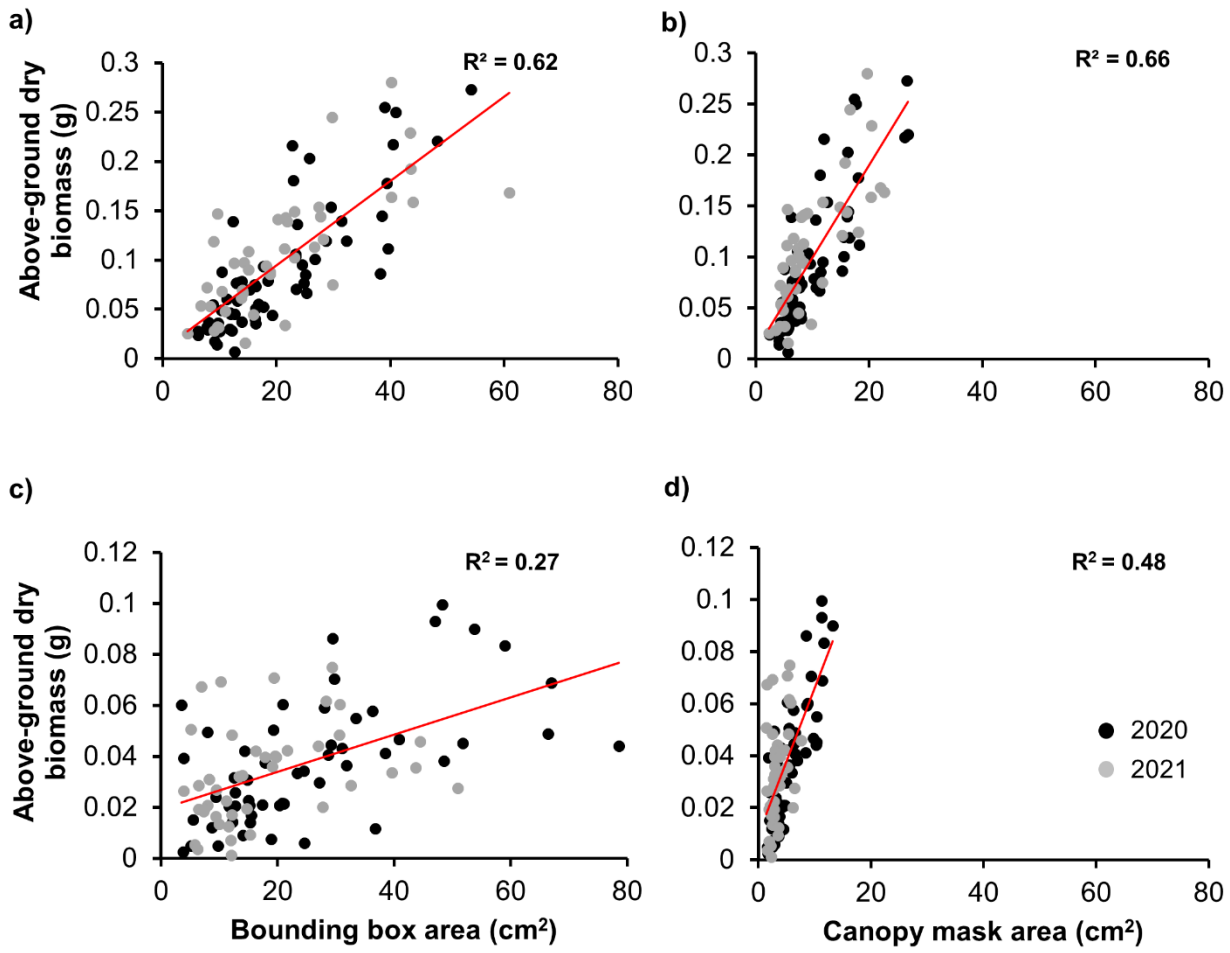

Figure 5.9. Regression analysis for estimating biomass for morningglories (a, b) and grasses (c, d) with bounding box and canopy mask area, respectively. The red line represents the best fitted line estimated by the regression analysis. Altogether, 99 (60 in 2020 & & 40 in 2021) MG and Grass individuals were sampled for biomass, respectively.

6. CONCLUSIONS

This dissertation explored and experimented with integrated geospatial and computer vision techniques to detect weeds in agricultural systems. Several image analysis techniques were evaluated for various crop-weed scenarios. The dissertation concludes that the row-detection method can be reliably used for mapping weed coverage in cotton at various density levels. It also concludes that accuracy might drop with an increase in weed density in the field. This research also suggests that image analysis-derived weed coverage can be confidently used to estimate the number of weeds in the field. The methodology demonstrated in this study can be a quick yet effective method for producing weed maps, which can be used for various purposes, including devising weed management plans for current and future cropping cycles.

This research also concludes that ryegrass can be detected and mapped in wheat fields using a pixel-based machine learning approach. The ryegrass-wheat study also suggests that hue and saturation features derived from color transformation can provide higher separability between ryegrass and wheat. In addition, it also suggests that image analyzed ryegrass coverage at the early growth stage can estimate the competitive effects on wheat in respect to biomass and grain yield reduction. In particular competition effects on biomass were better estimated with image-based coverage. These findings are expected to provide guidance on the site-specific ryegrass management in wheat and help farmers early predict the future ryegrass-wheat interactions for devising better management plans.

This dissertation concludes that the model trained to detect weed species in cotton can be used to detect the same given weed species in soybean and corn. The cross-crop applicability of

the detection model was higher for soybean compared to corn. Whether or not weeds are detected at meta-level or individual weed species level also determined the cross-applicability. The study also shows that the addition of non-cotton images can improve the cross-crop applicability differentially across corn and soybean. These findings are expected to help minimize the efforts in developing a crop-specific detection model, which in return would save huge time and money resources.

This research also demonstrates that synthetic images can provide comparable (~80%) accuracy to real images. The study suggests that the row orientation of cotton in the synthetic images can be beneficial compared to random orientation. This calls for a careful selection of crop positions in the images while generating synthetic images. The study shows that automatically-clipped plants can be as effective as human-clipped plants for generating synthetic images. In addition, the study also shows that the canopy mask area can be a great predictor for above-ground weed biomass. The findings of this study offer valuable insights for guiding future endeavors oriented towards using synthetic images for weed detection and segmentation and biomass estimation in row crops.

LITERATURE CITED

Akar, Ö., 2017. Mapping land use with using rotation forest algorithm from UAV images. European Journal of Remote Sensing 50, 269–279. https://doi.org/10.1080/22797254.2017.1319252

Aracena, P.A., 2013. Spatially-explicit decision support system for invasive weed species management. Ph.D. Thesis, University of Montana, Missoula, MT, USA.

Castaldi, F., Pelosi, F., Pascucci, S., Casa, R., 2017. Assessing the potential of images from unmanned aerial vehicles (UAV) to support herbicide patch spraying in maize. Precision Agriculture 18, 76–94. https://doi.org/10.1007/s11119-016-9468-3

Chen, L.-C., Papandreou, G., Kokkinos, I., Murphy, K., Yuille, A.L., 2018. DeepLab: Semantic image segmentation with deep convolutional nets, atrous convolution, and fully connected CRFs. IEEE Transactions on Pattern Analysis and Machine Intelligence 40, 834–848. https://doi.org/10.1109/TPAMI.2017.2699184

Christensen, S., Søgaard, H.T., Kudsk, P., Nørremark, M., Lund, I., Nadimi, E.S., Jørgensen, R., 2009. Site-specific weed control technologies. Weed Research 49, 233–241. https://doi.org/10.1111/j.1365-3180.2009.00696.x

De Castro, A.I., Torres-Sánchez, J., Peña, J.M., Jiménez-Brenes, F.M., Csillik, O., López-Granados, F., 2018. An automatic random forest-OBIA algorithm for early weed mapping between and within crop rows using UAV imagery. Remote Sensing 10, 285. https://doi.org/10.3390/rs10020285

Everitt, J.H., Fletcher, R.S., Elder, H.S., Yang, C., 2008. Mapping giant salvinia with satellite imagery and image analysis. Environmental Monitoring & Assessment 139, 35–40. https://doi.org/10.1007/s10661-007-9807-y

Ludovisi, R. Tauro, F., Salvati, R., Khoury, S., Scarascia, G.M., Harfouche, A.L., 2017. UAV-based thermal imaging for high-throughput field phenotyping of black poplar response to drought. Frontiers in Plant Science 8, 8.

Gao, J., Nuyttens, D., Lootens, P., He, Y., Pieters, J.G., 2018. Recognising weeds in a maize crop using a random forest machine-learning algorithm and near-infrared snapshot mosaic hyperspectral imagery. Biosystems Engineering 170, 39–50. https://doi.org/10.1016/j.biosystemseng.2018.03.006

Goudy, H.J., Bennett, K.A., Brown, R.B., Tardif, F.J., 2001. Evaluation of site-specific weed management using a direct-injection sprayer. Weed Science 49, 359–366. https://doi.org/10.1614/0043-1745(2001)049[0359:EOSSWM]2.0.CO;2

Hall, M.R., Swanton, C.J., Anderson, G.W., 1992. The critical period of weed control in grain corn (*Zea mays*). Weed Science 40, 441–447. https://doi.org/10.1017/S0043174500051882

Jensen, J.R., 2005. Digital image processing: a remote sensing perspective. Upper Saddle River, NJ: Prentice Hall.

Klette, R., 2014. Concise computer vision. Springer.

López-Granados, F., Torres-Sánchez, J., Serrano-Pérez, A., de Castro, A.I., Mesas-Carrascosa, Fco.-J., Peña, J.-M., 2016. Early season weed mapping in sunflower using UAV technology: variability of herbicide treatment maps against weed thresholds. Precision Agric 17, 183–199. https://doi.org/10.1007/s11119-015-9415-8

Medlin, C.R., Shaw, D.R., 2000. Economic comparison of broadcast and site-specific herbicide applications in nontransgenic and glyphosate-tolerant Glycine max. Weed Science 48, 653–661. https://doi.org/10.1614/0043-1745(2000)048[0653:ECOBAS]2.0.CO;2

Mirik, M., Ansley, R.J., Steddom, K., Jones, D.C., Rush, C.M., Michels, G.J., Elliott, N.C., 2013. Remote distinction of obnoxious weed (Musk Thistle: *Carduus nutans*) using airborne hyperspectral imagery and the support vector machine classifier. Remote Sensing 5, 612–630. https://doi.org/10.3390/rs5020612

Mohri, M., Rostamizadeh, A., Talwalkar, A., 2018. Adaptive computation and machine learning. Foundations of Machine Learning, 2nd ed.; The MIT Press: Cambridge, MA, USA.

Oerke, E.C., 2006. Crop losses to pests. The Journal of Agricultural Science 144, 31–43. https://doi.org/10.1017/S0021859605005708

Lamb, D.W., Brown, R.B., 2001. PA—Precision Agriculture: Remote-sensing and mapping of weeds in crops. Journal of Agricultural Engineering Research 78, 117–125. https://doi.org/10.1006/jaer.2000.0630

Pérez-Ruíz, M., Slaughter, D.C., Fathallah, F.A., Gliever, C.J., Miller, B.J., 2014. Co-robotic intra-row weed control system. Biosystems Engineering 126, 45–55. https://doi.org/10.1016/j.biosystemseng.2014.07.009

Sa, I., Popović, M., Khanna, R., Chen, Z., Lottes, P., Liebisch, F., Nieto, J., Stachniss, C., Walter, A., Siegwart, R., 2018. WeedMap: A large-scale semantic weed mapping framework using aerial multispectral imaging and deep neural network for precision farming. Remote Sensing 10, 1423. https://doi.org/10.3390/rs10091423

Shi, Y., Thomasson, J.A., Murray, S.C., Pugh, N.A., Rooney, W.L., Shafian, S., Rajan, N., Rouze, G., Morgan, C.L.S., Neely, H.L., Rana, A., Bagavathiannan, M.V., Henrickson,

J., Bowden, E., Valasek, J., Olsenholler, J., Bishop, M.P., Sheridan, R., Putman, E.B., Popescu, S., Burks, T., Cope, D., Ibrahim, A., McCutchen, B.F., Baltensperger, D.D., Jr, R.V.A., Vidrine, M., Yang, C., 2016. Unmanned aerial vehicles for high-throughput phenotyping and agronomic research. PLOS ONE 11, e0159781. https://doi.org/10.1371/journal.pone.0159781

Sugiura, R., Tsuda, S., Tamiya, S., Itoh, A., Nishiwaki, K., Murakami, N., Shibuya, Y., Hirafuji, M., Nuske, S., 2016. Field phenotyping system for the assessment of potato late blight resistance using RGB imagery from an unmanned aerial vehicle. Biosystems Engineering 148, 1–10. https://doi.org/10.1016/j.biosystemseng.2016.04.010

van Evert, F.K., Fountas, S., Jakovetic, D., Crnojevic, V., Travlos, I., Kempenaar, C., 2017. Big data for weed control and crop protection. Weed Research 57, 218–233. https://doi.org/10.1111/wre.12255

Yang, M.-D., Huang, K.-S., Kuo, Y.-H., Tsai, H.P., Lin, L.-M., 2017. Spatial and spectral hybrid image classification for rice lodging assessment through UAV imagery. Remote Sensing 9, 583. https://doi.org/10.3390/rs9060583